Form-Finding of Thin Shell Structures

Zaahir Asmaljee

A research report submitted to the Faculty of Engineering and the Built Environment, University of the Witwatersrand, in partial fulfilment of the requirements for the degree of Master of Science in Engineering.

Johannesburg, 2013

Table of Contents

Declaration 4
Abstract 5
Acknowledgements 6
List of Figures 7
List of Tables 12

1 Introduction 15
1.1 Background 15
1.2 Form Finding of Thin Shell Structures 18
1.2.1 Existing methods of form-finding 18
1.2.2 Proposed form-finding technique 23
1.3 Focus of the Research 26
1.4 Implementation of the design tool 27
1.5 Format of the study 29

2 Literature Review 31
2.1 Thin Shell Structures 31
2.2 Development of Thin Shell Structures in the Built Environment 39
2.2.1 Robert Hooke (1635 - 1703) 40
2.2.2 Giovanni Poleni 42
2.2.3 Karl Culmann (1821 – 1881) 44
2.2.4 Rafael Guastavino 45
2.2.5 Antonio Gaudi (1852 – 1926) 48
2.2.6 Eladio Dieste (1917 – 2000) 52
2.2.7 Heinz Isler (1926-2009) 58

3 Development of the Design Tool 62
3.1 The Computer Model 62
3.1.1 Design Approach 62
3.1.2 Background to the Finite Element Method 62
3.1.3 Theory of the Finite Element Method 65

3.1.4 Adapting the plate flexure element to the form-finding process100
3.1.5 Formulation of the computer program 105
3.2 Verification of the computer model 108
3.2.1 Mathematical model 109
3.2.2 Physical models 110

4 Results 112
4.1 Analysis of the forms generated 114
4.1.1 Shape 1: The Barrel Vault 114
4.1.2 Shape 2: All Edges Simply Supported 130
4.1.3 Shape 3: Corner Point Supports 142
4.1.4 Shape 4: Broad Corner Supports 153
4.1.5 Shape 5: Broad Corner and Centre Supports 164
4.1.6 Shape 6: Corner and Centre Point Supports 175
4.2 Summary of Results 188
4.2.1 Shape 1: Barrel Vault 188
4.2.2 Shape 2: All Edges Simply Supported 188
4.2.3 Shape 3: Corner Point Supports 189
4.2.4 Shape 4: Broad Corner Supports 189
4.2.5 Shape 5: Broad Corner and Centre Supports 190
4.2.6 Shape 6: Corner and Centre Point Supports 191
4.3 Discussion of Results 193

5 Conclusion and Recommendations 198

References 202

Appendix 1 205

DECLARATION

I declare that this research report is my own unaided work. It is being submitted for the Degree of Master of Science in Engineering to the University of the Witwatersrand, Johannesburg. It has not been submitted before for any degree or examination to any other University.

Zaahir Asmaljee

Signature:_____

ABSTRACT

The outstanding characteristics of structural efficiency, durability and aesthetic beauty make the thin shell structure a much more viable structural design solution as compared to the more traditional methods of design. However, the manifestation of these outstanding characteristics is directly related to the form of the structure. This makes the form of the structure a key factor in ensuring the success of the design.

The correct form of the structure is not known in advance and requires a process known as form-finding or shape-finding. Hence, the focus of this research is to enhance this form-finding process, through the development of a computer design tool that is capable of accurately predicting the form of a pure compression thin shell structure, quickly and easily, in a manner that ensures that the desired characteristics are obtained within the structure.

The analyses show that the computer model only corresponded to the shape of the physical chain model in two out of the six cases analyzed. The results suggest that the shapes produced by the computer model corresponded more closely to the shapes produced by the square slabs of yield-line analysis or the physical models developed using the hanging fabric modelling technique. In conclusion, the physical hanging chain models did not provide a correct representation of the shapes produced by the computer model.

ACKNOWLEDGEMENTS

My thanks extend to my supervisor, Professor Mitchell Gohnert. He has been supportive and engaged and has helped steer this process, while encouraging me to explore new possibilities along the way. My thanks also extend to my family, for their endless support and encouragement throughout the research. And thanks to everyone who gave me encouragement or assistance over the course of this research.

LIST OF FIGURES

Figure 1.1: Hanging cloth model (Liem 2011) 19
Figure 1.2: A completed thin shell low-cost housing structure (Gohnert n.d.) 28

Figure 2.1: Thin shell structures commonly found in nature a) hazelnut (www.123rf.com) b) eggshell (drmiddlebrook.hubpages.com) c) turtle shell and skeleton (informaticaseptimoabc.blogspot.com) d) snail shells (naplesseashellcompany.com)..... 31
Figure 2.2: Early 19th century Ottoman Mosque of Mohamed Ali Pasha at the Citadel in Cairo, Egypt (www.marktisdalephotography.com) 33
Figure 2.3: Arch formed by inverting the hanging chain model (masonrydesign.blogspot.com)..... 40
Figure 2.4: Forces present in a typical arch (www.bristol.ac.uk)..... 41
Figure 2.5: Poleni's drawing of Hooke's analogy between a hanging chain and an arch, and his analysis of the Dome of St. Peter's in Rome (Block et al. 2006)..... 43
Figure 2.6: Gaudi's string model with birdshot weights used in the design of the Colonia Guell. 50
Figure 2.7: Gaudi's magnum opus, the Sagrada Familia, in Barcelona, Spain (Patrick Mayon)..... 51
Figure 2.8: Dieste's vault supported on a single column (clippings.com)..... 54
Figure 2.9: Heinz Isler's hanging models (http://blog .buildllc.com/ 2009/04/heinz-isler-a-few-important-things/)..... 60
Figure 2.10: Heinz Isler's motorway service station in Deitingen (commons.wikimedia.org) 60

Figure 3.1: Rectangular element with co-ordinate system 76
Figure 3.2: Stress resultants acting on a rectangular element (www.sciencedirect.com) 82

Figure 3.3: Rectangular element with co-ordinate system 85
Figure 3.4: Internal bending moments per unit length 95
Figure 3.5: Catenary curves for various values of a (www.mathsinthecity .com) 110

Figure 4.1: Arches along which the analysis was conducted 113
Figure 4.2: Actual square grid on which the physical models were constructed 114
Figure 4.3: Barrel vault generated by the computer model – REGN Method 116
Figure 4.4: Barrel vault shape – 64 REGN elements – computer model vs catenary shape 117
Figure 4.5: Barrel vault shape – 100 REGN elements – computer model vs catenary shape 117
Figure 4.6: Barrel vault shape – 144 REGN elements – computer model vs catenary shape 118
Figure 4.7: Barrel vault generated by the computer model – ACM Method 119
Figure 4.8: Barrel vault shape – 64 ACM elements – computer model vs catenary shape 120
Figure 4.9: Barrel vault shape – 100 ACM elements – computer model vs catenary shape 121
Figure 4.10: Barrel vault shape – 144 ACM elements – computer model vs catenary shape 122
Figure 4.11: Barrel vault shape – 64, 100 & 144 ACM element comparisons – computer model vs catenary shape 128
Figure 4.12: Physical model with all edges simply supported 131
Figure 4.13: Computer model with all edges simply supported 131
Figure 4.14: All edges simply supported – centre arches – computer model vs catenary shape 132

Figure 4.15: All edges simply supported – diagonal arches – computer model vs catenary shape 133
Figure 4.16: All edges simply supported – centre arches – physical model vs catenary shape 135
Figure 4.17: All edges simply supported – diagonal arches – physical model vs catenary shape 137
Figure 4.18: All edges simply supported – centre arches – computer model vs physical model 139
Figure 4.19: All edges simply supported – diagonal arches – computer model vs physical model 140
Figure 4.20: Physical model with corner point supports 142
Figure 4.21: Computer model with corner point supports 142
Figure 4.22: Corner point supports – centre arches – computer model vs catenary shape 143
Figure 4.23: Corner point supports – diagonal arches – computer model vs catenary shape 145
Figure 4.24: Corner point supports – centre arches – physical model vs catenary shape 147
Figure 4.25: Corner point supports – diagonal arches – physical model vs catenary shape 148
Figure 4.26: Corner point supports – centre arches – computer model vs physical model 149
Figure 4.27: Corner point supports – diagonal arches – computer model vs physical model 151
Figure 4.28: Physical model with broad corner supports 153
Figure 4.29: Computer model with broad corner supports 154
Figure 4.30: Broad corner supports – centre arches – computer model vs catenary shape 155
Figure 4.31: Broad corner supports – diagonal arches – computer model vs catenary shape 156

Figure 4.32: Broad corner supports – centre arches – physical model vs catenary shape 158
Figure 4.33: Broad corner supports – diagonal arches – physical model vs catenary shape 159
Figure 4.34: Broad corner supports – centre arches – computer model vs physical model 161
Figure 4.35: Broad corner supports – diagonal arches – computer model vs physical model 163
Figure 4.36: Physical model with broad corner and centre supports..... 165
Figure 4.37: Computer model with broad corner and centre supports 165
Figure 4.38: Broad corner and centre supports – centre arches – computer model vs catenary shape 166
Figure 4.39: Broad corner and centre supports – diagonal arches – computer model vs catenary shape 168
Figure 4.40: Broad corner and centre supports – centre arches – physical model vs catenary shape 169
Figure 4.41: Broad corner and centre supports – diagonal arches – physical model vs catenary shape 171
Figure 4.42: Broad corner and centre supports – centre arches – computer model vs physical model 173
Figure 4.43: Broad corner and centre supports – diagonal arches – computer model vs physical model 174
Figure 4.44: Physical model with corner and centre point supports 176
Figure 4.45: Computer model with corner and centre point supports..... 176
Figure 4.46: Corner and centre point supports – centre arches – computer model vs catenary shape 177
Figure 4.47: Corner and centre point supports – diagonal arches – computer model vs catenary shape 179
Figure 4.48: Corner and centre point supports – centre arches – physical model vs catenary shape 181

Figure 4.49: Corner and centre point supports – diagonal arches – physical model vs catenary shape 182
Figure 4.50: Corner and centre point supports – centre arches – computer model vs physical model 184
Figure 4.51: Corner and centre point supports – diagonal arches – computer model vs physical model 186

LIST OF TABLES

Table 4.1: Barrel vault – computer model vs catenary shape – 64 ACM elements 120
Table 4.2: Barrel vault – computer model vs catenary shape – 100 ACM elements 121
Table 4.3: Barrel vault – computer model vs catenary shape – 144 ACM elements 123
Table 4.4: Barrel vault comparison – 64 ACM elements vs 100 ACM elements 129
Table 4.5: Barrel vault comparison – 64 ACM elements vs 144 ACM elements 129
Table 4.6: 64 ACM – Computer Model vs Catenary Shape – Centre Comparison – All Edges Simply Supported 132
Table 4.7: 64 ACM – Computer Model vs Catenary Shape – Diagonal Comparison – All Edges Simply Supported 134
Table 4.8: 64 ACM – Physical Model vs Catenary Shape – Centre Comparison – All Edges Simply Supported 136
Table 4.9: 64 ACM – Physical Model vs Catenary Shape – Diagonal Comparison – All Edges Simply Supported 138
Table 4.10: 64 ACM – Computer Model vs Physical Model – Centre Comparison – All Edges Simply Supported 139
Table 4.11: 64 ACM – Computer Model vs Physical Model – Diagonal Comparison – All Edges Simply Supported 141
Table 4.12: 64 ACM – Computer Model vs Catenary Shape – Centre Comparison – Corner Point Supports 144
Table 4.13: 64 ACM – Computer Model vs Catenary Shape – Diagonal Comparison – Corner Point Supports 146
Table 4.14: 64 ACM – Physical Model vs Catenary Shape – Centre Comparison – Corner Point Supports 147

Table 4.15: 64 ACM – Physical Model vs Catenary Shape – Diagonal Comparison – Corner Point Supports 148
Table 4.16: 64 ACM – Computer Model vs Physical Model – Centre Comparison – Corner Point Supports 150
Table 4.17: 64 ACM – Computer Model vs Physical Model – Diagonal Comparison – Corner Point Supports 151
Table 4.18: 64 ACM – Computer Model vs Catenary Shape – Centre Comparison – Broad Corner Supports 155
Table 4.19: 64 ACM – Computer Model vs Catenary Shape – Diagonal Comparison – Broad Corner Supports 157
Table 4.20: 64 ACM – Physical Model vs Catenary Shape – Centre Comparison – Broad Corner Supports 158
Table 4.21: 64 ACM – Physical Model vs Catenary Shape – Diagonal Comparison – Broad Corner Supports 159
Table 4.22: 64 ACM – Computer Model vs Physical Model – Centre Comparison – Broad Corner Supports 161
Table 4.23: 64 ACM – Computer Model vs Physical Model – Diagonal Comparison – Broad Corner Supports 163
Table 4.24: 64 ACM – Computer Model vs Catenary Shape – Centre Comparison – Broad Corner and Centre Supports 167
Table 4.25: 64 ACM – Computer Model vs Catenary Shape – Diagonal Comparison – Broad Corner and Centre Supports 168
Table 4.26: 64 ACM – Physical Model vs Catenary Shape – Centre Comparison – Broad Corner and Centre Supports 170
Table 4.27: 64 ACM – Physical Model vs Catenary Shape – Diagonal Comparison – Broad Corner and Centre Supports 171
Table 4.28: 64 ACM – Computer Model vs Physical Model – Centre Comparison – Broad Corner and Centre Supports 173
Table 4.29: 64 ACM – Computer Model vs Physical Model – Diagonal Comparison – Broad Corner and Centre Supports 175

Table 4.30: 64 ACM – Computer Model vs Catenary Shape – Centre Comparison – Corner and Centre Point Supports..... 178
Table 4.31: 64 ACM – Computer Model vs Catenary Shape – Diagonal Comparison – Corner and Centre Point Supports..... 179
Table 4.32: 64 ACM – Physical Model vs Catenary Shape – Centre Comparison – Corner and Centre Point Supports..... 181
Table 4.33: 64 ACM – Physical Model vs Catenary Shape – Diagonal Comparison – Corner and Centre Point Supports..... 183
Table 4.34: 64 ACM – Computer Model vs Physical Model – Centre Comparison – Corner and Centre Point Supports..... 185
Table 4.35: 64 ACM – Computer Model vs Physical Model – Diagonal Comparison – Corner and Centre Point Supports..... 186

1 INTRODUCTION

1.1 Background

The environment in which human beings exist today is almost completely structured by design. A considerable portion of this design consists of the structures that make up the built environment. These structures comprise of the many buildings that aim to fulfil the many purposes of life, by providing people with houses to live in, offices to work in, shops and warehouses to supply goods, cafes as meeting places, schools and universities for education, stadiums for sport, mosques and churches for religious purposes.

These buildings are a vital component of any community. They play an important role in improving the quality of people's lives, by firstly, providing shelter to their occupants in a manner that allows them to function in a shared environment and secondly, by satisfying the needs and wants of its occupants. These buildings should therefore be designed to be both functional and aesthetically appealing, so that they may achieve the purpose for which they were created in a manner that encourages their use and adds value to their surroundings.

The success of any building depends on the creation of a well-defined space. The creation of this space provides one of the main challenges to building design. Usually, it is achieved through the construction of surfaces that are

organized in a specific manner to define the space that they enclose. These surfaces comprise of elements that have been inspired by nature. Angerer (1961) mentions, that the elements found in nature like that of a tree trunk, a rock on the earth or a shell of a snail or egg, have been translated into man-made structures comprising of slender members, solid bodies and stressed surfaces. These man-made structures include the Eiffel Tower, the Egyptian Pyramids and the Dome of the Hagia Sophia.

The use of these basic elements in building construction has been translated into three different building methodologies, as mentioned by Angerer (1961). The first method is referred to as solid construction, where the basic element of building is a solid mass such as the present day brick wall. The second method is referred to as skeleton construction, such as the present day sky-scrapers, where the basic elements are the struts, columns and beams. The third method, which is between solid and skeleton construction is referred to as surface construction, with the basic element being the surface. In nature, these surface constructions are in the form of honeycombs, snail shells, grain stalks and flower petals, and in man-made structures they are in the form of arches, vaults and domes.

The third method of surface construction has been developed over many centuries into what is today known as the thin shell structure. The surface of this structure fulfils both the load bearing and space defining functions, with

the inner space and the external form being identical. This surface has progressed from the multi-curved dome structures constructed by the Byzantine builders, who had a very clear conception of the flow of forces within the structure, to the more complicated structures designed in more recent times. This progression was made possible through the development of improved methods of calculation, which allow for a better understanding of the behaviour of the thin shell structure.

These thin shell structures are of particular interest to structural designers, due to the manifestation of three very important characteristics: The first characteristic is its structural efficiency, which enables the usage of less material to enclose larger spaces. The second, is the durability and time-enduring properties of the shell structure, which has been proven from the design and construction of the many iconic buildings of the past that still exist to this day with very little maintenance. And the third characteristic is the natural aesthetic beauty exhibited by these thin shell structures, which is derived from the very nature of their form-finding process.

These outstanding characteristics make the thin shell structure a much more viable structural design solution as compared to the more traditional methods of design. However, since the mechanical behaviour of the structure is dependent on its form, the characteristics described above are also dependant on the form of the structure. This makes the form of the structure a

key factor in determining the accuracy of the structural design, which ultimately determines its success. Therefore, a thin shell structure can only be considered as a design alternative when the form of the completed structure is correct.

1.2 Form Finding of Thin Shell Structures

1.2.1 Existing methods of form-finding

The mechanical behaviour of a thin shell structure, which comprises of the complex force systems that exist within the structure, is closely related to the shape or form of the structure. This means that the success of the structure is directly dependant on the form of the structure. The correct form of the structure is not known in advance and requires a process known as form-finding or shape-finding. The early designers of thin shell structures employed the use of physical models in the form-finding process. Even in more recent times, these structures have been designed using form-finding techniques based on physical models.

The physical modelling techniques apply physical hanging models such as the hanging fabric model or the hanging string model. These models, under their own self-weight, form a funicular shape that accurately defines the form of a thin shell structure. In some instances, to simulate the hanging model, networks of chain models were calibrated with sand bags and in other

instances, fabric models were weighted with plaster or epoxy resin. The co-ordinances of the displacements along the models were then measured and the shape of the structure was defined. These hanging models produced a pure tension structure, which when inverted resulted in a structure that was in pure compression.

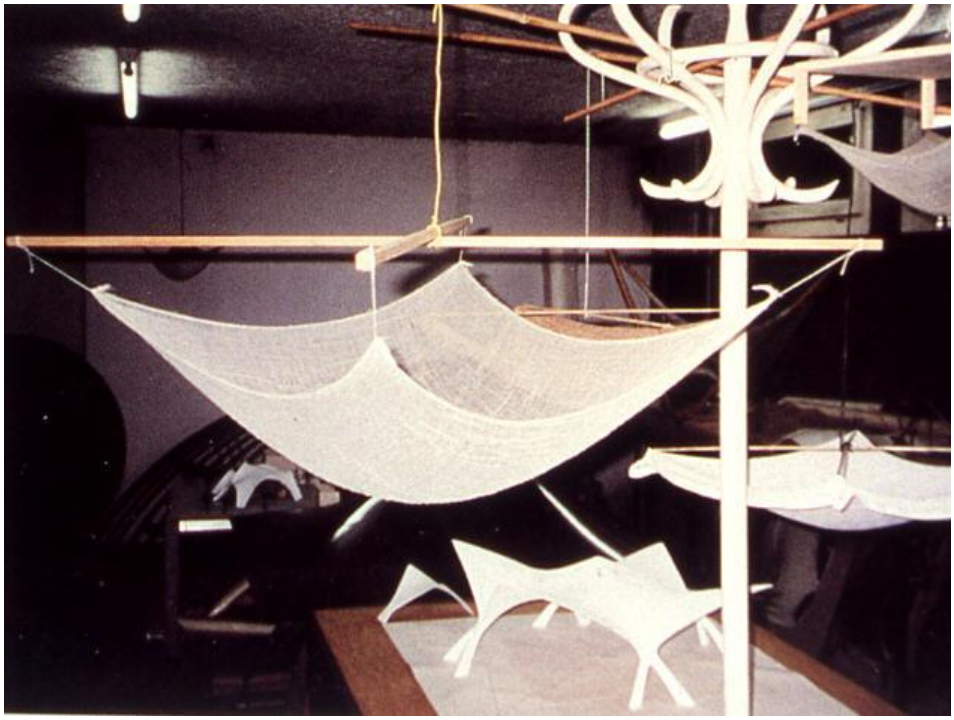

Figure 1.1: Hanging cloth model (Liem 2011)

The design of thin shell structures using form-finding techniques, like that of the physical hanging model, has worked well in the past. Killian (2004) points out that the equilibrium solutions obtained from these models accurately define the shape of a full-scale building design, provided that the proportional distribution of mass is kept and the geometry of the lines of forces are scaled

proportionally. This concept holds true, even though mass does not scale proportionally to geometric dimensions.

Nevertheless, there are certain factors that limit the application of physical hanging models in the design of thin shell structures. These limitations are presented in the following section.

1.2.1.1 Limitations to physical methods of form-finding

Although the physical hanging model form-finding process provides a very compelling design approach, there are certain factors that limit its application in the design of thin shell structures. These factors are provided below:

Firstly, the enormous amount of work that is required to construct a fully detailed hanging model makes it an extremely labour-intensive process. In addition to the initial construction, the inherently dependant nature of the model means that any major change to the geometry of the structure at a later stage, would require a large amount of additional work. Even small modifications to the design of the interdependent structure will ripple through to the larger parts of the model, which would require further adjustments that would result in further shifts elsewhere. Although the model will eventually reach a state of equilibrium, the new shape might not even match the desired

form. This would require even more adjustments and this iterative process makes the method even more labour-intensive.

The second major disadvantage of the physical hanging model is as a result of the difficulties that arise in accurately measuring the model, since measuring requires accessing the model. Weller (2011) states that the incorrect measuring of the model can lead to fatal flaws, since for a 1:100 model, an error of 0.5mm would scale to a design irregularity of 5cm, which could be the full thickness of the final shell. Therefore, the physical models need to be relatively big in scale to allow for accurate measurements with reasonable tolerances. This increase in the model size adds to the work required in building the model.

The third major disadvantage is the time-consuming nature of the physical design process. The large amount of work required for the initial construction of the model, together with the iterative adjustments (due to any modifications), makes the construction of the model very time-consuming. In addition to the physical design process, the difficulties that arise in the measurements associated with the model add to the time-consuming nature of the design process. Weller (2011) states, that although the building of the model is a slow process, the measuring of the final form is an even slower process. The time-consuming nature of the physical design process is also evident in Gaudi's Colonia Guell. Tomlow (1989), states that Gaudi's model

was developed by a highly qualified team, over a period of ten years between 1898 and 1908.

Fourthly, the emerging shape of the hanging model is influenced by the underlying fabric and fibre orientation. This, together with the human and environmental errors that can arise from the nature of the physical design process, results in shapes of inconsistent proportions. Therefore, by scaling these physical models up or down, it becomes very difficult to ensure that the properties of these structures remain constant and are in fact according to the design requirements.

Furthermore, these inconsistencies can result in uncertainties in the distribution of the stresses within the structure. It therefore becomes difficult to ensure that the stresses at all locations within the structure are optimally designed and are, in fact, within the design requirements. This is an important consideration, since an inadequate stress distribution results in areas of unnecessary weakness within the structure, which would consequently compromise the integrity of the structure.

1.2.2 Proposed form-finding technique

The previous section highlights the shortcomings of the physical modelling process and brings to the fore the need to develop an alternate form-finding technique. To meet the requirements of the highly competitive structural design environment, this technique needs to be able to efficiently produce a large number of structures that can be adapted to various locations, in a manner that will not compromise the strength and stability of the structure. Therefore, a more accurate, efficient and stable form-finding technique is required.

This can be achieved by incorporating the same principles of the physical hanging membranes into the development of a computer design tool that can accurately define the shape of a pure compression thin shell structure. The development of this computer design tool will be dedicated to accurately defining the form of a thin shell structure, in a manner that would eliminate the shortcomings of the form-finding process and allow the thin shell design approach to reach its full potential.

It now becomes necessary to determine whether any of the structural analysis packages that are already available on the market are in fact capable of accurately defining the shape of a pure compression thin shell structure. Some

of the more popular computer packages have been considered and the limitations of these packages are presented in the section that follows.

1.2.2.1 Limitations of existing computer packages

Since the advent of the digital computer, various computer packages have been developed to analyze the behaviour of a structure. Although, these packages can be effectively applied to the analysis of certain aspects of thin shell structures, none have been specifically developed for the purpose of determining the form of a funicular structure. This is evident from the research that has been conducted to determine the capacity of these packages in defining the form of a funicular thin shell structure.

One such package is NASTRAN, which was originally developed for NASA in the 1960's. This computer package is considered by many to be the most advanced finite element analysis package that is available on the market and many are convinced that it is the foremost in the field of finite element analysis. The NASTRAN program has the ability to analyze both static and dynamic systems in a wide variety of failure modes and it is the software of choice for the analysis of parts and systems for any mechanical application.

However, Pendergrast (2010) states that although NASTRAN is one of the most advanced finite element packages, the output of information is not

relevant to most architectural and form-finding applications. This makes the program more suited to determining the failure modes for a part of a mechanical system rather than defining the form of a thin shell structure. Therefore, although NASTRAN is a powerful structural analysis software, it is not designed to solve form-finding problems.

Dr. Frame 3D is another program that is considered to be more relevant to architectural design than NASTRAN. This is because this software provides an interface that allows the building of frames and structures, whereupon the user can apply loads and see the resulting deformations and moments. Other similar architectural CAD packages such as AutoCAD Architecture and Rhino are also available. These computer packages are very adept at constructing frames for bridges, skyscrapers and traditionally designed houses. However, Pendergrast (2010) mentions that the shortfall of all of the above programs is in the construction of an accurate funicular shape. This is because these packages do not possess the tools for easily creating an arbitrary stable frame.

Therefore, the available computer packages are more suited to the analysis of the behaviour of a structure or part of a structure, whereby the form or shape of the surface is already known. But when it comes to defining the actual shape of the surfaces, the form-finding procedures of these packages are inadequate. Therefore, although various computer packages do exist for structural analysis

and architectural modelling, it can be concluded that these packages are not particularly well-suited for the form-finding of a funicular thin shell structure.

1.3 Focus of the Research

The focus of this research is to develop a design tool that can accurately predict the shape of a thin shell structure, both quickly and easily. This will allow engineers, architects and designers to concentrate more on the design of their structures and less on ensuring that their buildings are structurally stable. The tool will be developed by means of a computer model that will allow designers to accurately simulate any irregularly shaped thin shell structure. This computer package will allow for greater flexibility and speed in designing this type of structure, which will enable a greater degree of optimization and ultimately lead to a more feasible design.

The development and correct functioning of this computer package will facilitate a considerable advancement in the design of thin shell structures. This is because the computer model will eliminate many of the shortcomings that cause the thin shell structural approach to fall out of favour with designers. Therefore, the availability of this design tool, which allows for the rapid and structurally efficient design of funicular thin shell structures, will broaden the scope of the application of this type of structure. This will revolutionize the use of thin shell structures and will encourage architects, designers and visionaries

to look beyond the constraints of existing technologies and towards the endless opportunities that exist through the use of funicular thin shell structures.

1.4 Implementation of the design tool

Within the South African context, one of the main areas for the application of thin shell structures, is in the design of low-cost housing, where the need to provide cost-effective housing of adequate quality still exists. Gohnert (n.d.) mentions that within the low income sector of the population, there is an estimated housing shortage of 2.1 million homes and an increase in new households of 200 000 per year. The National Housing Code of South Africa attributes much of the abnormalities in the housing sector to the policies and political turbulence of the Apartheid era.

In response to the housing abnormalities, the Department of Housing has developed a housing policy in an attempt to meet the needs of the housing sector. However, according to the DoH (2000), a major drawback of this policy is that the houses produced do not meet the standards set by the government, in terms of the quality and the affordability of the housing products. This presents the perfect opportunity for the application of the thin shell structural design approach, since the incorporation of the shell structure into the design of these low-cost houses will eliminate both problems of quality and affordability.

With regards to the quality, thin shell structures have proven themselves to be superior to the more traditional methods of design. This is evident from the time-enduring properties of the iconic buildings of the past that exist to this very day. The affordability of the thin shell structure is a direct result of its structural efficiency, which allows for the usage of both less and cheaper materials. This leads to a significant decrease in the cost of the structure. Therefore, the reduced cost, together with the improved quality of the thin shell structural design approach, makes it a viable solution to the current housing problem in South Africa.

Figure 1.2: A completed thin shell low-cost housing structure (Gohnert n.d.)

1.5 Format of the study

Following this introductory chapter, a review of the literature pertaining to the thin shell structure is presented in chapter two. The literature review will first introduce the concept of the thin shell structure and then provide the details that are relevant to this research. Thereafter, the development of the thin shell structure in the built environment is presented, whereby the contributions of the major personalities responsible for their developments are discussed. Chapter two therefore provides a comprehensive explanation of thin shell structures, together with how it has progressed to its current form.

In chapter three, the development of the design tool is discussed. The finite element method that forms the backbone of the design tool is firstly introduced. Thereafter, a detailed discussion of the theory behind the finite element method is presented, with particular emphasis on the rectangular finite element for plate flexure since it has been used in this research. The analysis was conducted using two different variations of the rectangular element and both derivations have been presented. Thereafter, the manner in which this rectangular element has been utilized in the form-finding process is explained. Chapter three is then concluded with an explanation of the formulation of the computer model, together with the physical and mathematical models that serve to verify the computer model.

In chapter four, the results of the analyses are presented and evaluated. Firstly, an initial accuracy test of the computer model is conducted using a barrel vault, which forms a pure catenary structure. This evaluation allowed for the most accurate rectangular finite element to be identified and implemented in all further computations. Thereafter, all the forms developed by the three types of models i.e. the computer, physical and mathematical models, are presented, compared and evaluated. The chapter is then concluded with a summary and discussion of the results. In the fifth and final chapter the conclusions and recommendations are presented.

2 LITERATURE REVIEW

2.1 Thin Shell Structures

Thin shell structures are the most optimal and efficient structural surfaces found in nature. They appear in a large variety of applications and are commonly found in forms such as egg shells, nut shells, turtle and snail shells, bamboo canes swaying in the wind, the leaves of trees, the skull and bones of humans and animals and even the root section of a bird's feather. Their application even extends as far as the cells in our bodies, where researchers such as Fung & Sechler (1974) have mentioned that at microscopic level, every cell in our body is in fact a thin shell structure.

(a)

(b)

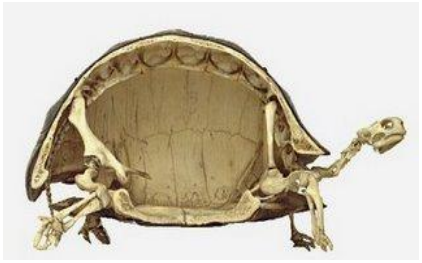

(c)

(d)

Figure 2.1: Thin shell structures commonly found in nature a) hazelnut (www.123rf.com) b) eggshell (drmiddlebrook.hubpages.com) c) turtle shell and skeleton (informaticaseptimoabc.blogspot.com) d) snail shells (naplesseashellcompany.com)

These naturally occurring thin shell structures have remarkable load-carrying capabilities and strength characteristics, and have been a source of inspiration for the creation of many man-made structures. These man-made structures encompass a wide range of applications that extend over many areas of specialization. There usage can be commonly found in the power industry, the chemical engineering industry, the aerospace industry, the vehicle manufacturing industry, the boat construction industry and the building industry. With regards to the building industry, these thin shell structures have played an important role in the design and architecture of the built environment.

In the built environment, the design and architecture of thin shell structures were often used to represent nations and cultures. This resulted in the incorporation of these shell structures into the design and construction of many iconic buildings that are symbols of great beauty, like the Pantheon in Rome, the Hagia Sophia in Istanbul, the Citadels in Egypt and the Sydney Opera House in Australia. However, their application was not restricted to the design of iconic buildings, but was also extended to the design of more economical structures such as vaults, domes, halls & theatres and the shell roofs that are found on many houses and factories.

Figure 2.2: Early 19th century Ottoman Mosque of Mohamed Ali Pasha at the Citadel in Cairo, Egypt (www.marktisdalephotography.com)

The early usage of thin shell structures are evident in the extraordinary dome constructions that were built long before the development of any shell theories or shell construction methods. The early Roman engineers and Gothic vault builders had a strongly empirical outlook that enabled them to develop a good understanding of the behaviour of the arch, which forms the basis of thin shell design. Angerer (1961) mentions, that they understood that where one stone block supported its neighbour, it was possible, by means of a skilful bond of wedge-shaped voussoirs to bridge a gap that was many times the size of the individual voussoirs. This understanding allowed the

Roman architects to design and construct shell structures, such as the Pantheon in Rome.

As the design of the built environment progressed, the need for building more economical structures became widespread. This required a greater precision in the design approach and ultimately led to the development of the theory of thin shell structures. Hence, the theory was developed over a century ago, when Lamé and Clapeyron (1828) developed the fundamental theory for shell membrane action and Aron (1874) investigated the bending behaviour of thin shells. However, the first general theory was developed by Love (1888) and all subsequent developments in the theory were directed at improvements to Love's formulation or the solution of the associated differential equations.

In today's understanding, a thin shell structure has been classified as a special type of structure that has a combination of two very important characteristics. The first characteristic is that in the unstressed state, the structure has a curved surface, which categorizes it as a shell structure. This curvature affects the strength and stiffness of the shell and is the main feature that differentiates a shell structure from a flat plate structure. The second characteristic is that the structure is thin i.e. it has a thickness that is relatively small as compared to its other dimensions. However, the structure should not be so thin that the deformations would be large as compared to the thickness

of the structure. These two characteristics provide a basic definition of a thin shell structure.

A more detailed definition requires that in addition to the curvature, the thin shell structure needs to be structurally continuous. This structural continuity requires that the forces within the surface of the shell should be able to be transmitted in a number of different directions. This may raise some doubts as to whether the ancient masonry domes fulfilled this condition of structural continuity, considering that they were made up of individual stone units that were not always cemented. The fact of the matter is that they were continuous, in that they were in a state of compression throughout the dome and each stone unit was held in compressive contact with the other (Calladine 1983).

With regards to shell theory, the mathematical solution is based on the assumption of an ideal material, which is developed assuming that Hooke's law applies to it. Angerer (1961) states that experience has shown that this degree of approximation, allows for the formulation of such calculations that when applied are sufficient to build economical surface structures. In this manner, Hooke's Law can be used to relate the deformation of a typical shell element to the stresses applied to it. The equilibrium and compatibility equations can now be expressed in terms of the initial geometry of the structure. Calladine (1983) mentions that the equilibrium equations relate the

stress resultants in the structure to the applied external forces and the compatibility equations express the geometrical connection between the strain in an element and the displacement of points on the structure.

The stresses that exist within the thin shell structure can be calculated by using either Membrane Theory or Bending Theory, depending on the type of stresses that are present within the structure. Membrane Theory is used when the structure is set up in such a manner that only membrane forces are present and the effects of normal shears, bending moments and torsions can be ignored. The structure is statically determinate and the stresses that remain within the structure are in equilibrium. On the other hand, Bending Theory is used when bending and torsion stresses cannot be eliminated and the structure will have to be designed to resist them. In this case, the structure will not be in equilibrium and it will be statically indeterminate. It should be noted that the calculations involved in Membrane Theory are much simpler than those involved in Bending Theory.

In addition to simplifying the calculations, the thin shell structure that comprises primarily of membrane forces also ensures that the structural efficiency of the shell structure is maximized. This structural efficiency is achieved as a result of the structure being designed to be free from any materially expensive forces such as bending, twisting and shear forces. And since the mechanical behaviour of the structure is directly related to the form

of the structure, it is through this form that the bending, twisting and shear forces can be eliminated from the structure. Therefore, ideally, the structure should be shaped and proportioned in such a manner that it is able to transmit the loads without bending, twisting and shear forces.

The ideal form of a pure compression thin shell structure is that of a funicular shape, which is capable of producing the ideal distribution of forces within the structure. The word ‘funicular’ is derived from the Latin word for “rope” since it refers to such structures that form a shape similar to that of a hanging rope, in response to the magnitude and location of the forces acting upon it. The hanging rope should be allowed to hang freely under its own self-weight whilst being supported at its ends. A combination of these ropes can be configured to form a three-dimensional shape, which would result in a type of funicular structure commonly referred to as a catenary thin shell structure. The suspended catenary structure will be in pure tension, which can then be inverted to form a pure compression structure that is free from any shear forces and bending moments.

These pure compression thin shell structures do experience some difficulties, which need to be considered in the design process. Calladine (1983) mentions that one of the main difficulties of these compression structures is that they are prone to buckling of a particularly unstable kind. This can lead to crumpling of the structure, which would result in a loss of the initial geometry

of the structure and render the structure less efficient and structurally unstable. Calladine (1983) also mentions that another difficulty arises due to unavoidable rigidity. This usually occurs as a result of thermal expansions, which can cause very large forces to be set up on account of the rigidity of the structure. The possibility of the occurrence of these difficulties needs to be identified and the necessary measures need to be put in place to counteract them.

Nevertheless, the funicular shape is a vital component in ensuring that no bending exists within the structure, and only axial and in-plane compression and/or tension occur. This allows for the most economical use of materials and the reduction or elimination of steel reinforcing from the design process. In addition, it also allows the thin shell structure to be constructed from no or low tensile materials such as masonry, since the funicular shape will either minimize or prevent the cracking of structures constructed from these materials. This will allow for the design of the most economical and structurally stable thin shell structure.

A deeper understanding of the behaviour of these thin shell structures can be obtained from the study of its development in the built environment, from its inception to its current form. This will identify how and to what extent this type of design has been applied and incorporated into the design of everyday structural designs.

2.2 Development of Thin Shell Structures in the Built Environment

Thin shell structures in the built environment have developed over many centuries, from the simple arch to the solid domes of the ancient buildings to the more irregularly shaped structures of today. The domes of the buildings of the past, like that of the Pantheon of Rome, built in 1 A.D or the Hagia Sophia in Istanbul, built in 538 A.D, were shaped and proportioned by intuition and tradition. This resulted in structures that were thick in cross-section, which rendered the structures uneconomical and not applicable to everyday structural design.

However, as time passed, the design of the thin shell structure moved away from its intuitive roots towards a design with an experimental and theoretical basis. This led to scientifically engineered structures that could be applied to a wider range of applications and allowed the thin shell structure to emerge as a practical approach to everyday structural design. The developments of thin shell design in the built environment can be attributed to various personalities, who have pioneered the design process and are responsible for its progression over the centuries. These personalities, together with their contributions, are discussed below:

2.2.1 Robert Hooke (1635 - 1703)

The foundation of the design of thin shell structures is deeply rooted in the design of the simple arch. Although the use of the arch dates back many centuries, its exact shape from a mathematical and structural point of view, was only developed towards the end of the seventeenth century by the English scientist, Robert Hooke. Allen & Zalewski (2010), claim that this celebrated scientist "discovered the true mathematical and mechanical form of all manner of arches". Hooke summarized his findings in a single phrase, which when translated from Latin reads:

"….*as hangs the flexible line, so but inverted will stand the rigid arch.*"

The principle of Hooke's observation was that the exact shape of the arch is obtained by hanging a chain or flexible line and recording the co-ordinates of the form it takes under its own self-weight. This arch can then be reversed to define an arch that is purely in compression.

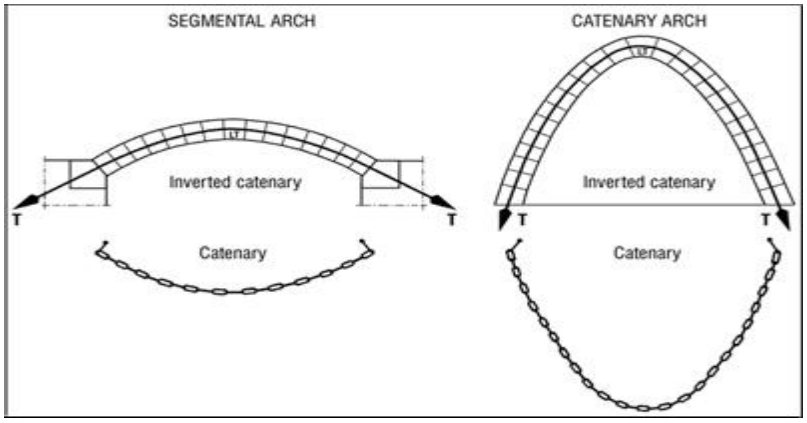

Figure 2.3: Arch formed by inverting the hanging chain model (masonrydesign.blogspot.com)

Hooke realized that an ideal shape of an arch can be obtained when the condition of equilibrium was satisfied within the arch. This occurs when the slope of the arch at each point exactly matches the combined horizontal and vertical forces acting at that point of the arch. The vertical component of the force is due to the gravity from the weight of the portion of the arch above the point. The horizontal component is as a result of the two sides of the arch leaning against each other. As one moves along the arch from the apex, the accumulation of load increases, resulting in a proportional increase in both the vertical force and the slope of the arch.

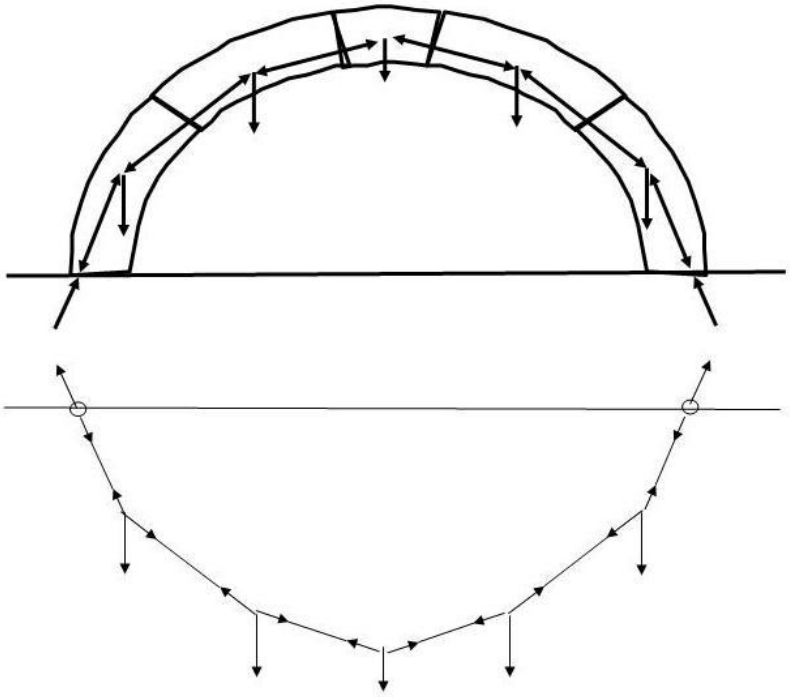

Figure 2.4: Forces present in a typical arch (www.bristol.ac.uk)

Hooke also realized that at the base of the arch, the horizontal force continues to increase. This led him to conclude that the bottom of the arch should be designed to be angled outwards and not vertical. Osserman (2010) mentions, that Hooke made this finding after the disastrous fire of 1966, when both he and Christopher Wren were among the chief architects rebuilding London. Hooke shared his findings with Wren, who was appointed to design the St. Paul's Cathedral. Wren then applied Hooke's finding to the design of the cathedral dome, which resulted in the dome being angled out at its base, rather than vertical.

In the centuries that followed, Hooke's principle has been widely used to understand and design many other thin shell structures.

2.2.2 Giovanni Poleni

In 1748, Giovanni Poleni was appointed to investigate the cracks that had appeared on the dome of the St. Peters Cathedral in Rome. He was given the task of determining whether these cracks affected the safety and stability of the cathedral. To analyze the dome, Poleni applied the arch theory previously developed by Hooke. Bulovic & Bhikoo (2011), mention that in keeping with Hooke's principle, Poleni hung thirty-two weights onto a chain in order to represent the self-weight of the dome. The resulting profile of the chain thus

represented the natural thrust line of the dome. This profile was then inverted and superimposed onto a cross-section of the dome walls.

Poleni hypothesized that the structure would be stable as long as the thrust line fell within the structure; and if the thrust line fell outside the structure tension cracking would occur and the structure would be rendered unstable. In the case of St Peters, the thrust lines fell within the dome structure and Poleni concluded that the structure was stable and safe for occupation. The cracking was attributed to the use of inferior construction materials. Poleni's theory has been substantiated with the passing of time, in that St Peters cathedral remains stable after nearly three centuries.

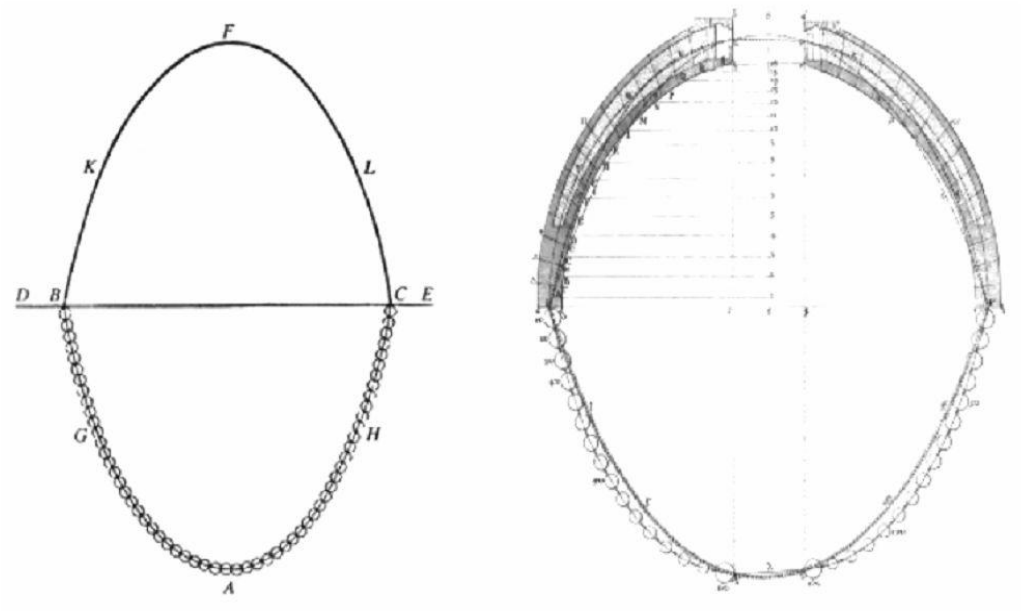

Figure 2.5: Poleni's drawing of Hooke's analogy between a hanging chain and an arch, and his analysis of the Dome of St. Peter's in Rome (Block et al. 2006)

2.2.3 Karl Culmann (1821 – 1881)

Karl Culmann was the man responsible for transforming Poleni's hypothesis into a simple and powerful method known as graphic statics. This method made it easy to find the correct forces and shapes of masonry arches and vaults. Anderson (2004) states that Culmann's , *Die graphische Statik,* which was published in 1866, provided the first comprehensive presentation of graphic statics, a method of structural design that uses scaled drawings instead of numerical operations.

The graphic statics method determines the form and forces within a masonry vault, in a manner that is both quick and simultaneous. The method requires that the vault be supported at two abutments and that it passes through a point on its vertical centreline. For the vault to be stable under the uniform gravity load, each segment of the vault must be in static equilibrium. This can be achieved when the gravity force for each segment and the two inclined compressive forces from the segments on either side, balance each other. This then develops a funicular shape that defines the ideal shape of a pure compression vault.

Culmann's method has been adopted by many designers in the design of vaults and shells.

2.2.4 Rafael Guastavino

Rafael Guastavino was a builder and an architect, who was born in 1842, in a place called Valencia in Spain. In 1861, he moved to Barcelona where he began his studies in building. His professional career started in 1866 in Catalonia, where he began building vaults. After this initial period, Guastavino built his vaults throughout Spain. Based on his background, his works were heavily influenced by the building traditions of Valencia and Barcelona.

Thereafter, in 1881, Guastavino left his home country of Spain and moved to the United States, where he later founded his own building company. In this manner, Guastavino transferred the knowledge of the ancient building technique of masonry vaulting to the United States, which at that time had little tradition of vault construction. Guastavino incorporated vaults in more than 300 buildings, some of which include the Cathedral of St. John (1908), Grand Central Station (1903-1913) and the Riverside Church (1930).

Guastavino revolutionized the use of masonry vaults by transforming the thick, heavy, and expensive vaults of the previous generations, into the thin brick shells of the late twentieth century. Anderson (2004) claims that Guastavino was responsible for producing the first scientifically engineered masonry structure, when he incorporated the technique of graphic statics to the design of traditional Catalan vaults.

Using the technique of graphic statics, Guastavino began producing vaults that were funicular in shape, thereby minimizing the bending stresses in the structure. Graphic statics made it possible for Guastavino to determine the minimum possible thicknesses of the vaults, which allowed him to use only as much material as was required. This enabled him to design and build economical masonry shell structures that are so durable that most survive in excellent condition to this day.

Guastavino's works were unique, in that he employed the Mediterranean technique of tile vaulting to his designs. Two main distinguishing features set these vaults apart from traditional vaults. The first distinguishing feature was that in tile vaults, the tiles were joined with plaster that set almost instantaneously, thereby immediately holding the tiles in place. This allowed the vault to be constructed without the costly wooden framework required in traditional vaults, which also resulted in the tile vaults having a faster speed of construction as compared to traditional vaults.

The second distinguishing feature was that in tile vaulting, thin tiles were laid flat and joined along the thin edges in accordance with the required shape of the surface of the vault. This was unlike traditional vaulting, where the masonry units were laid in a single layer that was vertical in orientation. This made the tile vaults thinner and thus more economical in its use of material as

compared to the traditional vaults. This ultimately led to the construction of a lighter vault, which subsequently reduced the size of the vault supports.

Guastavino considered his vaults to belong to another class of masonry design that he termed “cohesive construction”. He claimed that his vaults were held together as a result of the internal bonding together of the tiles and mortar. This allowed each vault to function as a unified material that was able to take tension and therefore exerted no thrust on the supports. However, in reality Guastavino’s vaults behave exactly the same as traditional vaults. Although the tile vaults might be lighter in weight, they still exert horizontal thrusts on their supports, which are generally lower than traditional vaults. Additionally, just like traditional vaults, the success of the tile vaults depends on the correct form and not on the strength of the material. For both types the material is brittle, making it strong in compression and weak in tension.

Nevertheless, the structural stability of Guastavino’s vaults remains outstanding. Ochsendorf (2010) highlights the fact that none of Guastavino’s vaults failed due a lack of load bearing capacity. He further goes on to prove the stability of Guastavino’s vaults through the example of the Registry Hall, built in 1917 on Ellis Islands, a place that had been deserted for many decades. All the other buildings in the area fell into terrible disrepair but the Guastavino vault remained in excellent condition, to such an extent that from the approximately thirty thousand tiles, only seventeen were ever replaced.

Therefore, although the architectural design of Guastavino's works fell out of fashion with designers who chose to move to materials such steel and concrete, the structural stability of his vaults remains unmatched.

2.2.5 Antonio Gaudi (1852 – 1926)

Antonio Gaudi was a Spanish Catalan architect, whose works have had a significant impact on the architecture of Spain. Although his complex curved surfaces grew from the traditions of Catalan masonry, his structures had a distinctive style of their own that was very different from that of his contemporaries. The uniqueness of his works has captured the attention of architects from around the world and many studies have been devoted to understanding his architectural designs. Gaudi's works are concentrated in and around the capital of Barcelona, including his most famous work, the Sagrada Familia.

Gaudi's works were influenced by many sources. According to Van Hensbergen (2001), as a student Gaudi studied photographs of Egyptian, Indian, Persian, Mayan, Chinese and Japanese art, together with the Moorish monuments in Spain. This left a deep impression on him and inspired many of his works. Flores (2002), also states that "Gaudi observed of Islamic art its spatial uncertainty, its concept of structures with limitless space; its feeling of sequences, fragmented with holes and partitions, which create a divide

without disrupting the feeling of open space by enclosing it with barriers". Furthermore, Saudi (2002), claims that Gaudi was most influenced by the Gothic Revival, promoted in the latter half of the 19th century by the French architect, Viollet-le-Duc.

Gaudi's study of nature also greatly influenced his work and it motivated his lifelong search for natural architecture. He realized that the forms found in nature were not only aesthetically appealing but also fully functional. This inspired him to imitate what he observed in nature and he tried to adapt the forms found in nature to the structural forms of architecture. This approach caused him to move away from the predetermined geometries of vertical piers and buttresses, towards structural forms derived from funicular lines.

One of the geometrical forms employed by Gaudi was that of the catenary arch, which at that time was only used in the design of suspension bridges. Gaudi utilized this catenary arch in his works such as the Casa Milá, the School of the Teresianas, the crypt of the Colonia Guell and the Sagrada Familia. The inherent properties of the catenary shape added great strength to Gaudi's structures and it also allowed him to construct his buildings from cheaper materials such as brick. He therefore frequently used brick with mortar in successive layers, a technique that was similar to how it was used in the traditional Catalan Vault.

Gaudi's method of design was unique, in that he used scale models to determine the shape of his structures. He rarely drew plans of his designs, but instead preferred to create them as three-dimensional scale models. Bassegoda (1989) mentions, that in the design of the Colonia Guell, Gaudi built a 1:10 scale model that was 4 meters in height. The model was set up using strings with small bags of birdshot hanging from them. The birdshot bags simulated the weight from the supporting points of the building i.e. the columns and the intersection of walls. The weights subsequently produced catenary curves in both the arches and vaults. Gaudi then took a picture of the model, which when inverted defined the shape of the structure.

Figure 2.6: Gaudi's string model with birdshot weights used in the design of the Colonia Guell.

Gaudi's quest for new structural solutions culminated in the design of the Sagrada Familia. Anderson (2004) mentions that Gaudi had taken the principle of graphic statics one step further when he used it to determine the directions of the thrusts that emerged from the bases of the vaults. He then aligned the supporting columns along these lines of thrust, which allowed him to avoid constructing buttresses that he considered unnatural. Therefore, in the Sagrada Familia, Gaudi created a new architectural style that was original, simple and aesthetic. He also employed this method of design in other structures such as the Parc Guell (1900 – 1914).

Figure 2.7: Gaudi's magnum opus, the Sagrada Familia, in Barcelona, Spain (Patrick Mayon)

2.2.6 Eladio Dieste (1917 – 2000)

Eladio Dieste was an engineer and architect; who was born, lived and predominantly built his structures in Uruguay, a country of limited resources. Dieste was greatly affected by the inequities suffered by the majority of the population of his country. This influenced the way in which he designed his structures, in that he considered how his designs would affect the local community, together with the social implications involved in their construction.

Dieste was opposed to the common trend of blindly emulating the developed world by importing technology from them, which was often very costly and inappropriate to his countries needs. Anderson (2004) mentions that Dieste felt that this approach not only increased the dependence of developing countries on developed countries, but also maintained a division between them and the developed world. Dieste also opposed the view that economic benefit at any cost was always beneficial and he believed that there was an important difference between economic development and human development. He argued that economic development was determined by national statistics in terms of the productive output per capita, rather than by human fulfilment.

Dieste chose to design his structures using the technique of reinforced masonry, which was not very popular and less exploited during his time. The

architecture of that time was more inclined towards the use of 'modern materials' such as steel, concrete and glass. However, Dieste was adamant that these new materials should not displace the earlier materials that have demonstrated their effectiveness. He therefore chose to go against the norm and he built his structures using brick, which in his hands fulfilled all the requirements of the modern material. He incorporated this technique into the design of many low-cost roofs for factories and storage facilities in Uruguay.

Dieste supported his preference of using masonry brick over concrete by suggesting that brick had various advantages over concrete. These advantages are mentioned by Anderson (2004) as: the relative strength for weight, the better resistance to temperature changes and aging, the better acoustics, the better environmental qualities and the lower cost for comparable quality. Anderson (2004) also states that Dieste believed that the tectonic sense of a durable material with the necessary qualities of colour and texture, which when constructed through sound craftsmanship, added a greater appeal to the structures built from them.

Dieste's first major innovation in reinforced brick masonry was what he termed "self carrying vaults". Unlike traditional vaults that required both a continuous sidewall support or buttress and a stiff arch under the vault at its ends, Dieste's vaults rested on columns and in some cases just a single column. The few supports of Dieste's vaults, which were spaced at

considerable distances from each other, together with the thin unsupported ends that cantilever over the supports, clearly highlight the efficiency and lightness of the structure.

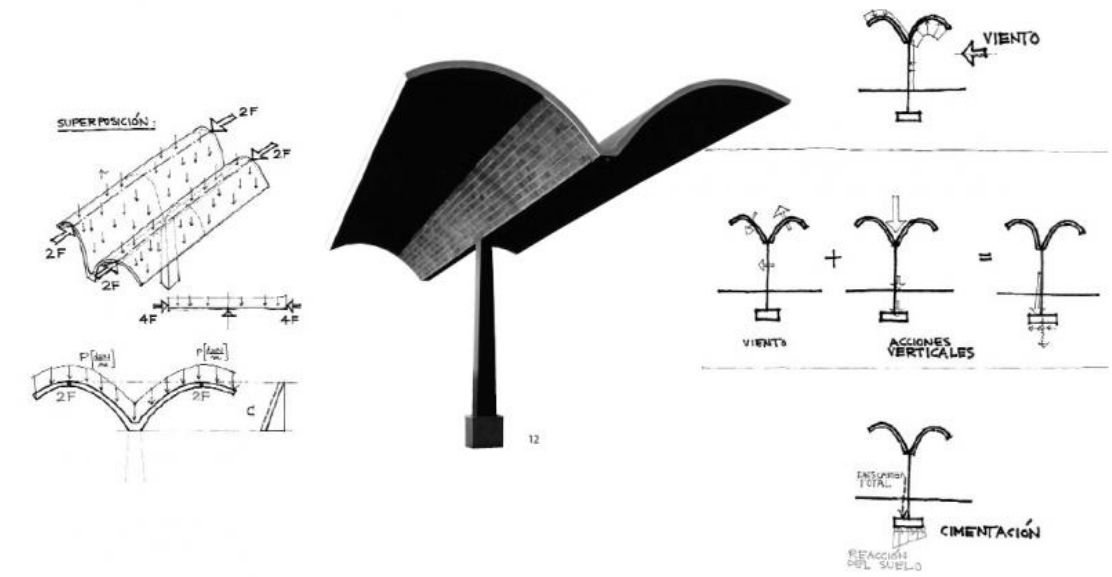

Figure 2.8: Dieste's vault supported on a single column (clippings.com)

Dieste was able to achieve the efficiency of his vaults through the form of the structure and the application of ordinary reinforcing bars between the rows of bricks. For the form of the structure, Dieste designed the cross section of the vault using the most effective structural form i.e. the catenary shape, which lightened the structure. However, lateral forces still existed within the vault and Dieste counteracted this by introducing a horizontal edge beam at the outer limit of any group of vaults. The lateral forces were collected on this

beam and transferred to the vertical buttresses at point supports (Anderson 2004).

The application of ordinary reinforcing bars between the rows of bricks became necessary in the long direction of the vault. This was because in this direction the vault acted as a beam that was supported on columns. This design scenario required that Dieste employ techniques in the design of his vaults that would resist bending moments. He therefore introduced the technique of pre-stressing that would pre-compress the vault. The pre-stressing was achieved by embedding successive loops of steel that were tensed into thin concrete layers on top of the brick masonry (Anderson 2004).

The second major innovation of Dieste was what he termed the “Gaussian” double curvature vault. It was developed in response to the barrel vault, which was not well suited to broad spans. The reason being that as the transverse span of the vault increased the vertical rise also had to be increased and if the vault was made any shallower the compressive stresses increased. Although the catenary shape of the vault aided in reducing the stresses and allowed for much larger spans to be constructed, the thickness of the vault still needed to be increased as the span increased. This additional thickness was necessary to ensure that the behaviour known as buckling does not occur.

Buckling causes the shell to collapse in on itself at lower stresses than that produced by its own weight. This makes the shell structurally unstable. One way to increase the resistance of the vault to buckling is to increase the thickness of the vault, which results in a subsequent increase in the weight of the structure, thereby increasing the thrust at the support points. The second way is to incorporate stiffening ribs into the design, which would cause the vault spanning between the ribs to act as a curved slab. The ribs become heavier and concentrate the forces at the support points. This approach however leads to a loss of the surface form of the structure.

Dieste was opposed to both of these methods and he instead chose to manipulate the surface of the vault to resist buckling in those areas where buckling was most likely to occur. Anderson (2004) mentions that Dieste designed his vaults in successive transverse bands, in which he increased the bending stiffness by means of three-dimensional curvature. The greatest forces were experienced at the centre of the vault, and to resist these forces, Dieste designed the mid-span band with a cross-section that had a reclining s-shape. The surface geometry was then progressively flattened until the vault became a continuous horizontal line at its edges and allowed for a simple connection with the side walls.

Dieste was able to improve the design and the aesthetics of his Gaussian vaults in a number of ways as mentioned by Anderson (2004). Firstly, he

used the s-shaped mid-span bands to add illumination to the structure at various intervals. Secondly, since the vaults were carried by edge beams, Dieste used continuous windows, framed with the simplest of small steel bars, in the walls below the beam. And thirdly, to enhance the stability of the vault, Dieste used exposed horizontal tie-bars to resist the large lateral forces that arose due to the long span and low rise of the Gaussian vaults.

Dieste's success in the design of his structures was as a result of his following of three important principles, which serve as a lesson for even the designers of today. The first principle is to understand the construction process, which is crucial to creating exceptional structures. The second principle is the use of a combination of traditional materials such as brick, and industrial materials such as steel, in the design. And the third principle is to adapt the design of the structure to the local conditions. Even today, these three principles can be incorporated into the design process and like Dieste's works; it can lead to the success of the design.

Dieste's work represents the structural artist of the past and provides a glimpse of the engineer of the future. His design philosophy addresses many of the challenges faced today: "creating economical, efficient and elegant structures in an ecologically and socially responsible manner" as stated by Anderson (2004). One remarkable characteristic of Dieste's works is that it

removed the boundaries between engineering and architecture, and it therefore serves as a valuable example for both engineers and architects.

2.2.7 Heinz Isler (1926-2009)

Heinz Isler was a Swiss engineer that many regard to be amongst the pioneers of thin shell structures. He gained much recognition through his experimental and physical methods of form-finding, which resulted in him designing expressive structures in thin-walled concrete. Isler presented his methods at the first congress of the International Association for Shell Structures in Madrid in1959. Seegers (2011) states that at this meeting, Isler presented his “New Shapes for Shells” which included his “freely shaped hill (of Earth), the membrane under pressure (an inflated rubber membrane creates the shape) and the reversed hanging cloth (a draped fabric defines the surface shape like a hanging cable defines a funicular line)”

Isler’s presentation triggered intense discussion amongst his colleagues. According to Kotnik and Schwartz (2011), these discussions revolved around three themes. Firstly, the problem of scale and the relationship between model and reality; secondly, the difficulty in describing the resulting form and the associated problem of whether it could be economically built; and thirdly, the self-sufficiency of the form-finding methods with regards to architectural

demands. Isler addressed the first two themes in great detail and he largely ignored the question regarding the integration of the architectural aspects.

Isler considered the forming of shells as a primarily technical problem whose solution would give way to the necessary architectural effect. Kotnik and Schwartz (2011) mention that Isler expressed his architectural design attitude in terms of the appropriateness of the built form and the related means of construction necessary to produce this form. The appropriateness refers to a built form that follows the laws of nature, has a low consumption of materials and energy, as well as a decades-long reduced need for maintenance, combined with the greatest possible degree of covered space.

Isler's design method involved the constructing of models by inflating surfaces or by hanging and then hardening them. The construction of these models eventually led him to a lifelong exploration of the inverted hanging membrane structure. Through continuous experimentation, Isler found numerous refinements to the core principles of the inverted hanging membrane method of form-finding. He applied these refinements to buildings such as the Wyss Garden Centre in Solothurn (1962), the Burgi garden centre in Camorino (1973) and the Motorway service station in Deitingen (1968). Structures like these also brought about the realization that thin shell structures could be employed in non-industrial applications.

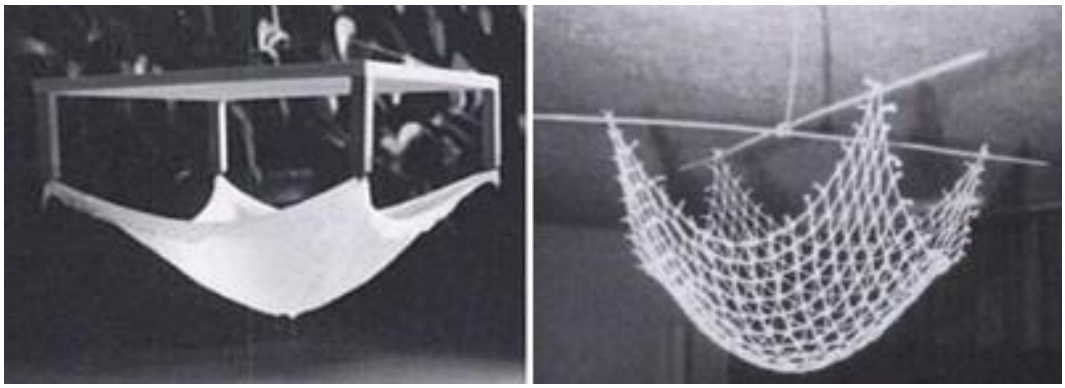

Figure 2.9: Heinz Isler's hanging models (http://blog .buildllc.com/ 2009/04/heinz-isler-a-few-important-things/)

Figure 2.10: Heinz Isler's motorway service station in Deitingen (commons.wikimedia.org)

Isler's design approach resulted in structures that took on a unique shape. Chilton (2000) states that while the majority of designers worked with curved surfaces that could be defined by mathematical formulae, Isler's free form

shells are of shapes that cannot be described by simple geometric formulae as they have a continuously varying double curvature across the whole body. Many consider Isler's shell forms to have taken shell building to the level of structural art. His structures shaped the built landscape of Switzerland, his native country, where he was able to produce almost 1400 shell structures.

Isler's methods of design were however not readily copied and reproduced mainly due to three reasons. Firstly, his models were based solely on physical modelling and no computer-aided design was involved in the design process. This meant that the models produced by Isler were either "one-offs" or built in limited numbers due the cost and complexity of the formwork. Secondly, Isler's methods were complex and required extreme precision. And thirdly, due to the infinite number of design alternatives that exist, he was required to make and test a large variety of examples to enable him to choose between the most economic designs, in terms of use of material, structurally efficiency and aesthetic appeal.

These shortcomings have forced designers to search for other alternatives and have motivated the development of a computer model, like the one developed in this research.

3 DEVELOPMENT OF THE DESIGN TOOL

3.1 The Computer Model

3.1.1 Design Approach

The development of the design tool primarily involved the formulation of a fully functional computer program that would be capable of developing the correct shape of a funicular thin shell structure. The computations of the computer model have been developed based on the Finite Element Method. The versatility of this method has been well demonstrated and it has formed the basis of many optimization techniques. It also displays great potential for refining a structural form to minimize bending. The finite element method discretizes the structure into a finite number of smaller regions called *finite elements.* These finite elements are available in many convenient geometrical shapes such as the rectangular, triangular and quadrilateral finite elements.

3.1.2 Background to the Finite Element Method

The application of the basic concept of the finite element method can be traced back many centuries. The ancient mathematicians applied the concept when trying to find the circumference of a circle, by approximating it by the perimeter of a polygon. In today's understanding of the finite element method, each side of the polygon would be classified as a *finite element.*

The concept had also been applied elsewhere. In 1851, Schellback applied the concept when he was attempting to find the differential equation of the minimum area bounded by a specified closed curve. Schellback sub-divided the surface into several triangles and used the finite difference expression to find the total discretized area. In today's representation of the finite element method, the differential equation is solved by replacing it by a set of algebraic equations. Thereafter, in the 1900's, the concept was applied to analyze the behaviour of structural frameworks. Rao (2011) states that these frameworks were composed of several bars arranged in a regular pattern, and were approximated by that of an isotropic elastic body.

The present form of the finite element method is believed to have been initially formulated in 1943, when Courant presented a method of determining the torsional rigidity of a hollow shaft. According to Rao (2011), Courant divided the cross section of the shaft into several triangles and he then used a linear variation of the stress function, Ø, over each triangle in terms of the values of Ø at net points (which is referred to as nodes in the present day finite element method). Further developments occurred in the mid 1940s when approximate methods were developed by the aircraft industry for the prediction of stresses that are induced in aircraft wings.

In 1946, Clough, Turner, Martin and Topp developed a method for modelling the wing skin using three-node triangles. At about the same time, Argyris and Kelsey also developed matrix procedures that contained some of the finite element ideas for the solution of structural analysis problems. However, it was only in the 1960s that the method was given the name *The Finite Element Method* by R.W. Clough. Thereafter, a broad interpretation of the method, together with its applicability to any general field problem was provided by Zienkiewics and Cheung, and the application of the method as the solution of stress analysis problems was provided by Przemieniecki.

Thereafter, the popularity of the finite element method increased with the establishment of the mathematical basis of the method. Although the method was originally developed based on intuition and physical argument, it was also recognized as a form of the classical Rayleigh-Ritz method. New finite elements began to be developed that could be applied to a variety of problems. With the advent of the digital computer, the viability of the method was greatly increased. The many calculations required in the finite element analysis could be rapidly carried out using the high speed computer.

With regards to thin shell structures, the Finite Element Method has been applied to the reliable and efficient design of these structures. The early development of the Finite Element Method in this field occurred in the aerospace industry, due to the growing need for the use of thin shells in new

structural configurations. The analytical solutions that had been previously applied as a solution to thin shell structural problems became limited in its scope and did not apply to many aspects of structural design, like that of arbitrary shape, load and support conditions. These complications were easily dealt with by the Finite Element Method, which very quickly became the preferred approach for thin shell structural analysis.

The Finite Element Method has therefore become the most powerful and widely used approach in the design and analysis of structures. The main reasons for its extensive use in solving structural problems are due to its versatility and complete generality. The method follows the same basic procedures for structures of any shape, loading and boundary conditions. This standard pattern makes the method universally adaptable to any form of structural problem and allows for the use of a single computer program to solve a variety of problems.

3.1.3 Theory of the Finite Element Method

The current form of the Finite Element Method was initially applied to the analysis of ‘skeletal’ structures, which are structures that are made up of individual components connected together at various points. Examples of these skeletal structures include the continuous beam and the multi-storey frame connected at ‘node points’. The behaviour of these structures was

analyzed by firstly analyzing the individual components or elements, and thereafter the elements were assembled together in such a way that equilibrium and compatibility of displacements were satisfied at each node.

In structures wherein bending existed, the relationship between the moments and rotations within each individual span was analyzed using methods such as the slope-deflection method. The individual spans were then connected together in such a manner that the equilibrium of moments and compatibility of rotations were satisfied at the connection points. Before the Finite Element Method, methods such as the slope-deflection method could only be applied to simple structures that were made up of a few members. When applied to structures that comprised of many members such as a multi-storey frame, a large number of simultaneous equations were set up.

The solution to these simultaneous equations made the method tedious and attempts were rather made to develop other analytical techniques that reduced the amount of simultaneous equations. Therefore, methods such as the Hardy Cross moment distribution method became the preferred choice of application since the solution could be obtained in a series of convenient steps. However, the availability of the digital computer has made the solution to a large number of simultaneous equations quick and easy and has prompted the return to fundamental methods such as the slope-deflection

method. The repetitive nature of these methods makes them ideally suited for the automatic computation by the computer.

Hence, the developments in the structural methods of analysis, from the 1960's till today, have been based on matrix algebra and a sub-division of the structure into an assembly of discrete structural elements. The matrix method assumes that an approximate displacement or stress distribution exists within the element. These displacement or stress distributions are then combined in such a manner that the force-equilibrium and displacement-compatibility requirements at all interfaces of the element are satisfied. The matrix method is suitable for the analysis of complex structures and it forms the basis of the Finite Element Method.

Thereafter, the matrix methods for skeletal structures were extended to the analysis of continuum structures, where the structural surface is continuous and not composed of individual components. These structural surfaces include plates, slabs and shell structures. The application of the finite element method to these continuum structures requires that the continuum be idealized as a structure that is divided along imaginary lines, to form a number of individual elements that are connected only at nodal points. Thus, the only difference between the standard matrix method for skeletal structures and that for continuum structures is in this idealization.

Zienkiewics (1977) defines the finite element method as a method of approximation to continuum problems such that:

a) "the continuum is divided into a finite number of parts (elements), the behaviour of which is specified by a finite number of parameters, and

b) The solution of the complete system as an assembly of its elements follows precisely the same rules as those applicable to *standard discrete problems*"

3.1.3.1 Selection of the appropriate finite element for continuum structures

The finite element of a continuum structure best describes the behaviour of a thin shell structure. Therefore, since the intended application of the finite element method was to determine the form of a thin shell structure, it was only fitting that the finite element of a continuum structure be employed in the analysis. This, then required the selection of the appropriate continuum finite element, from the various possibilities that exist, which would most closely approximate the behaviour of a thin shell structure and also ensure that the behaviour could be represented at each node in terms of the lateral displacements. This lateral displacement at each node would then define the form of the thin shell structure.

The available continuum finite elements, which are either curved or flat, have been developed to approximate the behaviour of a structure according to the applied loads and the stresses that are developed within the structure. With regards to the use of curved or flat elements, it was decided from the very beginning of the analysis that the curved surface of the thin shell structure would be approximated by a series of flat continuum elements. This then required the selection of the appropriate flat continuum element from the two possibilities that exist; the first being the finite element for plane elasticity and second being the finite element for plate flexure.

In the finite element for plane elasticity, the applied loads are in the plane of the surface and any stresses normal to the plane are neglected. The corresponding displacements are also in the plane of the surface. For the finite element for plate flexure, the applied loads need not be in the plane of the surface and the corresponding displacements also need not be in the plane of the surface. For the intended application, the applied loads were normal to the surface and the lateral displacement at each node was also normal to the surface. Therefore, the rectangular plate flexure element best suited the intended application and it was thus selected for the analysis.

The next step required the selection of the appropriate shape of the plate flexure element. The two main shapes of the plate flexure element are the rectangular element and the triangular element. Both these elements were

found to have certain advantages and disadvantages. For instance, the triangular element was more versatile in its application than the rectangular element - since it could be used for the analysis of plates having various boundary shapes. On the other hand, Wegmuller and Kostem (n.d.) mention that comparative studies have shown that the rectangular element shows a greater accuracy than the triangular element.

For this research, the rectangular plate flexure element had been selected as the first step in developing the theory to solve for a catenary shape. This element was deemed appropriate for the necessary computations and was therefore employed in the development of the computer model. A detailed explanation of the rectangular plate flexure finite element method is provided in the following section.

3.1.3.2 Rectangular plate flexure finite elements

The rectangular plate flexure finite element is based on the classical theory of thin plates, where three important assumptions are made. The first is that plane sections normal to the middle surface of the structure before deformation remain plane and normal during deformation. This is also known as Kirchoff's assumption. The second assumption is that the transverse displacement (w) is small in comparison to the thickness of the plate. And the third is that the stresses normal to the plane of the plate are negligible. The

first two assumptions imply that the shearing stresses in the transverse direction are neglected and that the deflection (w) at any point on the plate and the corresponding point on the middle plane of the plate are approximately equal. Thus, the state of deformation can be described in terms of the transverse displacement alone.

The rectangular plate flexure element, as with the other elements, can solve a structural problem using one of two methods. The first being the stiffness method and the second being the force method. Rockey et al (1983) mentions that the differences between the two methods are due to the order in which the two basic equations of nodal equilibrium and compatibility are treated. In the stiffness method, the displacement compatibility conditions are firstly satisfied and the equations of equilibrium are set up and solved to yield the unknown nodal displacements. In the force method, the conditions of joint equilibrium are first satisfied and the equations arising from the need for compatibility of nodal displacements are solved to yield the unknown forces in the members. In this research, the stiffness approach was employed in the derivation of the rectangular finite element.

The first step of the stiffness approach involved the sub-division of the surface of the structure into a suitable number of finite elements. By default, the surface of the structure was continuous and the corresponding natural sub-division did not exist within the actual structure. Therefore, the continuum had

to be artificially divided into a number of finite elements, in a manner that allowed for the accurate analysis of the structure without excessive computational effort. Although the elements were connected all along their boundaries, the method assumed that each element is only connected to the adjacent elements at nodal points. In addition, each element was assumed to possess simple elastic properties.

This configuration of the structure allowed for the matrix method of analysis to be applied to the structure. The matrix method assumed that the elements were inter-connected only at their nodes, which was in conformance with how the structure had been modelled. The behaviour of the entire element was therefore represented at its nodes, with the basic unknown parameters being the displacements at the nodal points. The combination of the nodal displacements of all of the elements within the structure allowed for the behaviour of the entire structure to be approximated.

Thereafter, the state of deformations of the elements in terms of the nodal values was determined. This was done through the formulation of a displacement or shape function for each element. The functions were formulated in such a way that it ensured continuity both within the element and along the element boundaries. This continuity ensured that the displacement field was compatible, which ensured that the displacement field uniquely defined the state of strain within an element in terms of its nodal

displacements. These strains together with any initial strains defined the state of stress both within the element and on its boundaries.

Next, the force-displacement action of the structure was described by means of a series of simultaneous equations that was expressed by the following equation:

$$\{F\} = [K]\{\delta\}$$

Where: $\{F\}$ is the vector of nodal loads; $\{\delta\}$ is the vector of nodal displacements; and $[K]$ is the stiffness matrix of the structure.

The above equation required that the force vector, the displacement vector and the stiffness matrix be formulated. The force vector was formed from the loads acting on the structure. These loads were approximated by a set of equivalent concentrated nodal forces, which were in equilibrium with the internal boundary stresses, the distributed loads and the forces due to the initial strains. The entries within the force vector simply required the entry of the magnitude and location of the nodal forces. The displacement vector was what was needed to be determined and this required the formulation of the stiffness matrix, which allowed the above equation to be solved.

The stiffness matrix related the applied nodal forces, $\{F\}$, to the unknown nodal displacements,$\{\delta\}$. The terms within the element stiffness matrices were a function of the geometric and elastic properties of the element. These terms were made to conform to a common co-ordinate system. This allowed for the formulation of the global stiffness matrix, which was a combination of all the element stiffness matrices, whereby the appropriate element stiffness contributions framing into a common node were added together. Wegmuller & Kostem (n.d.) state that to ensure the efficient solution of large systems of simultaneous equations, the structure of the stiffness matrix should be well-conditioned, sparsely populated and narrowly banded. This was achieved through the appropriate nodal numbering of nodal points.

Once the relationships for the entire structure were established by the appropriate superposition of the individual element stiffness matrices into the global stiffness matrix, the kinematic restraints were then imposed. Thereafter, the solution to the finite element relationship was obtained through standard structural procedures. This allowed for the unknown nodal displacements at every node to be determined, which subsequently made it possible for the form of the pure compression thin shell structure to be defined.

For the intended application in this research two different rectangular plate flexure elements were utilized in the analysis. The difference between the two elements was in the derivation of the element stiffness matrices. The first derivation of the stiffness matrix was based on the Rockey, Evans, Griffiths & Nethercot Method (REGN Method) and the second derivation of the stiffness matrix was based on the Adini, Clough & Melosh Method (ACM Method). The derivations of both these methods are presented in the sections that follow.

3.1.3.3 The ACM Method of deriving the element stiffness matrix

One of the methods used in deriving the element stiffness matrix for a rectangular plate flexure element was the Adini-Clough-Melosh method (the ACM method). The ACM method has been explained in detail by Zienkiewics, (1977) and Wegmuller & Kostem (n.d.). Although the ACM element is a non-conforming type, Wegmuller & Kostem (n.d.) state that it nevertheless produces accurate results. The complete derivation is presented below:

Each of the rectangular elements comprises of four nodal points, I, J, K and L. A typical rectangular element is presented in the diagram below:

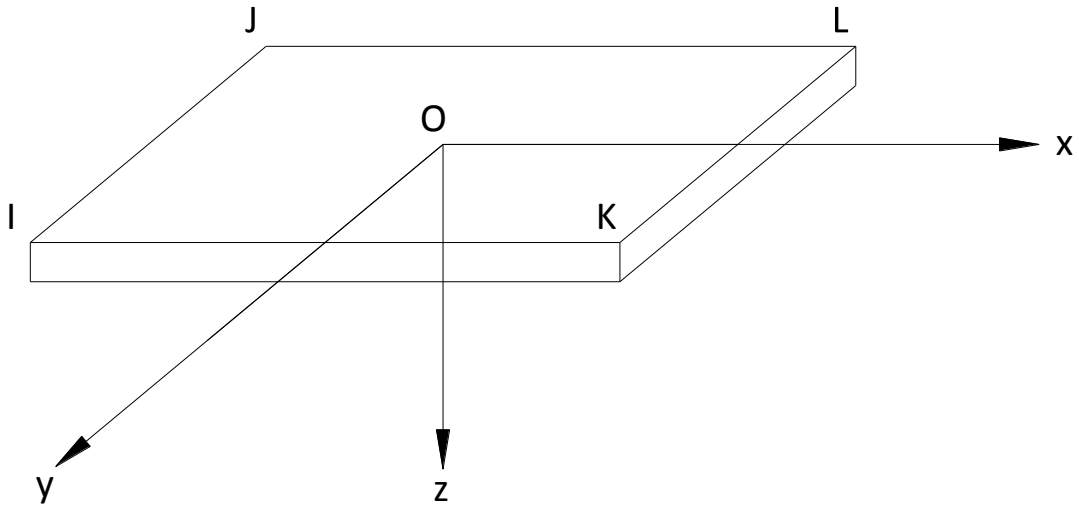

Figure 3.1: Rectangular element with co-ordinate system

At each node of the above element there are three displacement components. The first is a vertical displacement in the z-direction, the second is a rotation about the x-axis (θ_x), and the third is a rotation about the y-axis (θ_y). The three displacements are entered into the displacement vector at node i, to yield the following expression:

$$\{d_i\} = < w \;\; \theta_x \;\; \theta_y >$$

Therefore, the three displacement components at each node result in the complete element consisting of twelve unknown displacement parameters. These parameters make up the element displacements and are represented by the following nodal displacements:

$$\{d^e\}^T = < \; d_i^T \;\; d_j^T \;\; d_k^T \;\; d_l^T >$$

In a similar manner, the element forces can be expressed by the following relationship:

$$\{f^e\}^T = < f_i^T \;\; f_j^T \;\; f_k^T \;\; f_l^T >$$

Thereafter, the stiffness matrix of the structure needs to be derived. This derivation of the stiffness matrix is much more complicated than any of the above procedures. The derivation continues as follows:

Firstly, a shape function has to be defined in terms of the twelve parameters. This is done by means of a polynomial expression in which certain terms have been omitted from a complete fourth order polynomial. The polynomial is expressed as:

$$w = \alpha_1 + \alpha_2 x + \alpha_3 y + \alpha_4 x^2 + \alpha_5 xy + \alpha_6 y^2 + \alpha_7 x^3 + \alpha_8 x^2 y + \alpha_9 xy^2 + \alpha_{10} y^3 + \alpha_{11} x^3 y + \alpha_{12} xy^3$$

The use of the above format of the polynomial will ensure that the displacement of w will vary as a cubic along any x = constant or y = constant line. These lines make up the boundaries and interfaces of the element.

According to Zienkiewics (1977), a cubic is uniquely defined by four constants, the two end values of slopes and the displacements at the ends of

the boundaries, which will define the displacements along this boundary uniquely. Since such end values are common to adjacent elements, continuity of w will be imposed along any surface.

Zienkiewics (1977) also states that the gradient of w normal to any of the boundaries also varies along it in a cubic manner. For example, if we have to consider $\partial w/\partial x$ along a line on which x is constant, then two values of the normal slope are defined and the cubic is not specified uniquely, and in general a discontinuity of the slope will occur. This causes the function to be 'non-conforming'.

To evaluate the constants α_1 to α_{12}, the twelve simultaneous equations linking the values of w and its slopes at the nodes can be determined when the co-ordinates take up their appropriate values.

Listing all twelve equations in matrix form, results in the following equation:

$$\{d^e\} = B\alpha$$

Where, B is a twelve by twelve matrix depending on nodal co-ordinates and α is a vector of twelve unknown constants.

The above equation can be inverted to yield the following expression:

$$\{\alpha\} = [\underline{B}]^{-1}[T]\{d^e\} = B^{-1}\{d^e\}$$

Where $[\underline{B}]$ is the connection matrix comprising of numbers only and can be found in appendix 1. And, $[T]$ is a twelve by twelve transformation matrix that relates the modified element displacement vector to the actual displacement vector.

According to Wegmuller & Kostem (n.d.), the relationship between the in-plane displacements and the transverse displacements, w, can be expressed as:

$$U = u - z\frac{\partial}{\partial x}$$

$$V = v - z\frac{\partial w}{\partial y} \qquad equation\ 1$$

Where u and v are the displacements in the x or y direction of a point lying in the middle plane of the plate, and U and V are the displacements in the x or y direction of a point lying at a distance z from the reference point. In the classical theory of plates both u and v are assumed to be negligible.

From the differentiation of equation 1, the strain-displacement relationships are obtained as follows:

$$\varepsilon_x = \frac{\partial u}{\partial x} = \frac{\partial u}{\partial x} - z\,\frac{\partial^2 w}{\partial x^2}$$

$$\varepsilon_y = \frac{\partial v}{\partial y} = \frac{\partial v}{\partial y} - z\,\frac{\partial^2 w}{\partial y^2}$$

$$\gamma_{xy} = \frac{\partial U}{\partial y} + \frac{\partial V}{\partial x} = \frac{\partial u}{\partial y} + \frac{\partial v}{\partial x} - 2\,z\,\frac{\partial^2 w}{\partial x \partial y} \qquad equation\ 2$$

And the stresses that are required to satisfy the following two equations of equilibrium are:

$$\frac{\partial \sigma_x}{\partial x} + \frac{\partial \tau_{yx}}{\partial y} = 0$$

$$\frac{\partial \tau_{xy}}{\partial x} + \frac{\partial \sigma_y}{\partial y} = 0$$

Using the strain-displacement relationships in equation 2, Hooke's law can be written in terms of the derivatives of displacement w as:

$$\sigma_x = -\frac{Ez}{1-\nu^2}\left[\frac{\partial^2 w}{\partial x^2} + \nu\frac{\partial^2 w}{\partial y^2}\right]$$

$$\sigma_y = -\frac{E\,z}{1-\nu^2}\left[\frac{\partial^2 w}{\partial y^2} + \nu\frac{\partial^2 w}{\partial x^2}\right]$$

$$\tau_{xy} = -2\,G\,z\,\frac{\partial^2 w}{\partial xy}$$

Where, E is the Modulus of Elasticity, G is the Shear Modulus and ν is Poisson's Ratio.

The shear modulus,G, is related to the modulus of elasticity, E, by the following relationship:

$$G = \frac{E}{2(1+\nu)}$$

The following figure shows the stress resultants acting per unit width of the plate, which can be found by integrating the appropriate stress components over the plate thickness:

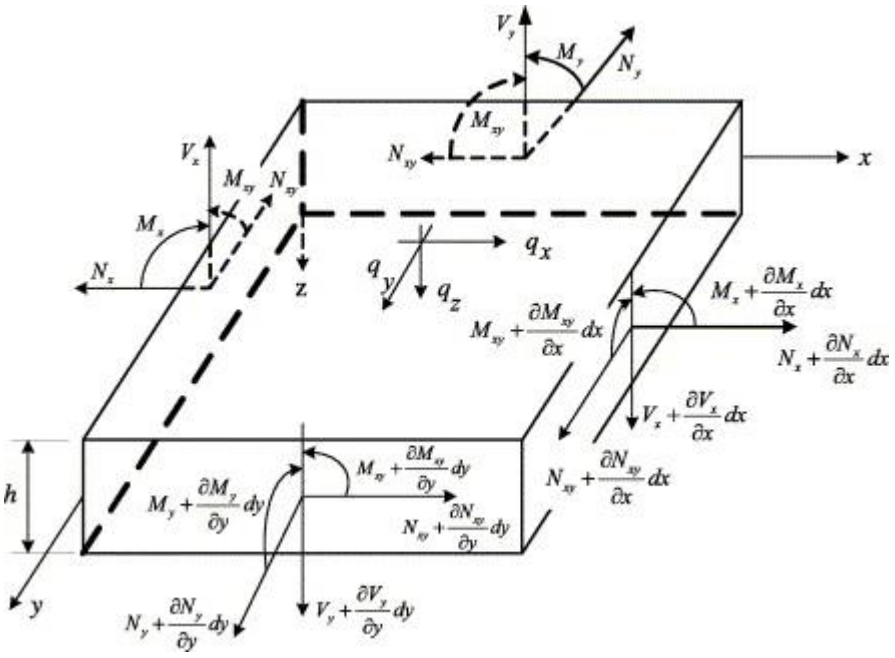

Figure 3.2: Stress resultants acting on a rectangular element (www.sciencedirect.com)

This can be written as:

$$M_x = \int_{-h/2}^{h/2} \sigma_x \, z \, dz$$

$$M_y = \int_{-h/2}^{h/2} \sigma_y \, z \, dz$$

$$M_{xy} = -\int_{-h/2}^{h/2} \tau_{xy} \, z \, dz$$

$$Q_x = \int_{-h/2}^{h/2} \tau_{xz}\, z\, dz$$

$$Q_y = \int_{-h/2}^{h/2} \tau_{yz}\, dz$$

These terms lead to the well-known moment curvature relationships for an isotropic material:

$$\begin{bmatrix} M_x \\ M_y \\ M_{xy} \end{bmatrix} = \begin{bmatrix} D_{11} & D_{12} & 0 \\ D_{21} & D_{22} & 0 \\ 0 & 0 & D_{33} \end{bmatrix} \begin{vmatrix} \emptyset_x \\ \emptyset_y \\ \emptyset_{xy} \end{vmatrix}$$

Where: $D_{11} = D_{22} = Eh^3/12(1-\nu^2)$

$$D_{12} = D_{21} = \nu D_{11}$$

$$D_{33} = (1-\nu)\, D_{11}/2$$

For a general anisotropic material, matrix $[D]$ is fully populated and is given by the following relationship:

$$\begin{bmatrix} D_{11} & D_{12} & D_{13} \\ D_{21} & D_{22} & D_{23} \\ D_{31} & D_{32} & D_{33} \end{bmatrix}$$

The two vectors can be defined as:

$$\{M\}^T = \langle M_x \; M_y \; M_{xy} \rangle$$

$$\{\emptyset\}^T = \langle -\frac{\partial^2 w}{\partial x^2} - \frac{\partial^2 w}{\partial y^2} \; 2\frac{\partial^2 w}{\partial \partial y} \rangle$$

Therefore, the relationship between the generalised stresses and strains for a linearly elastic material is given by:

$$\{M\} = [D]\{\emptyset\}$$

Now, the generalised strains can be expressed in terms of the element displacements by:

$$\{\emptyset\} = [Q][B]^{-1}\{d^e\} = [C]\{d^e\}$$

The minimization of the total potential energy results in the formulation of the stiffness relation governing the out-of-plane behaviour of the plate element:

$$\{f^e\} = \left[\int_A \int [C]^T [D][C] dxdy\right]\{d^e\}$$

The stiffness matrix is therefore given by:

$$[K^e]_{12\times 12} = \int_A \int [C]^T [D][C] dxdy$$

The integration in the above element should be taken over the area of the plate element. By carrying out the necessary operations, the following relationship is obtained:

$$[K^e]_{12\times12} = [B^{-1}]^T[D_{11}[K_1] + D_{12}[K_2] + D_{13}[K_3] + D_{22}[K_4] + D_{23}[K_5] + D_{33}[K_6]][B^{-1}]$$

The component matrices are provided in appendix 1. The final assemblage of the stiffness matrix is then performed with the aid of the digital computer.

3.1.3.4 The Rockey, Evans, Griffiths & Nethercot Method (REGN Method) of deriving the stiffness matrix

The element stiffness matrix for the rectangular element for plate flexure as derived by Rockey, Evans, Griffiths & Nethercot proceeds as follows:

The first step is to choose a suitable co-ordinate system and the number of element nodes.

The co-ordinate system has been chosen with the x, y and z axis as shown in the following figure:

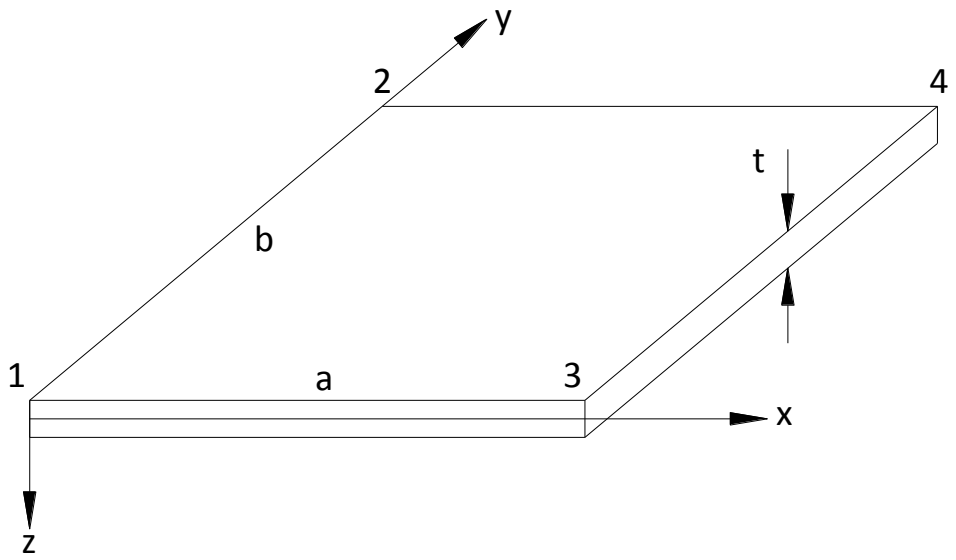

Figure 3.3: Rectangular element with co-ordinate system

At each of the nodes in the above element, there are three degrees of freedom: the lateral deflection w and a rotation about the x - axis denoted by θ_x and a rotation about the y - axis as denoted by θ_y. The directions of these rotations are defined according to the right-hand corkscrew rule. The element therefore has a total of twelve degrees of freedom.

The displacements at any particular node can be written as:

$$\{\delta_1\} = \begin{pmatrix} \theta_{x1} \\ \theta_{y1} \\ w_1 \end{pmatrix}$$

The moments and forces any particular node can be written as:

$$\{F_1\} = \begin{pmatrix} T_{x1} \\ T_{y1} \\ F_{z1} \end{pmatrix}$$

From the above relationships the complete displacement and force vectors can be expressed as:

$$\{\delta^e\} = \begin{bmatrix} \{\delta_1\} \\ \{\delta_2\} \\ \{\delta_3\} \\ \{\delta_4\} \end{bmatrix} = \begin{bmatrix} \theta_{x1} \\ \theta_{y1} \\ w_1 \\ \theta_{x2} \\ \theta_{x2} \\ w_2 \\ \theta_{x3} \\ \theta_{y3} \\ w_3 \\ \theta_{x4} \\ \theta_{y4} \\ w_4 \end{bmatrix}$$

And

$$\{F^e\} = \begin{bmatrix} \{F_1\} \\ \{F_2\} \\ \{F_3\} \\ \{F_4\} \end{bmatrix} = \begin{bmatrix} T_{x1} \\ T_{y1} \\ F_{z1} \\ T_{x2} \\ T_{y2} \\ F_{z2} \\ T_{x3} \\ T_{y3} \\ F_{z3} \\ T_{x4} \\ T_{y4} \\ F_{z4} \end{bmatrix}$$

Since the above vectors contain twelve terms, the stiffness matrix is required to be a 12 x 12 matrix. This is evident from the following relationship:

$$\{F^e\} = [K^e]\{\delta^e\}$$

The second step requires the choosing of the displacement function $[f(x, y)]$ that will define the displacements $\{\delta(x, y)\}$ at any point in the element.

The deflections are small for the plate flexure case and this allows the displacement at any point within the element to be represented by three components, i.e.

$$\{\delta(x, y)\} = \begin{bmatrix} \theta_x \\ \theta_y \\ w \end{bmatrix}$$

The relationship between the two slopes, θ_x and θ_y are related to the lateral displacement, w, by the following expressions:

$$\theta_x = -\partial w/\partial y$$

$$\theta_y = \partial w/\partial x$$

The above expressions are automatically defined once a displacement function is chosen for w. Since the element has twelve degrees of freedom

the polynomial expression chosen to represent w will also require twelve parameters. This polynomial is expressed as follows:

$$w = \alpha_1 + \alpha_2 x + \alpha_3 y + \alpha_4 x^2 + \alpha_5 xy + \alpha_6 y^2 + \alpha_7 x^3 + \alpha_8 x^2 y + \alpha_9 xy^2 + \alpha_{10} y^3 + \alpha_{11} x^3 y + \alpha_{12} xy^3 \qquad equation\ 3$$

The displacement function can now be substituted into the expressions of the rotations, to yield the following expressions:

$$\theta_x = -{}^{\partial w}/_{\partial y} = -(\alpha_3 + \alpha_5 x + 2\alpha_6 y + \alpha_8 x^2 + 2\alpha_9 xy + 3\alpha_{10} y^2 + \alpha_{11} x^3 + 3\alpha_{12} xy^2)$$

$$\theta_y = {}^{\partial w}/_{\partial x} = (\alpha_2 + 2\alpha_4 x + \alpha_5 y + 3\alpha_7 x^2 + 2\alpha_8 xy + \alpha_9 y^2 + 3\alpha_{11} x^2 y + \alpha_{12} y^3)$$

The function must ensure that the continuity of deflections and slopes are maintained in the solution. This can be checked as follows:

Consider the edge of the element i-j, where x is constant and equal to zero. The slopes and lateral displacements at any point on this edge can be obtained from the following equations:

$$\theta_x = -(\alpha_3 + 2\alpha_6 y + 3\alpha_{10} y^2)$$

$$\theta_y = (\alpha_2 + \alpha_5 y + \alpha_9 y^2 + \alpha_{12} y^3)$$

$$w = \alpha_1 + \alpha_3 y + \alpha_6 y^2 + \alpha_{10} y^3$$

Taking into account the conditions at the ends of this edge i.e. at nodes 1 and 2, when $y = 0$ (which is essentially at node 1), then:

$$w = w_1 = \alpha_1$$

$$\theta_x = \theta_{x1} = -\alpha_3$$

$$\theta_y = \theta_{y1} = \alpha_2$$

And when $y =$ width of element (b) (which is essentially node 2)

$$\theta_x = \theta_{x2} = -(\alpha_3 + 2\alpha_6 b + 3\alpha_{10} b^2)$$

$$\theta_y = \theta_{y2} = (\alpha_2 + \alpha_5 b + \alpha_9 b^2 + \alpha_{12} b^3)$$

$$w = w_2 = \alpha_1 + \alpha_3 b + \alpha_6 b^2 + \alpha_{10} b^3$$

It now becomes evident that to solve for the eight unknown constants only six equations are available and consequently, the constants cannot be determined. However, it is also evident that w and θ_x contain the same four constants (α_1, α_3, α_6, α_{10}), whereas θ_y contains four different constants

(α_2, α_5, α_9, α_{12}).Therefore, a sufficient number of equations are available to solve for the constants related to these quantities. Since four of the boundary equations refer to w and θ_x , they can be expressed in terms of the nodal displacements.

The remaining two equations are not sufficient to solve the four unknown constants in θ_y. Hence, the lateral displacement, w, and the rotation along the edge θ_x are completely defined by the end movements, whilst θ_y, the rotation normal to the edge is not uniquely specified. When obtaining the solution, the end movements are made compatible and this ensures that the continuity of w and θ_x is maintained along the edges where x is a constant. However, on the other hand, θ_y is discontinuous along this edge. Generally, along any edge a discontinuity of the normal slope can exist. The function chosen is therefore not ideal and is referred to as a 'non-conforming function'.

The third step is to express the state of displacement $\{\delta(x,y)\}$ within the element in terms of the nodal displacements $\{\delta^e\}$

Firstly, equation 3 can be summarized in the general equation:

$$\{\delta(x,y)\} = [f(x,y)]\{\alpha\}$$

The substitution of the nodal co-ordinate values into the above equation leads to the formation of the 12 x 12 $[A]$ matrix (presented in appendix 1), which is expressed in the following relationship:

$$\{\delta^e\} = [A]\{\alpha\}$$

The matrix is then inverted and it can now be substituted into the required general equation to yield the following relationship:

$$\{\delta(x,y)\} = [f(x,y)][A]^{-1}\{\delta^e\}$$

The fourth step requires the relating of the strains $\{\varepsilon(x,y)\}$ at any point to displacements $\{\delta(x,y)\}$ and hence, to nodal displacements $\{\delta^e\}$

The state of strain at any point can be represented by three components, the curvature in the x direction, the curvature in the y direction and the twist. The curvature in the x direction is equal to the rate of change of the slope in the x direction with respect to x. This is expressed by the following relationship:

$$-\frac{\partial}{\partial x}\left(\frac{\partial w}{\partial x}\right) = -\frac{\partial^2 w}{\partial x^2}$$

Similarly, the curvature in the y direction is expressed by the following relationship:

$$-\frac{\partial}{\partial y}\left(\frac{\partial w}{\partial y}\right) = -\frac{\partial^2 w}{\partial y^2}$$

The twist is equal to the rate of change of the slope in the x direction with respect to y. This is expressed in the following relationship:

$$\frac{\partial}{\partial y}\left(\frac{\partial w}{\partial x}\right) = -\frac{\partial^2 w}{\partial x \partial y}$$

The state of strain can now be represented as follows:

$$\{\varepsilon(x,y)\} = \begin{pmatrix} -\partial^2 w/\partial x^2 \\ -\partial^2 w/\partial y^2 \\ 2\,\partial^2 w/\partial x \partial y \end{pmatrix}$$

From equation 3, w is now substituted into the equation, to yield:

$$\{\varepsilon(x,y)\} = \begin{pmatrix} -(2\alpha_4 + 6\alpha_7 x + 2\alpha_8 y + 6\alpha_{11} xy \\ -(2\alpha_6 + 2\alpha_9 x + 6\alpha_{10} y + 6\alpha_{12} xy \\ 2(\alpha_5 + 2\alpha_8 x + 2\alpha_9 y + 3\alpha_{11} x^2 + 3\alpha_{12} y^2) \end{pmatrix}$$

This can also be expressed as:

$$\{\varepsilon(x,y)\} = \begin{bmatrix} 0 & 0 & 0 & -2 & 0 & 0 & -6x-2y & 0 & 0 & -6xy & 0 \\ 0 & 0 & 0 & 0 & 0 & -2 & 0 & 0 & -2x-6 & 0 & -6xy \\ 0 & 0 & 0 & 0 & 2 & 0 & 0 & 4x & 4y & 0 & 6x^2 & 6y^2 \end{bmatrix} \begin{bmatrix} \alpha_1 \\ \alpha_2 \\ \alpha_3 \\ \alpha_4 \\ \alpha_5 \\ \alpha_6 \\ \alpha_7 \\ \alpha_8 \\ \alpha_9 \\ \alpha_{10} \\ \alpha_{11} \\ \alpha_{12} \end{bmatrix}$$

The above expression can be concisely written in matrix notation as:

$$\{\varepsilon(x,y)\} = [B]\{\alpha\}$$

The required relationship between the strains and the nodal displacements can now be obtained as follows:

$$\{\varepsilon(x,y)\} = [B]\{\delta^e\}$$

Where:

$$[B] = [C][A]^{-1} \qquad equation\ 4$$

The fifth step involves relating the internal stresses $\{\sigma(x,y)\}$ to the strains $\{\varepsilon(x,y)\}$ and the nodal displacements $\{\delta^e\}$.

The state of 'stress' can be represented by three components: the internal bending moments per unit length, M_x and M_y, and the internal twisting moment per unit length, M_{xy}. This is expressed as follows:

$$\{\sigma(x,y)\} = \begin{pmatrix} M_x \\ M_y \\ M_{xy} \end{pmatrix}$$

These are shown in the following figure where $M_{xy} = M_{yx}$:

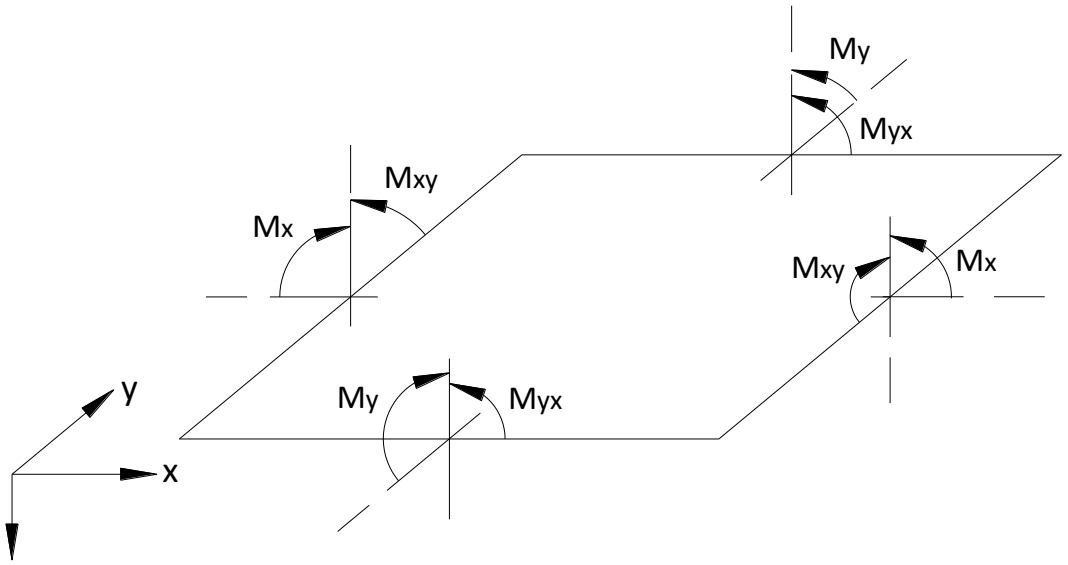

Figure 3.4: Internal bending moments per unit length

The ‘stress-strain’ i.e. moment-curvature relationships from plate bending theory are given as:

$$M_x = -\left(D_x \frac{\partial^2 w}{\partial x^2} + D_1 \frac{\partial^2 w}{\partial y^2}\right)$$

$$M_y = -(D_y \frac{\partial^2 w}{\partial y^2} + D_1 \frac{\partial^2 w}{\partial x^2})$$

$$M_{xy} = 2D_{xy} \frac{\partial^2 w}{\partial x \partial y}$$

Where: D_x and D_y are the flexural rigidities in the x and y direction respectively; and D_1 is a ‘coupling’ rigidity representing a Poisson’s ratio type of effect; and D_{xy} is the torsional rigidity.

For this particular case:

$$D_x = D_y = D = Et^3/12(1-\nu^2)$$

$$D_1 = \nu D$$

$$D_{xy} = 1/2\,(1-\nu)D$$

This leads to the following expression:

$$\{\sigma(x,y)\} = \begin{pmatrix} M_x \\ M_y \\ M_{xy} \end{pmatrix} = \begin{bmatrix} D_x & D_1 & 0 \\ D_1 & D_y & 0 \\ 0 & 0 & D_{xy} \end{bmatrix} \begin{bmatrix} -\partial^2 w/\partial x^2 \\ -\partial^2 w/\partial y^2 \\ 2\partial^2 w/\partial x \partial y \end{bmatrix}$$

This can be written in simplified form as:

$$\{\sigma(x,y)\} = [D]\{\varepsilon(x,y)\}$$

The substitution of $\{\varepsilon(x,y)\}$ from equation 4, will allow the relationship between the element stresses and the nodal displacements to be expressed as follows:

$$\{\sigma(x,y)\} = [D][B]\{\delta^e\}$$

The final step involves replacing the internal stresses $\{\sigma(x,y)\}$ with statically equivalent nodal forces,$\{F^e\}$, thereby relating the nodal forces to the nodal displacements,$\{\delta^e\}$, and hence, obtaining the element stiffness matrix,$[K^e]$

The relationship between the nodal loads, $\{F^e\}$ and the displacements, $\{\delta^e\}$ is given by the general equation:

$$\{F^e\} = [\int [B]^T [D][B] d(vol)]\{\delta\}$$

During a virtual displacement of the element, the total work done, together with the twists per unit length, can be obtained by integrating the product of these moments and twists and their associated curvature over the surface

area of the element. Therefore, for a general case, the $\int d(vol)$ expression is replaced by the expression $\int_0^b \int_0^a dxdy$

The expression can be rewritten as:

$$\{F^e\} = [\int_0^b \int_0^a [B]^T [D][B] dxdy]\{\delta^e\}$$

Subsequently, the element stiffness matrix, $[K^e]$, can be defined as:

$$[K^e] = \int_0^b \int_0^a [B]^T [D][B] dxdy$$

The final stiffness matrix for a general orthotropic case is presented below:

$$[K^e] = 1/15ab \begin{bmatrix} SA & & & & & & & & & & & \\ SB & SC & & & & & & & & & & \\ SD & SE & SF & & & & & & & & & \\ SG & 0 & SH & SA & & & & & & & & \\ 0 & SI & SJ & SB & SC & & & & & & & \\ SH & SJ & SM & SD & SE & SF & & & & & & \\ SN & 0 & SO & SP & 0 & SQ & SA & & & & & \\ 0 & SR & SS & 0 & ST & SU & SB & SC & & & & \\ SO & SS & SX & SQ & SU & SY & SD & SE & SF & & & \\ SP & 0 & SQ & SN & 0 & SO & SG & 0 & SH & SA & & \\ 0 & ST & SU & 0 & SR & SS & 0 & SI & SJ & SB & SC & \\ SQ & SU & SY & SO & SS & SX & SH & SJ & SM & SD & SE & SF \end{bmatrix}$$

Where:

$p = a/b$

$$SA = 20a^2D_y + 8b^2D_{xy}$$

$$SB = 15abD_1$$

$$SC = 20b^2D_x + 8a^2D_{xy}$$

$$SD = 30apD_y + 15bD_1 + 6bD_{xy}$$

$$SE = 30bp^{-1}D_x + 15aD_1 + 6aD_{xy}$$

$$SF = 60p^{-2}D_x + 60p^2D_y + 30D_1 + 84D_{xy}$$

$$SG = 10a^2D_y - 2b^2D_{xy}$$

$$SH = -30apD_y - 6bD_{xy}$$

$$SI = 10b^2D_x - 8a^2D_{xy}$$

$$SJ = 15bp^{-1}D_x - 15aD_1 - 6aD_{xy}$$

$$SM = 30p^{-2}D_x - 60p^2D_y - 30D_1 - 84D_{xy}$$

$$SN = 10a^2D_y - 8b^2D_{xy}$$

$$SO = -15apD_y + 15bD_1 + 6bD_{xy}$$

$$SP = 5a^2D_y + 2b^2D_{xy}$$

$$SQ = 15apD_y - 6bD_{xy}$$

$$SR = 10b^2D_x - 2a^2D_{xy}$$

$$SS = 30bp^{-1}D_x + 6aD_{xy}$$

$$ST = 5b^2D_x + 2a^2D_{xy}$$

$$SU = 15bp^{-1}D_x - 6aD_{xy}$$

$$SX = 60p^{-2}D_x + 30p^2D_y - 30D_1 - 84D_{xy}$$

$$SY = -30p^{-2}D_x - 30p^2D_y + 30D_1 + 84D_{xy}$$

3.1.4 Adapting the plate flexure element to the form-finding process

The two methods of the rectangular plate flexure element selected for the analysis were sufficiently capable of representing the behaviour of the structure and also expressing this behaviour in terms of the lateral displacements. However, both methods could not be applied exactly in its original form. This was because the original form of the plate flexure element assumed that the surface of the structure exhibited out-of-plane displacements such as bending and twisting. To represent this bending and twisting, both methods assumed that at each node of the element, there existed in addition to the transverse displacement both a rotation about the x-axis, θ_x , and a rotation about the y - axis, θ_y.

Since the ideal shape of a pure compression thin shell structure needed to be developed; only in-plane forces with no bending and twisting were required to be developed within the structure. This meant that the design methodology employed in the analysis was required to translate the loads applied normal to the surface of the structure into lateral displacements at each node, in a

manner that would produce no bending or twisting within the structure. Therefore, to continue using the rectangular plate flexure element in the analysis, the two rotations at each node needed to be eliminated, leaving only the lateral displacements.

For these rotations to be eliminated, the computer model needed to be idealized in the appropriate manner. This was achieved by ensuring that the computer model was idealised to behave in exactly the same way a chain made out of a series of individual links supported at specified points would behave, when it was allowed to hang freely under its own self-weight. Each link of the chain was represented by a finite element and the rotation free connection at each link was represented by a pin support. In this manner, the computer model was made up of a series of finite elements that were connected to each other by means of pin supports. This representation of the model ensured that no moments were transmitted within the structure and only in-plane forces existed.

The next step involved adapting the theory of the Finite Element Method to represent a computer model that was pinned at every node. This involved the degeneration of the element stiffness matrix from its original form into one that represented the behaviour of a rotation free element, with only a lateral displacement at each node. For both the ACM method and the REGN method of deriving the stiffness matrix the exact same procedure was followed in

reducing the stiffness matrix to the required form. For this reason, the procedure will be explained using only the stiffness matrix of the REGN Method.

The original REGN stiffness matrix is as presented below:

$$[K^e] = 1/15ab \begin{bmatrix} SA & & & & & & & & & & & \\ SB & SC & & & & & & & & & & \\ SD & SE & SF & & & & & & & & & \\ SG & 0 & SH & SA & & & & & & & & \\ 0 & SI & SJ & SB & SC & & & & & & & \\ SH & SJ & SM & SD & SE & SF & & & & & & \\ SN & 0 & SO & SP & 0 & SQ & SA & & & & & \\ 0 & SR & SS & 0 & ST & SU & SB & SC & & & & \\ SO & SS & SX & SQ & SU & SY & SD & SE & SF & & & \\ SP & 0 & SQ & SN & 0 & SO & SG & 0 & SH & SA & & \\ 0 & ST & SU & 0 & SR & SS & 0 & SI & SJ & SB & SC & \\ SQ & SU & SY & SO & SS & SX & SH & SJ & SM & SD & SE & SF \end{bmatrix}$$

Considering the three components that exist at each of the nodes *i, j, k & l* of a typical element, each entry within the stiffness matrix can be represented by a column displacement parameter and a row displacement parameter. The column and row displacement parameters for each node and its position in the element stiffness matrix are presented below:

θ_{xi}	θ_{yi}	w_i	θ_{xj}	θ_{yj}	w_j	θ_{xk}	θ_{yk}	w_k	θ_{xl}	θ_{yl}	w_l	
SA												θ_{xi}
SB	SC					*Symmetric*						θ_{yi}
SD	SE	SF										w_i
SG	0	SH	SA									θ_{xj}
0	SI	SJ	SB	SC								θ_{yj}
SH	SJ	SM	SD	SE	SF							w_j
SN	0	SO	SP	0	SQ	SA						θ_{xk}
0	SR	SS	0	ST	SU	SB	SC					θ_{yk}
SO	SS	SX	SQ	SU	SY	SD	SE	SF				w_k
SP	0	SQ	SN	0	SO	SG	0	SH	SA			θ_{xl}
0	ST	SU	0	SR	SS	0	SI	SJ	SB	SC		θ_{yl}
SQ	SU	SY	SO	SS	SX	SH	SJ	SM	SD	SE	SF	w_l

The degeneration of the element stiffness matrix to include only the lateral displacements, w, required that all the columns and rows containing the parameters of the rotations in the x and y direction, for nodes *i, j, k & l* to be eliminated. This resulted in the following reduced element stiffness matrix that contained only the terms that represent the lateral displacements, w, at each node:

$$[K^e] = 1/15ab \begin{array}{c} \begin{matrix} w_i & w_j & w_k & w_l \end{matrix} \\ \begin{bmatrix} SF & SM & SX & SF \\ SM & SF & SY & SX \\ SX & SY & SF & SM \\ SY & SX & SM & SF \end{bmatrix} \end{array} \begin{matrix} w_i \\ w_j \\ w_k \\ w_l \end{matrix}$$

This 4 x 4 matrix represented the stiffness matrix of a REGN element pinned at each node, which ensured that only the lateral displacement, w, was developed at each node. The identical procedure was conducted for the degeneration of the stiffness matrix of the ACM element.

Once the theory had been adapted to represent the pinned computer model, all the other idealizations and computations could then be carried out. The analysis began by sub-dividing a flat plate square structure into an appropriate number of rectangular finite elements. The flat surface was divided into a 64, 100 and 144 rectangular finite element sub-division. Thereafter, to simulate the uniformly distributed load due to the self-weight of the structure, a unit load was then applied at each node within the structure and the displacement of the nodal points along the structure was determined.

These displacements determined the shape that the structure will form under a uniformly distributed unit load. This made it possible for the maximum displacement of the centre-most node of the structure to be determined. This maximum displacement was then scaled by a factor equal to the maximum centre deflection of the physical hanging model. All the other nodal displacements were also scaled by the same factor. This allowed the computer model to correspond with the different shapes produced by the

physical models, based on the maximum centre displacement of the actual structure.

3.1.5 Formulation of the computer program

The computer program was formulated using the Matlab programming language, which provided a simple yet efficient platform for the necessary computations to be carried out. However, a major challenge in formulating the computer program still existed due to the difficulties in constructing the single global stiffness matrix from the combination of all the element stiffness matrices.

To simplify the formulation of the global stiffness matrix, all the elements were modelled to be exactly the same shape and size. This allowed for the element stiffness matrices to be identical for each and every element within the structure. Nevertheless, the challenge of combining each element stiffness matrix into the single global stiffness matrix still existed, since every entry of every element stiffness matrix needed to be entered into the correct position within the global stiffness matrix. Any mistake in this procedure would compromise the accuracy of the computer model.

To overcome this challenge of developing the global stiffness matrix, the structure was first sub-divided into a few elements, whereby the entries of the

element stiffness matrices could be placed manually into the global stiffness matrix. The accuracy of the results was then verified through hand calculations. The element sub-divisions were then increased in a specified pattern and the analysis was repeatedly checked by means of hand calculations. Once it was determined that the analyses produced accurate results, the configuration of the global stiffness matrix for each predetermined sub-division was analyzed until the pattern of the location of the entries within the global stiffness matrix could be identified.

Once the pattern of the movement of the entries within the global stiffness matrix was identified, the pattern was then simulated by the computer program. Therefore, as long as the number of elements was increased in the same pattern as those verified by means of the hand calculations, the program would automatically place each entry of the element stiffness matrix correctly into the global stiffness matrix. This ensured the correct formulation of the global stiffness matrix and made it possible to analyze a series of finite element sub-divisions that included the 64, 100 and 144 element sub-divisions.

Thereafter, the force vector entries were entered into the program, based on the position and magnitude of the applied forces. The boundary conditions, which are the support conditions, were then entered into the program according to the design requirements. In this manner, the computations were

completed and the program was able to then calculate the displacements at each node within the structure by solving the finite element equations. These displacements then defined the shape of the pure compression thin shell structure.

3.1.5.1 Inputs of the computer program

To allow for the flexibility of the computer program, the user would need to input the following:

- The dimensions of the rectangular element i.e. the length, width and thickness of the rectangular element.
- The width and height of the cross-section of the structure. This is required to calculate the moment of inertia along the x-x axis i.e. Ixx.
- The Young's Modulus and Poisson's Ratio of the material. This allows for the use of different materials.
- The magnitude and location of the applied nodal forces, which simulate the uniformly distributed load. This will allow the user to scale the model up or down according to the design requirements. It will also allow the user to analyze the effects of various load combinations in defining the shape of the structure.
- The number of elements required to sub-divide the structure. Varying the number of elements will allow the user to determine the convergence of the solution. This will ensure that the subdivision is

neither too coarse nor too fine, which would make the program either inaccurate or too cumbersome.

- The boundary conditions also need to be inputted. The boundary conditions simulate the support conditions of the structure. Therefore, the computer program can accommodate for varying support conditions. This maintains the flexibility of the program and accommodates for different design requirements.

3.1.5.2 Outputs of the computer program

The main output of the program is to define the shape of the funicular thin shell structure based on the inputs. To achieve this, the computer program determines the lateral displacement that occurs at every node of the structure. The program then outputs the node number and displacement that occurs at that node. This allows for the resulting three-dimensional shape of the structure to be defined.

3.2 Verification of the computer model

The accuracy of the computer model needed to be verified, and this was achieved through the development of two other models in the form of the mathematical model and the physical hanging chain model. Since the success of these funicular thin shell structures depend on their form, the

comparison of the results from the three models will determine whether the form is indeed correct. This would ensure that the distribution of the stresses within the structure is optimal and according to the design requirements. This will determine whether the computer model developed using the finite element method can accurately define a funicular structure. The development of the mathematical and physical models is described in the following sections.

3.2.1 Mathematical model

An initial verification of the accuracy of the computer model was conducted by comparing it to mathematical models. The mathematical model was developed using the following mathematical expression of the catenary developed by Gregory (1706):

$$y = a \cosh(x/a)$$

The shapes obtained from this mathematical expression were then inscribed on the shapes obtained from the computer model and this provided a quick and easy accuracy check before the arduous task of actually constructing the physical models. The mathematical models were developed using Excel and the comparison of the mathematical and computer models were also conducted in Excel.

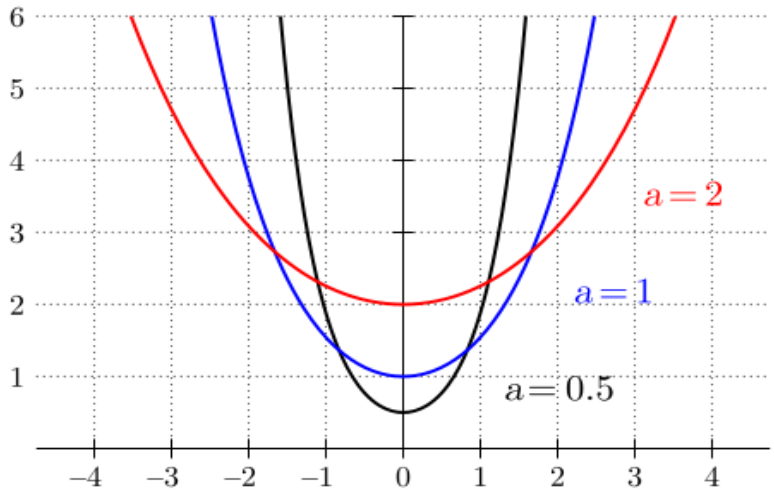

Figure 3.5: Catenary curves for various values of a (www.mathsinthecity .com)

However, the shapes obtained from the mathematical expressions were only two dimensional and therefore, only a two-dimensional comparison against the computer model was possible. This provided a starting point for the analysis and once sufficiently accurate results were obtained, three-dimensional models were then developed using the physical hanging chain modelling technique. A comparison was then made between the mathematical and physical models i.e. the two-dimensional and three-dimensional models, which provided more insight into the development of the ideal shapes of these structures.

3.2.2 Physical models

The physical models were constructed to correspond with the computer models. This three-dimensional shape corresponds more closely to a three-

dimensional shell structure and when compared to the computer model yields a more realistic analysis of the accuracy of the computer model. The physical models were constructed using interconnected hanging chains. Each of these hanging chains comprised of interconnected steel rings, which are commonly used in the jewellery industry to make neck chains and bracelets.

The models were then constructed on a frame that had been specifically built for this purpose. The hanging chains were then supported at varying locations on the frame and were allowed to hang freely under their own self-weight. The interconnections of the various chains allowed for the development of the required shapes. Once the required shape was obtained, the displacements along the chains were measured at locations that corresponded to the nodes of the computer model.

The measurements of displacement were conducted using a thin steel rod supported at its bottom edge by a square ruler, which ensured that it remained perfectly perpendicular to the ground surface. This ensured that the measurements were accurate and consistent. The co-ordinances of the displacements were then mapped out in Excel to reconstruct the shape, which was then compared to the computer model. A sufficient number of shapes were analyzed in order that conclusive results could be obtained.

4 RESULTS

The analysis was conducted using six different structural forms for each of the three types of models i.e. the computer model, the mathematical model and the physical model. In addition to varying the structural form, the support conditions were also varied for each form. This variation allowed for sufficient comparisons to be made between the three types of models, which made it possible to determine the accuracy and versatility of the computer model. This ultimately determined the extent to which the design tool had achieved the purpose for which it was developed.

Comparisons were firstly conducted between the overall three-dimensional shape of the physical and computer models, and thereafter, more detailed comparisons were conducted along the centre and diagonal arches of the three types of models. The curves of these arches were developed by plotting the co-ordinances of the displacements that occurred at the specified points along the arches. This resulted in two-dimensional curves that defined the shape of the structures and allowed for an accurate comparison of the forms generated by the computer, physical and mathematical models. These comparisons determined the exact extent to which the computer program achieved the design requirement of developing an accurate form of a thin shell structure.

All of the forms generated for the three types of models were developed on exactly the same square grid. The layout of the element sub-divisions, together with the centre and diagonal arches along which the analysis was conducted, is illustrated in the diagrams below:

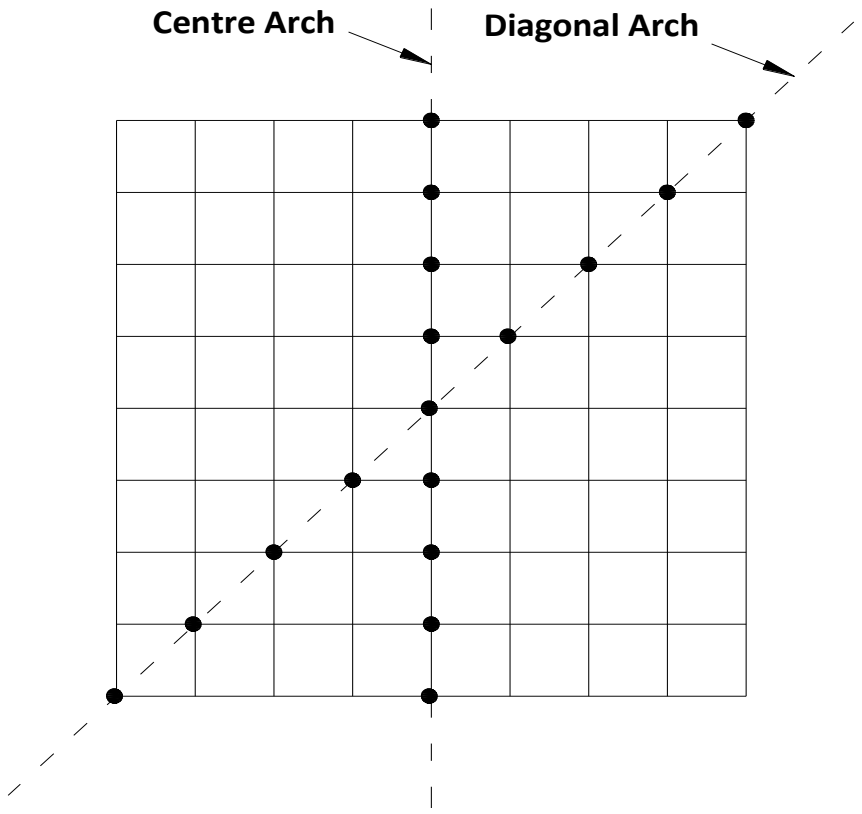

Figure 4.1: Arches along which the analysis was conducted

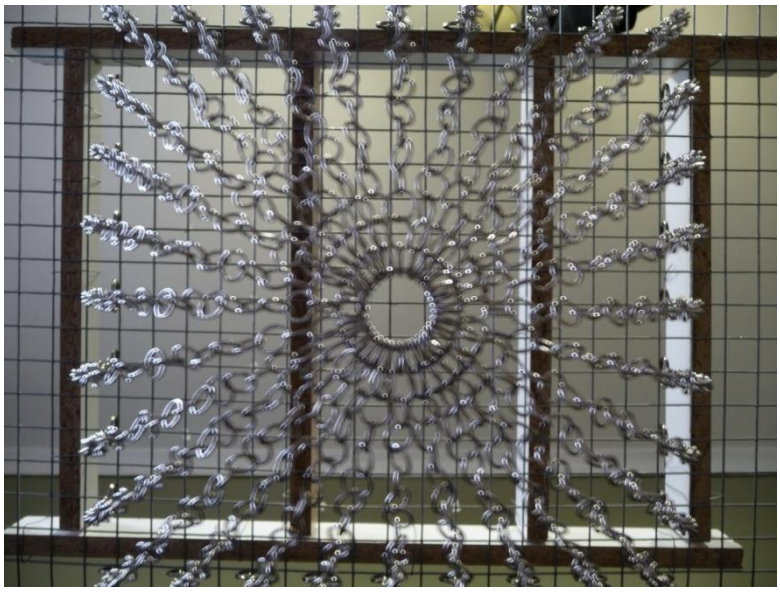

Figure 4.2: Actual square grid on which the physical models were constructed

4.1 Analysis of the forms generated

Each of the forms generated for the three types of models i.e. the computer, mathematical and physical models are presented and evaluated in the sections that follow:

4.1.1 Shape 1: The Barrel Vault

The first shape analysed was that of the Barrel vault. It was specifically chosen as the starting point of the analysis due to the simplicity of its shape. The singly-curved shape of the barrel vault meant that for the structure to be in pure compression, it could assume no other shape except that of a

catenary. This allowed for a simple and straight-forward initial comparison between the computer model and the catenary shape.

This comparison provided an initial estimation of the accuracy of the computer model before the arduous task of actually constructing the physical model. The level of correspondence between the computer model and the catenary shape verified whether the design philosophy employed in the development of the computer model was indeed correct. This subsequently determined whether its application could be extended to the design of the more complex doubly-curved forms.

The comparisons were conducted using both the REGN and ACM finite element methods. This allowed for the accuracy of each method to be determined and for the most accurate method to be applied to all further analyses. Thereafter, further comparisons were conducted between the different element sub-divisions of the 64, 100 and 144 elements. This determined how the accuracy of the computer model was affected by the change in element sub-divisions and it also determined which element sub-division would be the most suitable for all further analyses i.e. between the 64, 100 or 144 element sub-divisions.

4.1.1.1 Analysis of the Barrel Vault

4.1.1.1.1 The Rockey, Evans, Griffiths & Nethercot Method (REGN Method)

The three-dimensional shape developed by the computer model is presented below:

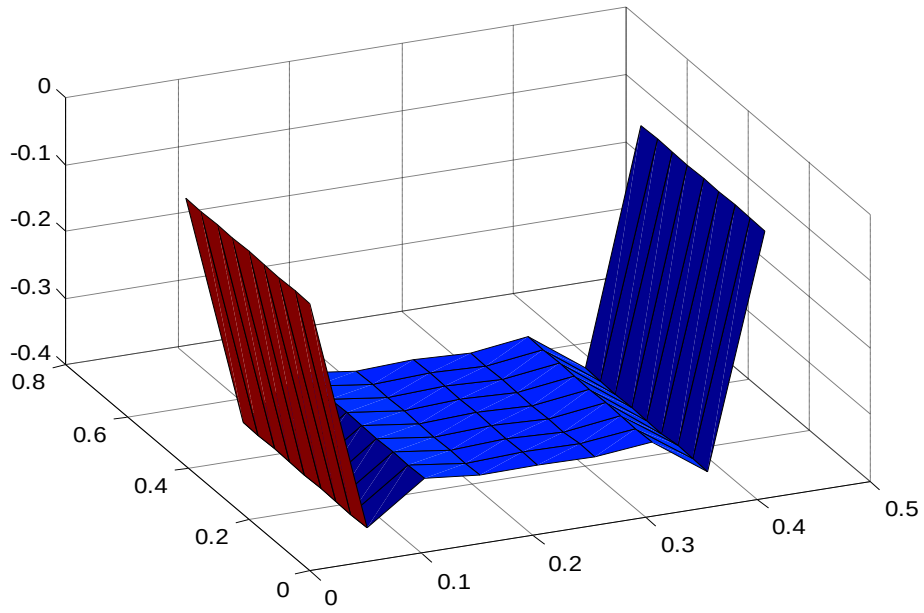

Figure 4.3: Barrel vault generated by the computer model – REGN Method

The shape formed above does not even resemble the curvature of a barrel vault. Therefore, the above shape clearly indicates that the computer model developed by the REGN finite element method was not capable of accurately defining the shape of a pure compression barrel vault. The individual curves of the barrel vault developed by the 64, 100 and 144 element sub-divisions are now compared to that of a catenary arch. This allows for a more detailed comparison of the forms generated. The results are presented below:

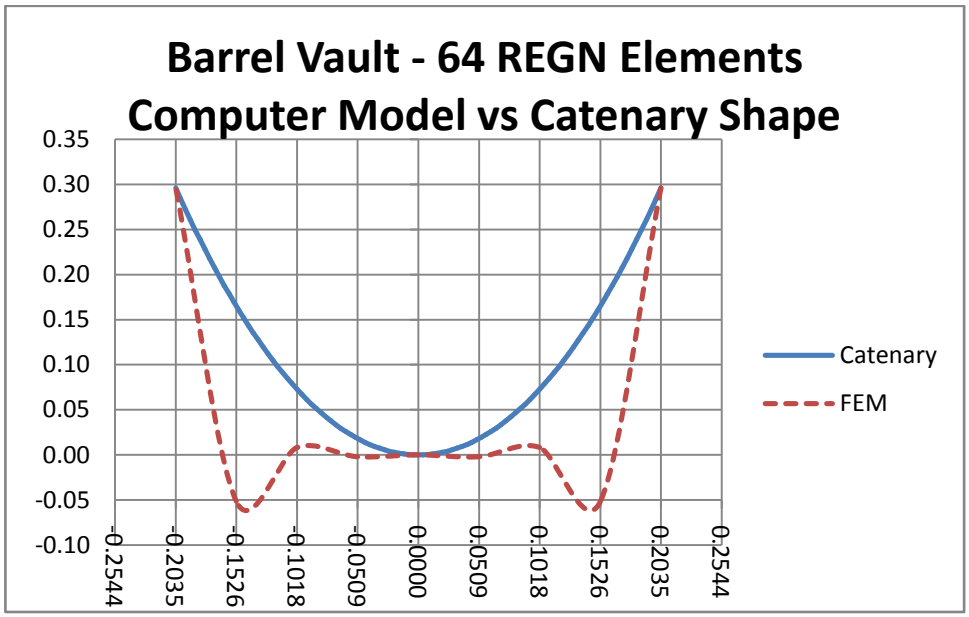

Figure 4.4: Barrel vault shape – 64 REGN elements – computer model vs catenary shape

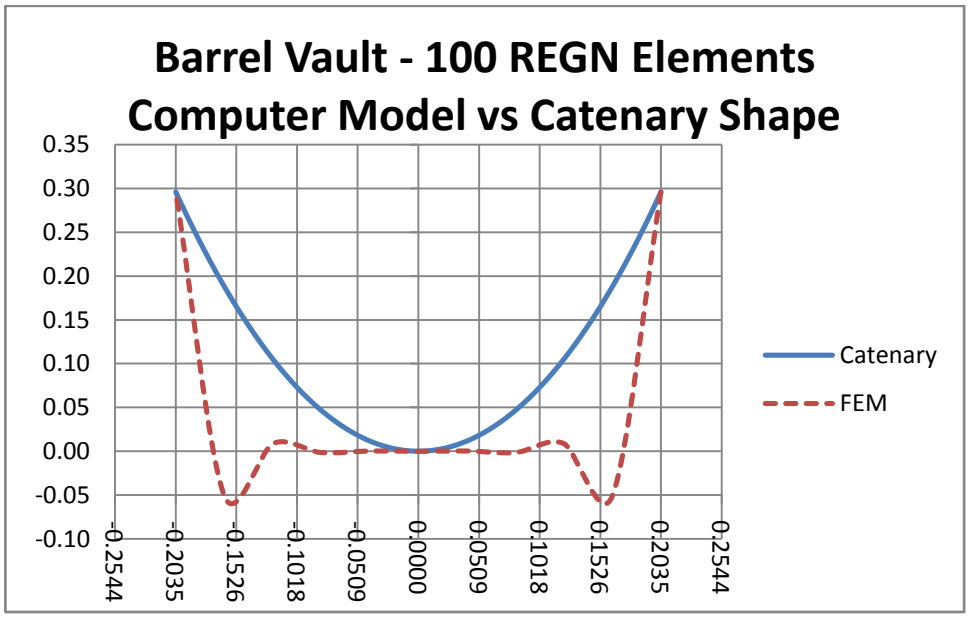

Figure 4.5: Barrel vault shape – 100 REGN elements – computer model vs catenary shape

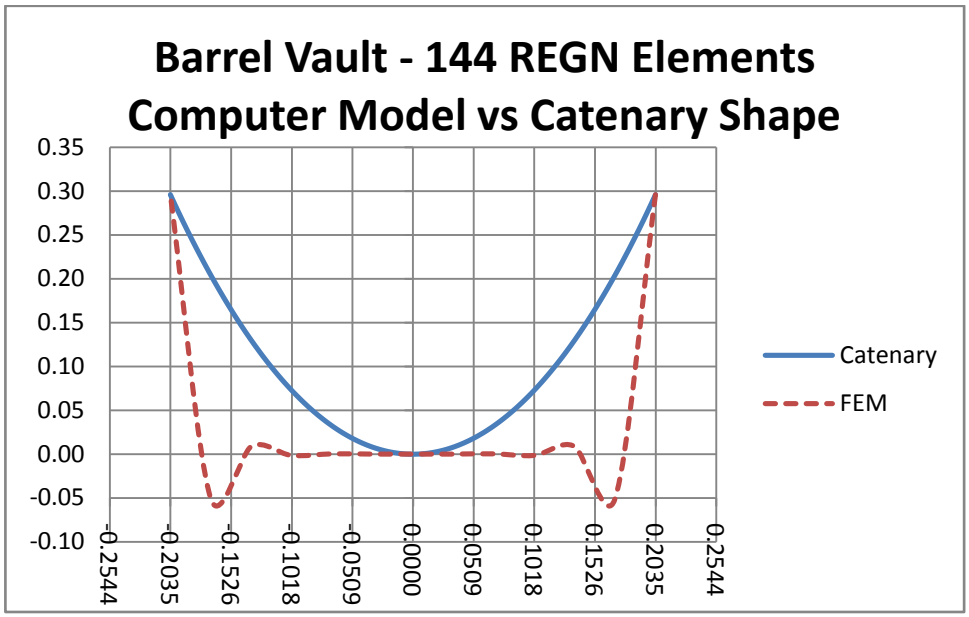

Figure 4.6: Barrel vault shape – 144 REGN elements – computer model vs catenary shape

The above comparisons of the individual arches of the barrel vault indicate that the computer model was not capable of modelling the catenary shape of the barrel vault for all three sub-divisions of 64, 100 or 144 elements. This proved that the REGN Method of analysis was definitely not capable of determining an accurate shape of a pure compression barrel vault. Hence, the REGN Method had to be discarded and the alternative approach of the ACM Method was introduced. The reasons as to why the REGN Method was not capable of defining an accurate shape of a pure compression structure will be discussed after the results of the ACM Method have been presented.

4.1.1.2 ACM Method of analysis

The three-dimensional barrel vault shape developed by the computer model is presented below:

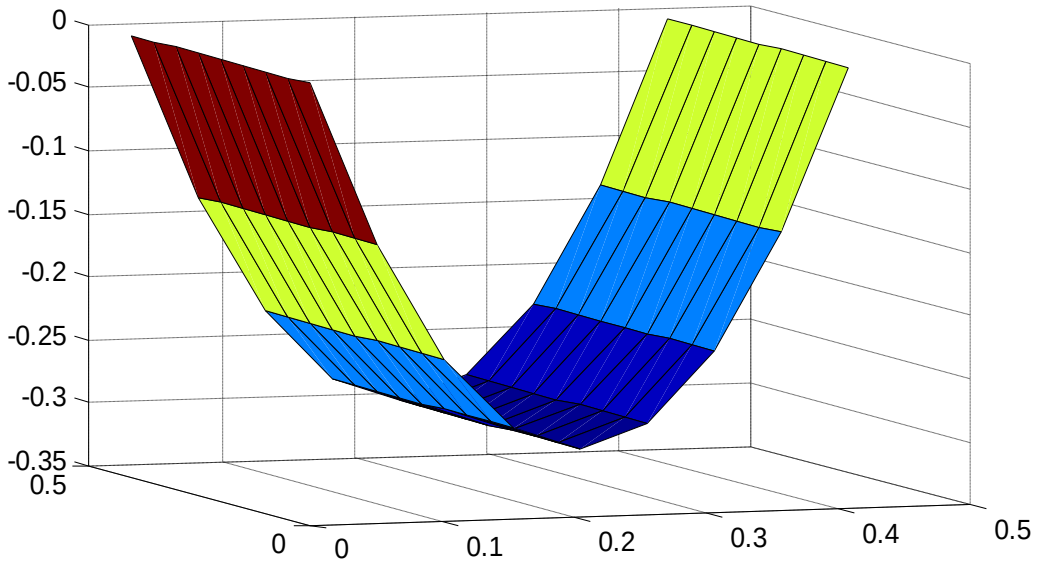

Figure 4.7: Barrel vault generated by the computer model – ACM Method

The above form generated by the computer model resembles that of a pure compression barrel vault. It should be noted that in the above three-dimensional graph the finite elements appear to be rectangular, although they are square in shape. The square finite elements appear rectangular due to the inconsistent sub-divisions along the different axes of the graph.

As with the previous method, the exact extent of the correspondence of the computer model to that of a pure compression barrel vault required a more detailed analysis. This analysis was conducted in the exact same manner, by

comparing the individual curves of the barrel vaults developed by the 64, 100 and 144 element sub-divisions to that of a catenary arch. The results are presented below:

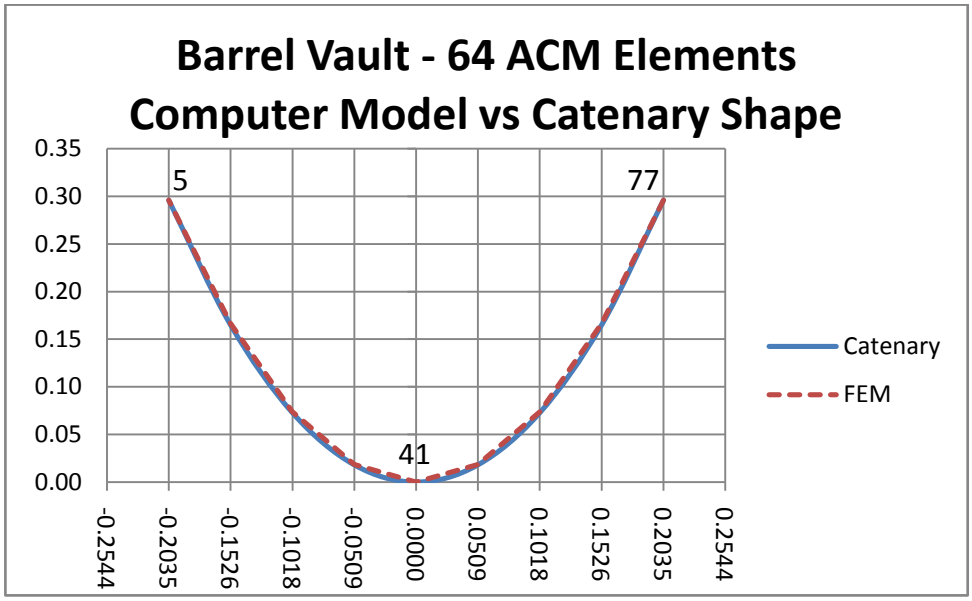

Figure 4.8: Barrel vault shape – 64 ACM elements – computer model vs catenary shape

Table 4.1: Barrel vault – computer model vs catenary shape – 64 ACM elements

Nodes	Distance (m)	Computer (m)	Catenary (m)	% Error
5	0.2035	0.2960	0.2960	0.0
14	0.1526	0.1665	0.1650	0.9
23	0.1018	0.0740	0.0729	1.5
32	0.0509	0.0185	0.0181	1.9
41	0.0000	0.0000	0.0000	0.0
50	-0.0509	0.0185	0.0181	1.9
59	-0.1018	0.0740	0.0729	1.5
68	-0.1526	0.1665	0.1650	0.9
77	-0.2035	0.2960	0.2960	0.0

For the 64 element sub-division, the shape produced in the graph and the results presented in the table indicate an excellent conformance of the computer model to the catenary shape. The variations ranging from 0.9 to 1.9% are relatively small. Therefore, it can be concluded that the form generated by the computer model using the 64 ACM element sub-division accurately defined the shape of a pure compression barrel vault

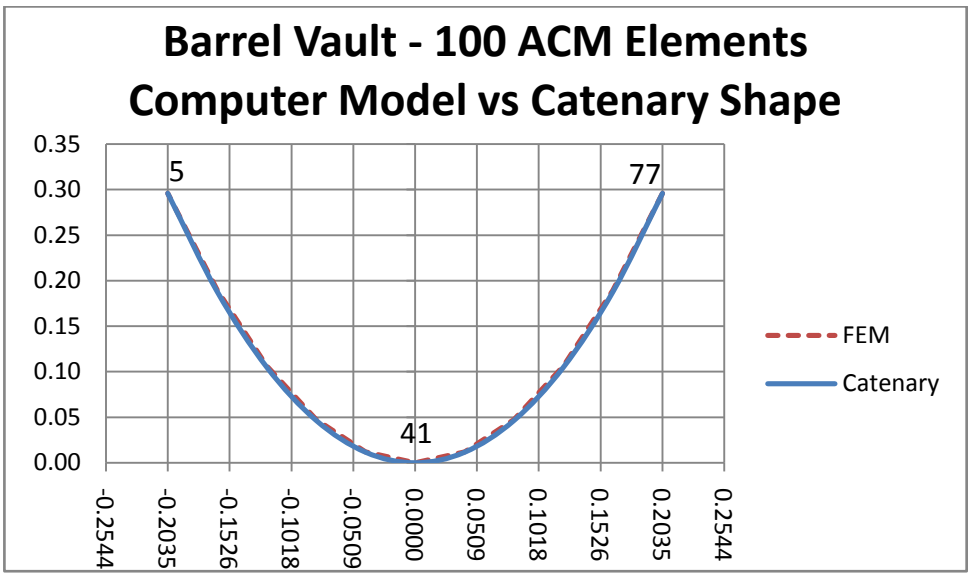

Figure 4.9: Barrel vault shape – 100 ACM elements – computer model vs catenary shape

Table 4.2: Barrel vault – computer model vs catenary shape – 100 ACM elements

Nodes	Distance (m)	Computer (m)	Catenary (m)	% Error
5	0.2035	0.2960	0.2960	0.0
14	0.1526	0.1663	0.1650	0.8
23	0.1018	0.0739	0.0729	1.4
32	0.0509	0.0183	0.0181	0.9
41	0.0000	0.0000	0.0000	0.0
50	-0.0509	0.0183	0.0181	0.9

59	**-0.1018**	**0.0739**	**0.0729**	**1.4**
68	**-0.1526**	**0.1664**	**0.1650**	**0.8**
77	**-0.2035**	**0.2960**	**0.2960**	**0.0**

Similarly, for the 100 element sub-division it is clear from both the form produced in the graph and the results presented in the table that there was an excellent conformance of the computer model and the shape of the catenary. The slight variations ranging from 0.8 to 1.4% are relatively small. Therefore, it can be concluded that the computer model generated using the 100 element sub-division accurately defined the shape of a pure compression barrel vault.

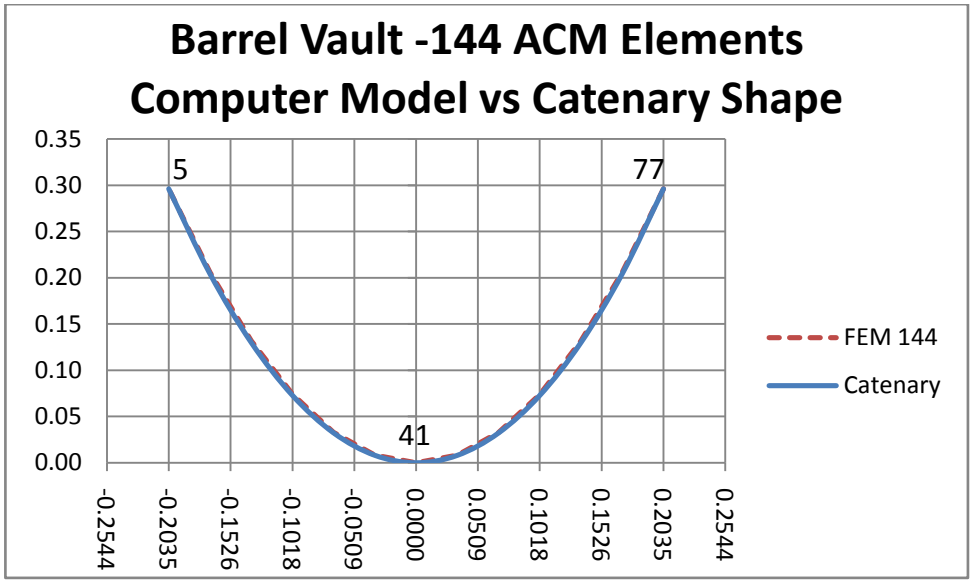

Figure 4.10: Barrel vault shape – 144 ACM elements – computer model vs catenary shape

Table 4.3: Barrel vault – computer model vs catenary shape – 144 ACM elements

Nodes	Distance (m)	Computer (m)	Catenary (m)	% Error
5	0.2035	0.2960	0.2960	0.0
14	0.1526	0.1660	0.1650	0.6
23	0.1018	0.0737	0.0729	1.1
32	0.0509	0.0183	0.0181	0.6
41	0.0000	0.0000	0.0000	0.0
50	-0.0509	0.0183	0.0181	0.6
59	-0.1018	0.0737	0.0729	1.1
68	-0.1526	0.1660	0.1650	0.6
77	-0.2035	0.2960	0.2960	0.0

For the 144 element sub-division, it is evident from both the form produced in the graph and the results presented in the table that the computer model had an excellent conformance to that of a catenary arch. The slight variations ranging from 0.6 to 1.1% are relatively small. Therefore, it can be concluded that the computer model formulated using the 144 element sub-division accurately defined the shape of a pure compression barrel vault.

All three element sub-divisions produced excellent results, with the maximum error reducing from 1.9% to 1.1% as the number of elements increased from 64 to 144 elements. Therefore, all three ACM element sub-divisions were fully capable of defining the shape of a pure compression structure and this proved that the design philosophy employed was indeed correct. It also proved that the ACM Method was much more accurate than the REGN Method.

Determining the source of the inaccuracies within the REGN Method required a more detailed analysis to be carried out. Since the inaccuracies found in the REGN Method were not present in the ACM Method, the first logical step in this analysis was to compare the REGN Method to the ACM Method. This comparison is presented below:

On close examination of the derivation of the two methods, it is clear that the fundamental approach in deriving the necessary equations for both the ACM and REGN methods are very similar. In both methods, the nodes of the elements have been defined in exactly the same manner and the displacements and forces have also been expressed in exactly the same manner. Furthermore, both methods define the shape function by using the exact same polynomial expression given below, in which certain terms have been omitted from a complete fourth order polynomial:

$$w = \alpha_1 + \alpha_2 x + \alpha_3 y + \alpha_4 x^2 + \alpha_5 xy + \alpha_6 y^2 + \alpha_7 x^3 + \alpha_8 x^2 y + \alpha_9 xy^2 + \alpha_{10} y^3 + \alpha_{11} x^3 y + \alpha_{12} xy^3$$

As has been fully explained in the derivation of the methods, the above format of polynomial will vary as a cubic along any x = constant or y = constant line. Since the four constants that uniquely define the cubic (i.e. the two end values of slopes and the displacements at the ends of the boundaries) are common to adjacent elements, continuity of w will be imposed along any

surface. However, the gradient of w normal to any of the boundaries also varies along it in a cubic manner. For example, if we have to consider $\partial w/\partial x$ along a line on which x is constant, then two values of the normal slope are defined and the cubic is not specified uniquely, and in general a discontinuity of the slope will occur. This causes the function to be 'non-conforming'.

This 'non-conformity' was initially assumed to be the source of the inaccuracies within the REGN Method. However, from the comparison of the two methods, it is clear that both methods utilise the exact same 'non-conforming' function and despite this, the ACM Method is still capable of producing a more accurate shape that is free from the major variations present in the REGN Method. Thus, it can be concluded that although this 'non-conforming' element might have resulted in some inaccuracies, it is not the cause of the major variations present in the REGN method, since these variations are not present in the ACM method.

Therefore, the source of the large variations in the REGN method had to be due to some other reason. Looking further into the derivation of the two methods, it can be seen that both methods define the moment-curvature relationships in ways that lead to exactly the same functions, whose components are exactly the same. Furthermore, the general equations

between the nodal loads and the displacements are exactly the same for both methods. And similarly, the general function that defines the element stiffness matrix is also exactly the same. The stiffness matrix is therefore given by:

$$[K^e]_{12\times12} = \int_A \int [C]^T [D][C]dxdy \ldots\ldots\ldots\ldots\ldots\ldots\ldots\ldots ACM\ Method$$

$$[K^e] = \int_0^b \int_0^a [B]^T [D][B]dxdy \ldots\ldots\ldots\ldots\ldots\ldots\ldots\ldots\ldots REGN\ Method$$

It is in the solution of this last step i.e. the derivation of the final stiffness matrix, that the differences between the two methods become apparent. From the above equations it can be seen that in order for the final stiffness matrix to be determined integration needed to take place over the area of the plate element. Both methods used different approaches in solving the above equation, which resulted in each method formulating a final stiffness matrix different from the other.

Therefore, since the final stiffness matrix of both methods differ from each other, it can be assumed that the source of the inaccuracies within the REGN Method occurred somewhere within this last step. This implies that the technique employed in the formulation of the final stiffness matrix for the ACM Method proved to be more accurate than the technique employed in the

formulation of the final stiffness matrix of the REGN Method. This resulted in the ACM Method being able to more accurately define the shape of a pure compression structure.

Since the ACM Method had been proven to be the most accurate method of analysis, it was then applied to the modelling of the three-dimensional doubly-curved surfaces. It then became necessary to determine the most suitable element sub-division that would be employed in all further analyses. This was done by comparing the results obtained from the 64, 100 and 144 element sub-divisions.

4.1.1.3 Comparison of the 64, 100 and 144 element sub-divisions using the ACM Method

All three finite element sub-divisions produced excellent results. However, only one element sub-division from the three available sub-divisions needed to be employed in all further analyses. From a practical point of view, a 64 element sub-division would be ideal, since the framework on which the physical models were constructed contained a grid that comprised of 64 sub-divisions. Hence, a 64 element sub-division of the computer model would ensure that the position of the nodal displacements of the two models corresponded exactly, which would reduce the experimental errors and increase the accuracy of the results.

To determine the effect that the three element sub-divisions had on the results of the computer model, a comparison between them was conducted. This ultimately determined whether the use of the 64 element sub-division compromised the accuracy of the computer model. The comparisons are presented below:

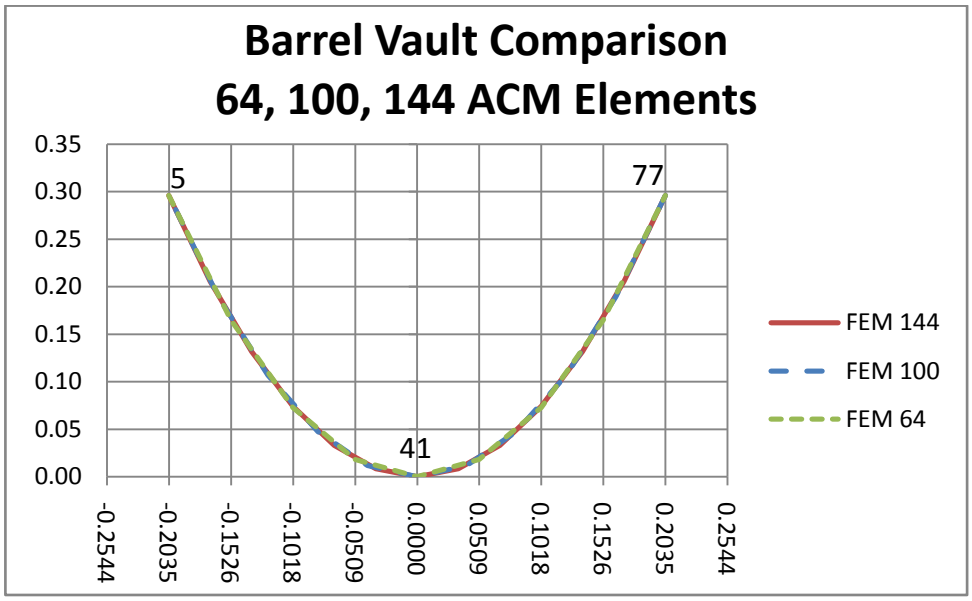

Figure 4.11: Barrel vault shape – 64, 100 & 144 ACM element comparisons – computer model vs catenary shape

From the above graph, the forms produced by the three element sub-divisions seem to be identical. All three element sub-divisions were capable of producing an accurate barrel vault shape. To identify the differences in the three sub-divisions a more detailed comparison of each individual node was conducted. This comparison is presented in the tables below:

Table 4.4: Barrel vault comparison – 64 ACM elements vs 100 ACM elements

Nodes	Distance (m)	64 FEM (m)	100 FEM (m)	% Error
5	0.2035	0.2960	0.2960	0.00
14	0.1526	0.1665	0.1663	0.12
23	0.1018	0.0740	0.0739	0.14
32	0.0509	0.0185	0.0183	1.08
41	0.0000	0.0000	0.0000	0.00
50	-0.0509	0.0185	0.0183	1.08
59	-0.1018	0.0740	0.0739	0.14
68	-0.1526	0.1665	0.1663	0.12
77	-0.2035	0.2960	0.2960	0.00

The comparison between the 64 and 100 element sub-division presented in the above table, clearly indicates that the two shapes were almost identical, with a maximum difference of only 1.08%. This led to the conclusion that the increase in element sub-division from 64 to 100 elements resulted in a very slight variation in the results. Therefore, compared to the 100 element sub-division the 64 element sub-division was sufficiently accurate in modelling a thin shell barrel vault.

Table 4.5: Barrel vault comparison – 64 ACM elements vs 144 ACM elements

Nodes	Distance (m)	64 FEM (m)	144 FEM (m)	% Error
5	0.2035	0.2960	0.2960	0.00
14	0.1526	0.1665	0.1660	0.30
23	0.1018	0.0740	0.0737	0.41
32	0.0509	0.0185	0.0183	1.35
41	0.0000	0.0000	0.0000	0.00
50	-0.0509	0.0185	0.0183	1.35
59	-0.1018	0.0740	0.0737	0.41
68	-0.1526	0.1665	0.1660	0.30
77	-0.2035	0.2960	0.2960	0.00

Again, the comparison between the 64 and 144 element sub-division presented in the above table, clearly indicates that the two shapes were almost identical, with a maximum difference of only 1.35%. This again led to the conclusion that the increase in the element sub-division from 64 to 144 elements resulted in a very slight variation in the results. Therefore, compared to the 144 element sub-division the 64 element sub-division was sufficiently accurate in modelling a thin shell structure.

Therefore, the 64 element sub-division has been proven to be sufficiently accurate for the determination of the form of a pure compression thin shell structure. This together with the correlation of the nodal displacements between the physical and computer model make the 64 element sub-division the most appropriate sub-division for all further analyses.

4.1.2 Shape 2: All Edges Simply Supported

4.1.2.1 Physical and Computer Model

For the second shape, all the edges of the models were simply supported. The resulting shapes are presented below:

Figure 4.12: Physical model with all edges simply supported

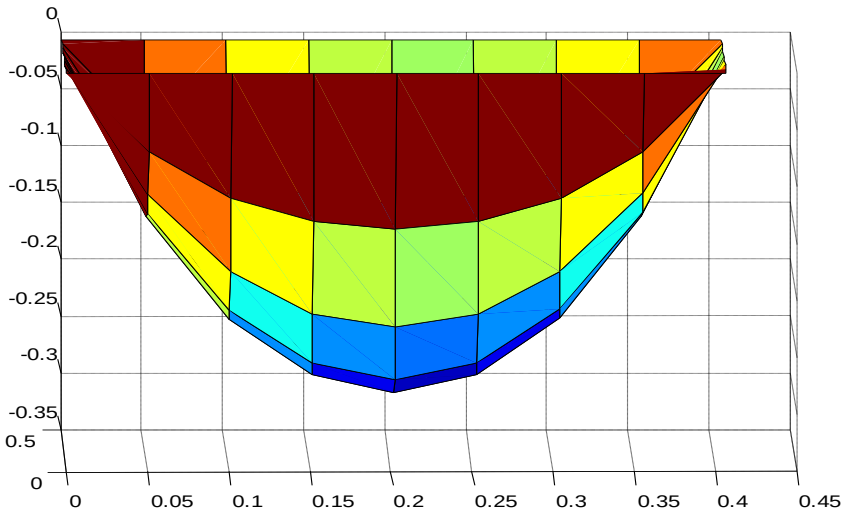

Figure 4.13: Computer model with all edges simply supported

The above models indicate that the overall shape formed by the computer model corresponded to that of the physical model. As with the previous case, to determine the exact correspondence between the models, a more detailed analysis was conducted along the centre and diagonal arches of the models. These comparisons are presented below:

4.1.2.2 Computer Model vs Catenary Shape

4.1.2.2.1 Centre Arch

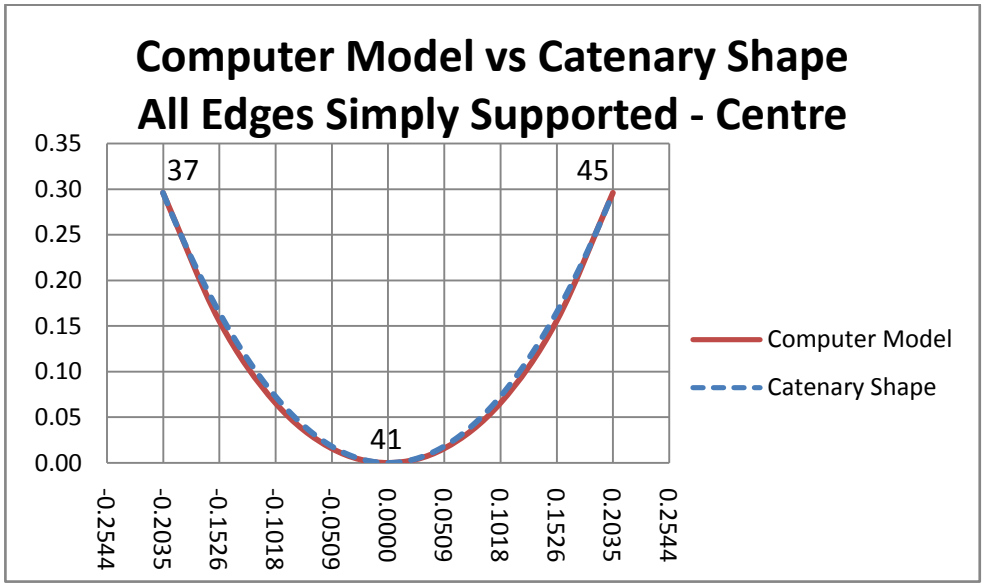

Figure 4.14: All edges simply supported – centre arches – computer model vs catenary shape

Table 4.6: 64 ACM – Computer Model vs Catenary Shape – Centre Comparison – All Edges Simply Supported

Node	Distance (m)	Computer (m)	Catenary (m)	% Error
37	0.2035	0.296	0.296	0.0
38	0.1526	0.156	0.165	3.2
39	0.1018	0.066	0.073	2.5
40	0.0509	0.016	0.018	0.8
41	0.0000	0.000	0.000	0.0
42	-0.0509	0.016	0.018	0.8
43	-0.1018	0.066	0.073	2.5
44	-0.1526	0.156	0.165	3.2
45	-0.2035	0.296	0.296	0.0

With regards to the centre arches, the above graph and table clearly indicate that the computer model corresponded closely to the shape of the

mathematical model i.e. the catenary shape. The maximum variation is 3.2%. This variation could be due to the way in which the computer model formed the arch. The computer model formed the arch by approximating it by a series of rigid finite elements that had no bending capacity. This led to the formation of an arch that was not completely smooth, which varied slightly from a completely smooth arch. The accuracy of the computer model could be further increased by decreasing the size of the finite elements.

Nevertheless, for this particular sag distance and support condition, the centre arch of the computer model corresponded closely to the catenary shape.

4.1.2.2.2 Diagonal Arch

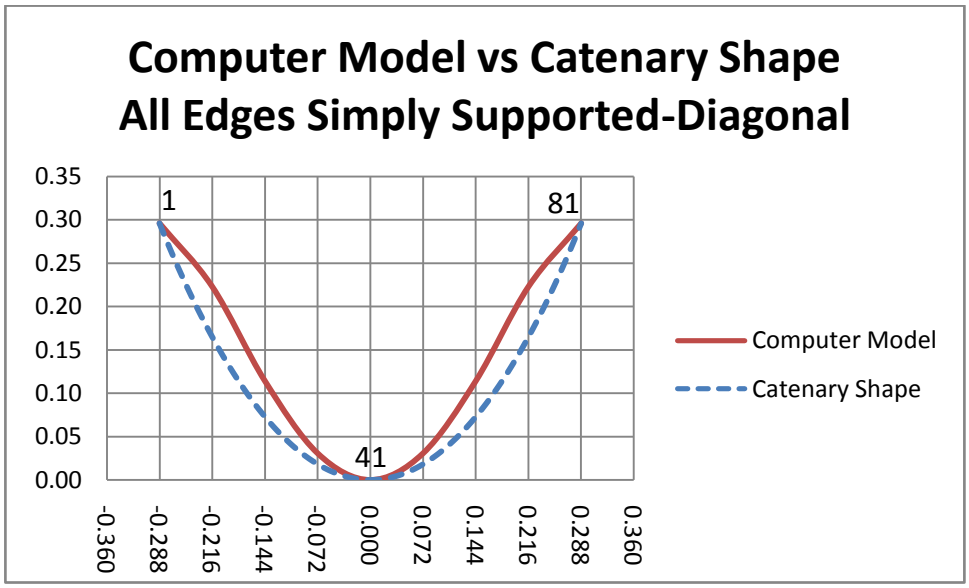

Figure 4.15: All edges simply supported – diagonal arches – computer model vs catenary shape

Table 4.7: 64 ACM – Computer Model vs Catenary Shape – Diagonal Comparison – All Edges Simply Supported

Node	Distance (m)	Computer (m)	Catenary (m)	% Error
1	0.288	0.296	0.296	0.0
11	0.216	0.223	0.165	19.6
21	0.144	0.114	0.073	13.9
31	0.072	0.031	0.018	4.2
41	0.000	0.000	0.000	0.0
51	-0.072	0.031	0.018	4.2
61	-0.144	0.114	0.073	13.9
71	-0.216	0.223	0.165	19.6
81	-0.288	0.296	0.296	0.0

The above graph and table indicate some variation in form along the diagonal arch of the computer model and catenary shape. The computer model was narrower than the catenary shape, with the most significant variation of 19.6% occurring at the node closest to the supports. Also, a slight reverse bending occurs as the curve approaches the edge of the structure closer to the supports.

The formation of this reverse bending at the corners of the computer model corresponds closely to the corner effects that are manifested in yield-line analysis - when a uniformly distributed load is applied to a square slab that is simply supported along all edges. These corner effects produce what is known as “corner levers” at the corner edges of the slab. Johansen (1962) maintains that the existence of these corner levers is solely due to the shape of the edge of the slab and does not depend on whether it is anchored or not.

Therefore, for this particular sag distance and support condition, the computer model did not correspond to the catenary shape, but it corresponded to the shape that is expected of a square slab that is simply supported along its edges. It can therefore be concluded that the computer model accurately defined the expected shape of the arch and not the catenary shape, since the catenary shape did not take into account the corner effects.

4.1.2.3 Physical Model vs Mathematical Model

4.1.2.3.1 Centre Arch

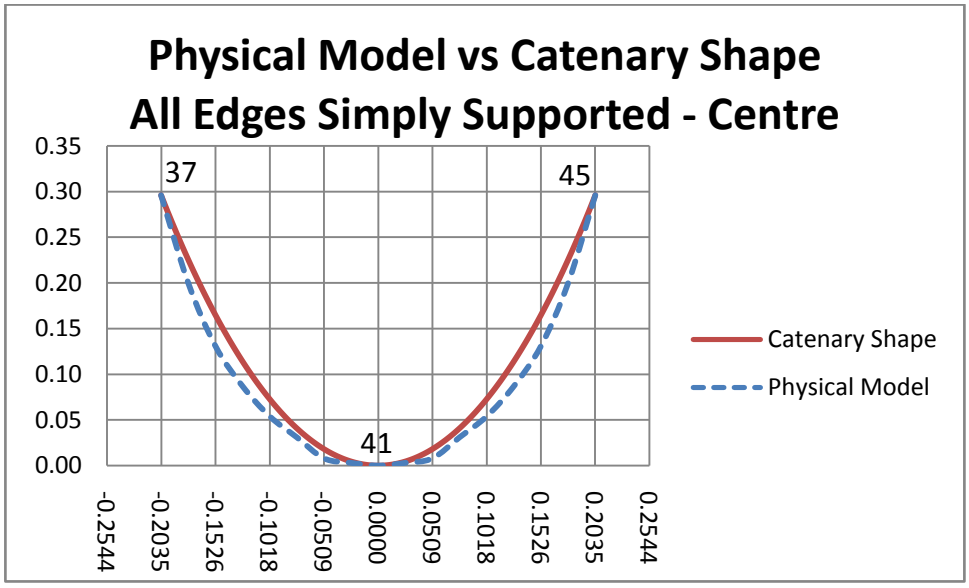

Figure 4.16: All edges simply supported – centre arches – physical model vs catenary shape

Table 4.8: 64 ACM – Physical Model vs Catenary Shape – Centre Comparison – All Edges Simply Supported

Node	Distance (m)	Physical (m)	Catenary (m)	% Error
37	0.2035	0.296	0.296	0.0
38	0.1526	0.131	0.165	11.5
39	0.1018	0.054	0.073	6.4
40	0.0509	0.008	0.018	3.4
41	0.0000	0.000	0.000	0.0
42	-0.0509	0.008	0.018	3.4
43	-0.1018	0.054	0.073	6.4
44	-0.1526	0.131	0.165	11.5
45	-0.2035	0.296	0.296	0.0

With regards to the form of the centre arches of the physical model and the catenary shape, the above graph and table indicate a variation in the two forms. The physical model was a bit broader than the catenary shape and the largest variation of 11.5% occurred at the node closest to the support. Since the form produced by the physical model had to be correct, the slight variation can be attributed to either errors in modelling or the difficulties in accurately measuring the co-ordinances of the physical model.

One very apparent shortcoming of the physical modelling process occurred when constructing the three-dimensional shape from individual arches along the model. Each arch was constructed using identical links that were combined together to form a chain. The uniform size of the link meant that the length of each chain could only be increased or decreased according to the link size. This resulted in adjacent arches being either too long or too short as

one moved along the physical chain model. This produced a three-dimensional shape that had slight inconsistencies along the model. This definitely caused slight inaccuracies in the arches of the physical model and could explain the variations seen above.

Therefore, for this particular sag distance and support condition, the centre arch of the physical model corresponded to the shape of the catenary model.

4.1.2.3.2 Diagonal Arch

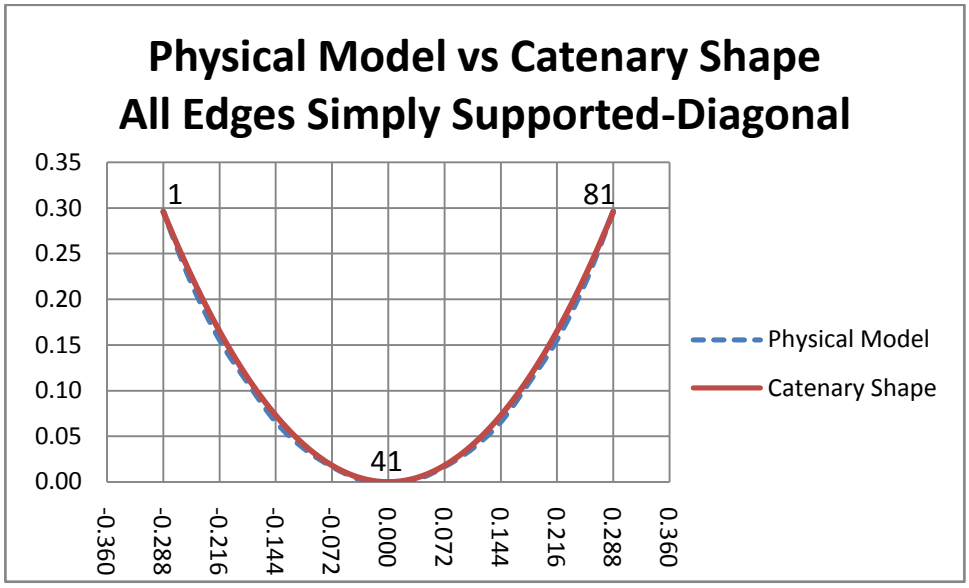

Figure 4.17: All edges simply supported – diagonal arches – physical model vs catenary shape

Table 4.9: 64 ACM – Physical Model vs Catenary Shape – Diagonal Comparison – All Edges Simply Supported

Node	Distance (m)	Physical (m)	Catenary (m)	% Error
1	0.288	0.296	0.296	0.0
11	0.216	0.156	0.165	3.0
21	0.144	0.066	0.073	2.3
31	0.072	0.017	0.018	0.4
41	0.000	0.000	0.000	0.0
51	-0.072	0.017	0.018	0.4
61	-0.144	0.066	0.073	2.3
71	-0.216	0.156	0.165	3.0
81	-0.288	0.296	0.296	0.0

With regards to the diagonal arches, the above graph and table clearly indicate that the physical model corresponded very closely to the shape of the mathematical model i.e. the catenary shape. The two shapes were almost identical with a maximum variation of only 3%. Therefore, for this particular sag distance the diagonal arch of the physical model corresponded closely to the shape of the catenary.

4.1.2.4 Computer Model vs Physical Model

4.1.2.4.1 Centre Arch

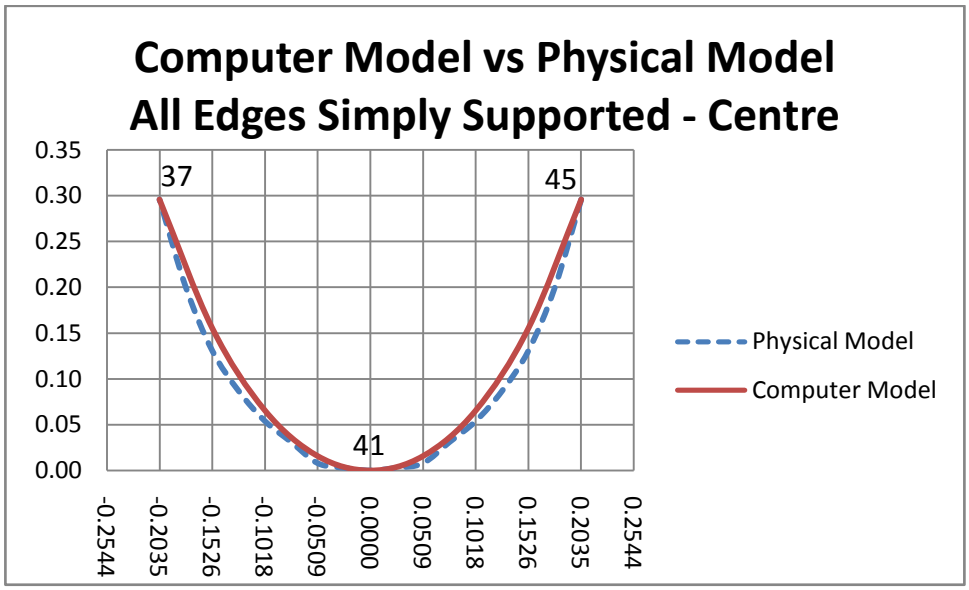

Figure 4.18: All edges simply supported – centre arches – computer model vs physical model

Table 4.10: 64 ACM – Computer Model vs Physical Model – Centre Comparison – All Edges Simply Supported

Node	Distance (m)	Computer (m)	Physical (m)	% Error
37	0.2035	0.296	0.296	0.0
38	0.1526	0.156	0.131	8.3
39	0.1018	0.066	0.054	3.9
40	0.0509	0.016	0.008	2.6
41	0.0000	0.000	0.000	0.0
42	-0.0509	0.016	0.008	2.6
43	-0.1018	0.066	0.054	3.9
44	-0.1526	0.156	0.131	8.3
45	-0.2035	0.296	0.296	0.0

With regards to the shape of the centre arches of the computer model and the physical model, the above graph and table indicate a slight variation in the two forms. The computer model produced an arch that was slightly narrower

than the physical model, with the maximum variation of 8.3% at the node closest to the support. This variation could be due to a combination of errors in the computer model and the physical model. For the physical model the errors arose due to the differing lengths of arches along the three-dimensional model and for the computer model the errors arose due to the rigid nature of the finite elements used in the analysis.

Nevertheless, this small variation can be accommodated by increasing the thickness of the constructed arch such that the arch of the computer model fits within this constructed arch.

4.1.2.4.2 Diagonal Arch

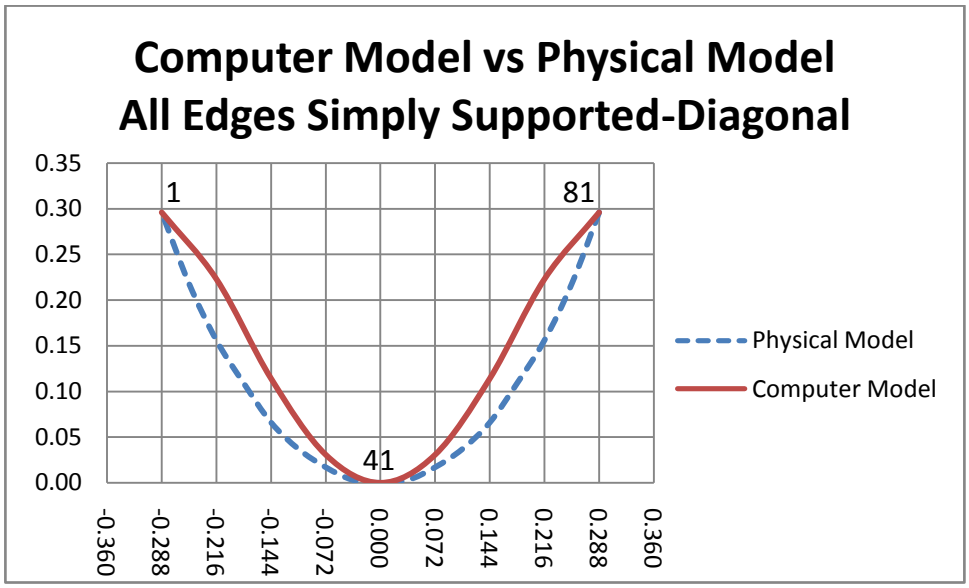

Figure 4.19: All edges simply supported – diagonal arches – computer model vs physical model

Table 4.11: 64 ACM – Computer Model vs Physical Model – Diagonal Comparison – All Edges Simply Supported

Node	Distance (m)	Computer (m)	Physical (m)	% Error
1	0.288	0.296	0.296	0.0
11	0.216	0.223	0.156	22.6
21	0.144	0.114	0.066	16.3
31	0.072	0.031	0.017	4.6
41	0.000	0.000	0.000	0.0
51	-0.072	0.031	0.017	4.6
61	-0.144	0.114	0.066	16.3
71	-0.216	0.223	0.156	22.6
81	-0.288	0.296	0.296	0.0

The above graph and table indicate a significant variation in the form along the diagonal arches of the computer and physical models. The computer model was narrower than the physical model, with the maximum variation of 22.6% occurring at the node closest to the support. A slight reverse bending towards the edge of the structure can also be seen.

As has been fully explained earlier, the formation of this reverse bending at the corners of the computer model corresponds closely to the corner effects that are manifested in yield-line analysis - when a uniformly distributed load is applied to a square slab that is simply supported along all edges. This led to the same conclusion, that for this particular sag distance and support condition, the computer model did not correspond to the physical hanging chain model, but it corresponded to the shape that is expected of a square slab that is simply supported along its edges.

4.1.3 Shape 3: Corner Point Supports

For the third shape, only the corner points of the models were supported. The resulting shapes are presented below:

4.1.3.1 Physical and Computer Model

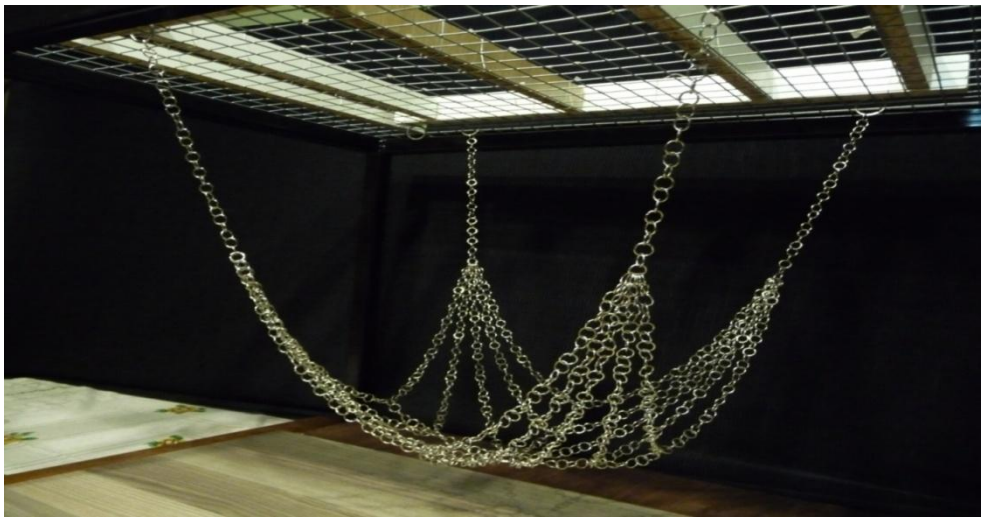

Figure 4.20: Physical model with corner point supports

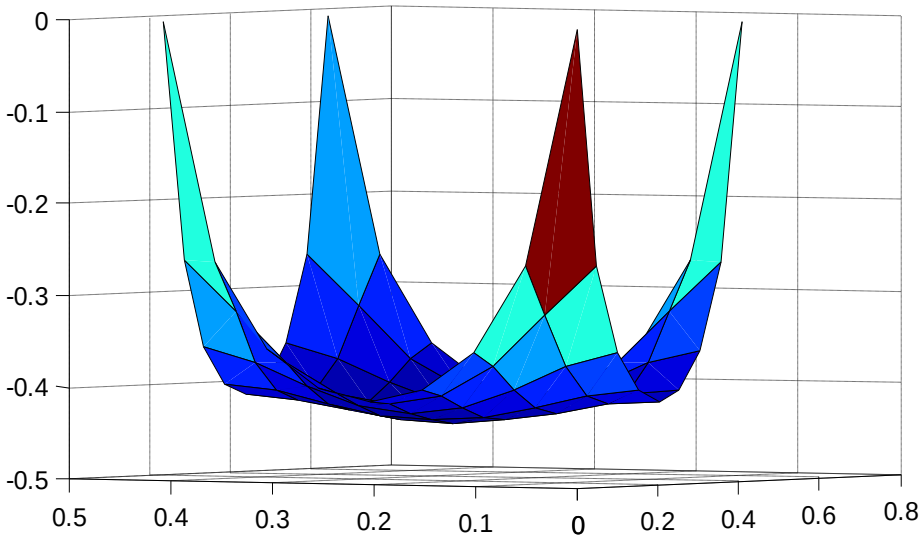

Figure 4.21: Computer model with corner point supports

A comparison of the shapes formed by the computer and physical models indicate that the overall shape between the two models was very similar. However, the computer model produced a slight reverse bending or lip towards the edge of the structure.

The results of the more detailed analyses are presented below:

4.1.3.2 Computer Model vs Mathematical Model

4.1.3.2.1 Centre Arch

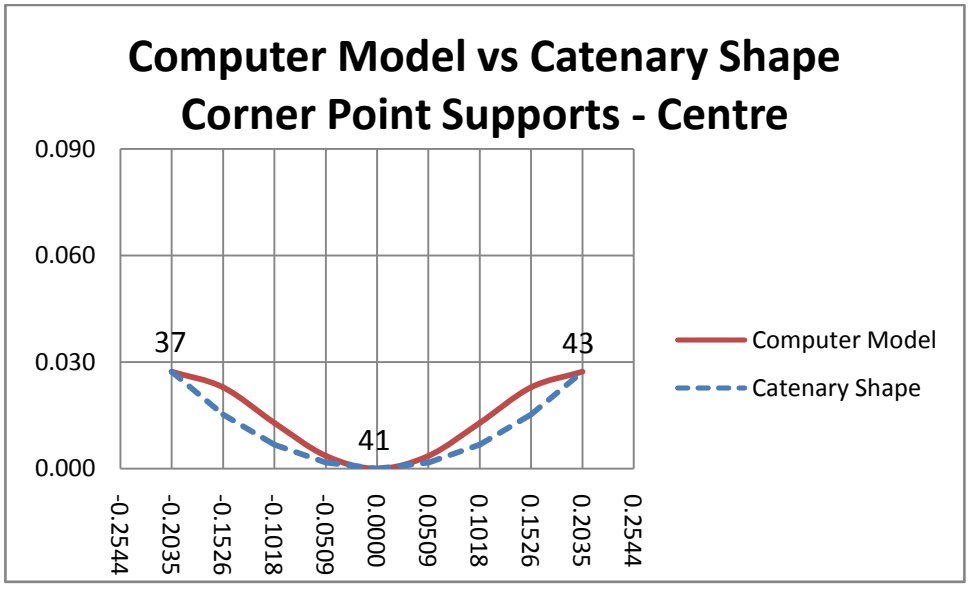

Figure 4.22: Corner point supports – centre arches – computer model vs catenary shape

Table 4.12: 64 ACM – Computer Model vs Catenary Shape – Centre Comparison – Corner Point Supports

Node	Distance (m)	Computer (m)	Catenary (m)	% Error
37	0.2035	0.027	0.027	0.0
38	0.1526	0.023	0.015	28.5
39	0.1018	0.013	0.007	22.9
40	0.0509	0.004	0.002	7.1
41	0.0000	0.000	0.000	0.0
42	-0.0509	0.004	0.002	7.1
43	-0.1018	0.013	0.007	22.9
44	-0.1526	0.023	0.015	28.5
45	-0.2035	0.027	0.027	0.0

With regards to the centre arches, the above graph and table clearly indicate the variation that occurred between the shape of the computer model and the shape of the mathematical model i.e. the catenary shape. The maximum variation of 28.5% occurred at the node closest to the edge. From the above graph it can be seen that a slight reverse bending occurred towards the edge of the structure. This reverse bending is also referred to as a lip.

The formation of this lip is more commonly found in the designs of previous engineers, who modelled their shell structures using fabric models. These fabric models were able to accurately predict the shape of shallow shells. Therefore, since the centre arch of the model produced a shallow shell, its shape corresponded more to the shape produced by a fabric model. Since the fabric model is interconnected at every point within the structure, the formation of the lip at the edge of the structure also affected the other points

towards the interior of the structure. In a similar manner, the computer model was also interconnected at every point within the structure and it therefore behaved in exactly the same manner as the fabric model, to produce the variation in shape indicated by the above graph.

Therefore, for this particular sag distance and support condition, the centre arch of the computer model did not correspond to the catenary shape but it corresponded more to the shape expected of a fabric model.

4.1.3.2.2 Diagonal Arch

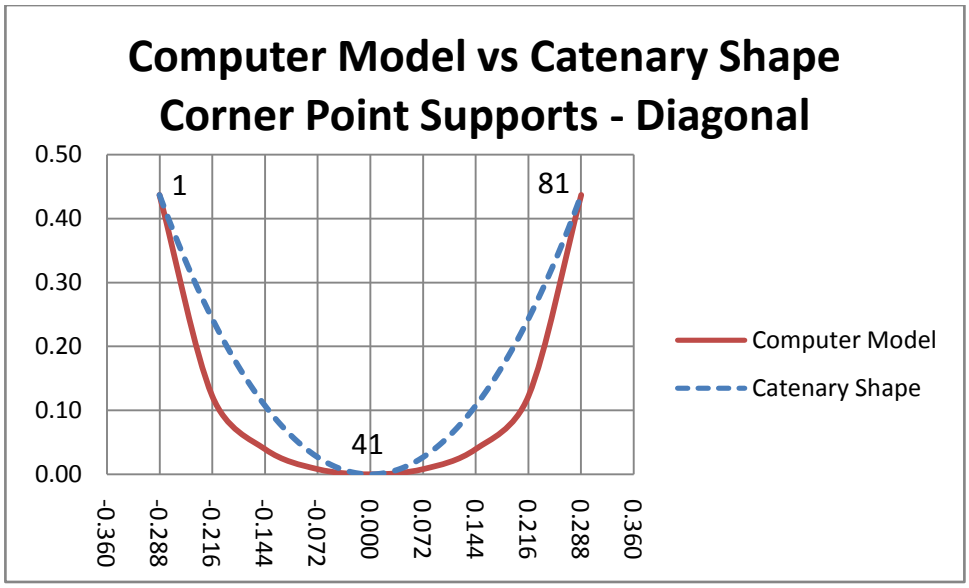

Figure 4.23: Corner point supports – diagonal arches – computer model vs catenary shape

Table 4.13: 64 ACM – Computer Model vs Catenary Shape – Diagonal Comparison – Corner Point Supports

Node	Distance (m)	Computer (m)	Catenary (m)	% Error
1	0.288	0.437	0.437	0.0
11	0.216	0.123	0.244	27.7
21	0.144	0.040	0.108	15.6
31	0.072	0.008	0.027	4.3
41	0.000	0.000	0.000	0.0
51	-0.072	0.008	0.027	4.3
61	-0.144	0.040	0.108	15.6
71	-0.216	0.123	0.244	27.7
81	-0.288	0.437	0.437	0.0

The above graph and table clearly indicate the significant variation in the shape of the diagonal arch of the computer model and that of the catenary shape. It is clear that the arch of the computer model did not correspond to the arch of the catenary model. The computer model developed a much broader bell-shaped arch, with the largest variation of 27.7% occurring at the node closest to the support.

This variation could have occurred due to the formation of the lip towards the edge of the model - which is evident from the graphs presented earlier. Due to the computer model being fully interconnected at every point within the structure, it is very possible that the lip that occurred at the edge of the structure affected the diagonal arch of the structure in a manner that contributed to the variations indicated above.

Therefore, for this particular sag distance and support condition, the diagonal arch of the computer model did not correspond to the catenary shape.

4.1.3.3 Physical Model vs Mathematical Model

4.1.3.3.1 Centre Arch

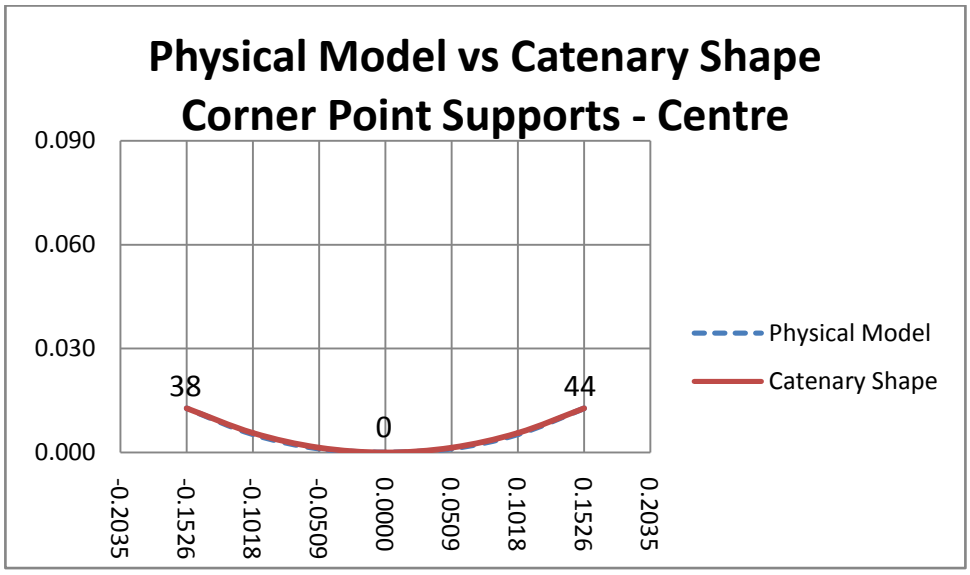

Figure 4.24: Corner point supports – centre arches – physical model vs catenary shape

Table 4.14: 64 ACM – Physical Model vs Catenary Shape – Centre Comparison – Corner Point Supports

Node	Distance (m)	Physical (m)	Catenary (m)	% Error
38	0.1526	0.013	0.013	0.0
39	0.1018	0.005	0.006	2.9
40	0.0509	0.001	0.001	2.2
41	0.0000	0.000	0.000	0.0
42	-0.0509	0.001	0.001	2.2
43	-0.1018	0.005	0.006	2.9
44	-0.1526	0.013	0.013	0.0

From the above graph and table it is clear that there was a very small variation in the shape of the arch along the centre of the physical model and the catenary shape. The two shapes were almost identical with a maximum variation of only 2.9% towards the edge of the structure. Therefore, for this particular sag distance the centre arch of the physical model corresponded to the shape of the catenary.

4.1.3.3.2 Diagonal Arch

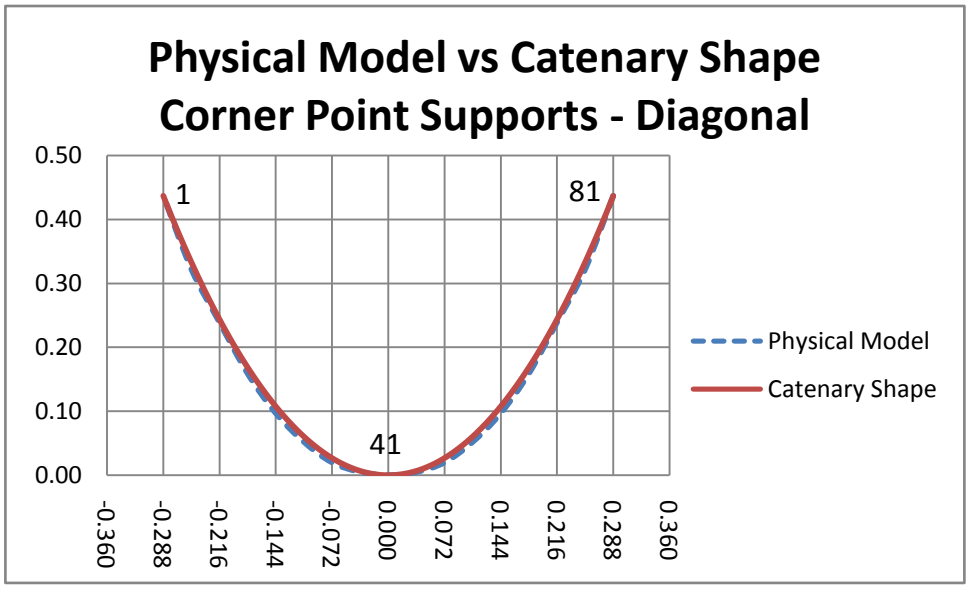

Figure 4.25: Corner point supports – diagonal arches – physical model vs catenary shape

Table 4.15: 64 ACM – Physical Model vs Catenary Shape – Diagonal Comparison – Corner Point Supports

Node	Distance (m)	Physical (m)	Catenary (m)	% Error
1	0.288	0.437	0.437	0.0
11	0.216	0.239	0.244	1.1
21	0.144	0.097	0.108	2.4

31	**0.072**	**0.020**	**0.027**	**1.6**
41	**0.000**	**0.000**	**0.000**	**0.0**
51	**-0.072**	**0.020**	**0.027**	**1.6**
61	**-0.144**	**0.097**	**0.108**	**2.4**
71	**-0.216**	**0.239**	**0.244**	**1.1**
81	**-0.288**	**0.437**	**0.437**	**0.0**

For the arch along the diagonal of the physical model, the shape corresponded closely to that of the catenary arch. The two shapes were almost identical, with a maximum variation of only 2.4% occurring towards the centre of the arch. Therefore, for this particular sag distance and support condition, the diagonal arch of the physical model conformed to the shape of the catenary.

4.1.3.4 Computer Model vs Physical Model

4.1.3.4.1 Centre Arch

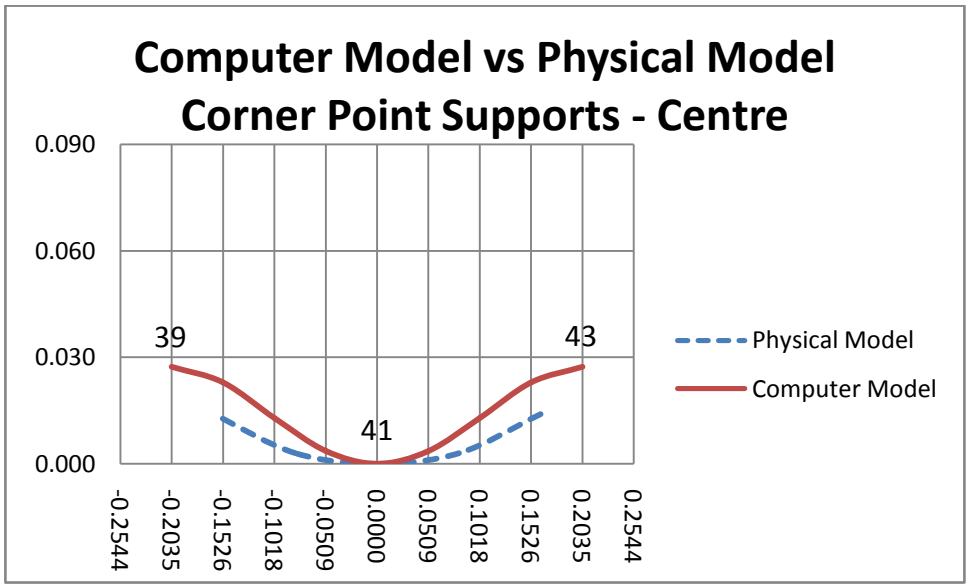

Figure 4.26: Corner point supports – centre arches – computer model vs physical model

Table 4.16: 64 ACM – Computer Model vs Physical Model – Centre Comparison – Corner Point Supports

Node	Distance (m)	Computer (m)	Physical (m)	% Error
37	0.2035	0.027		
38	0.1526	0.023	0.013	44.3
39	0.1018	0.013	0.005	33.5
40	0.0509	0.004	0.001	10.9
41	0.0000	0.000	0.000	0.0
42	-0.0509	0.004	0.001	10.9
43	-0.1018	0.013	0.005	33.5
44	-0.1526	0.023	0.013	44.3
45	-0.2035	0.027		

The above graph and table clearly indicate the large variation in the shape of the centre arch of the computer model and the physical model. From the table it can be seen that the maximum variation of 44.3% occurred towards the edge of the structure. From the graph it can be seen that the computer model produced a slight reverse bending or lip towards the edge of the structure.

As has been fully explained earlier, the formation of this lip is more commonly found in the designs of previous engineers, who modelled their shallow shell structures using fabric models as opposed to chain models. The fabric models produced this lip, whereas the chain models were not capable of producing this lip and therefore formed a shape completely different to the computer model. This explains the large variation between the two shapes as indicated by the above graph.

Therefore, for this particular sag distance and support condition, the physical chain model may not be a correct representation of the shape produced by the computer model.

4.1.3.4.2 Diagonal Arch

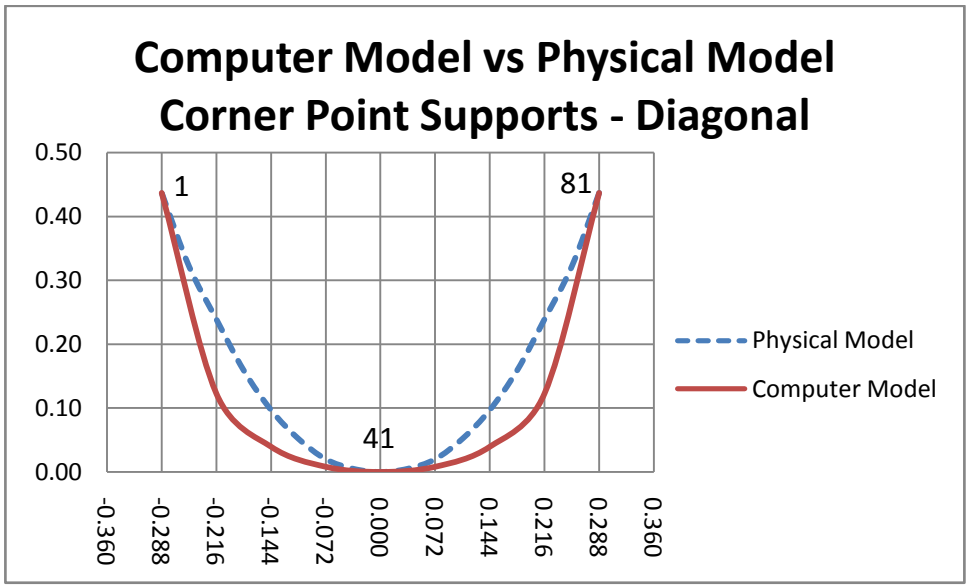

Figure 4.27: Corner point supports – diagonal arches – computer model vs physical model

Table 4.17: 64 ACM – Computer Model vs Physical Model – Diagonal Comparison – Corner Point Supports

Node	Distance (m)	Computer (m)	Physical (m)	% Error
1	0.288	0.437	0.437	0.0
11	0.216	0.123	0.239	26.6
21	0.144	0.040	0.097	13.2
31	0.072	0.008	0.020	2.7
41	0.000	0.000	0.000	0.0
51	-0.072	0.008	0.020	2.7
61	-0.144	0.040	0.097	13.2
71	-0.216	0.123	0.239	26.6
81	-0.288	0.437	0.437	0.0

The above graph and table clearly indicate the significant variation in the shape of the diagonal arch of the computer model and that of the physical model. It is clear that the arch of the computer model did not correspond to the arch of the physical model. The computer model developed a much broader bell-shaped arch, with a maximum variation of 26.6% at the node closest to the support.

Again, this variation could have occurred due to the formation of the lip towards the edge of the model - which is evident from the graphs presented earlier. Due to the computer model being fully interconnected at every point within the structure, it is very possible that the lip that occurred at the edge of the structure affected the diagonal arch of the structure in a manner that contributed to the variations indicated above. The physical chain model on the other hand was not capable of producing this lip and therefore formed a shape completely different to the computer model. This explains the large variation between the two shapes as indicated by the above graph.

Therefore, for this particular sag distance and support condition, the physical chain model may not be a correct representation of the shape produced by the computer model.

4.1.4 Shape 4: Broad Corner Supports

For the fourth shape, the models were supported at the corner edges, together with the adjacent edges on either side of the corner edges i.e. the structure was supported at three points at each corner of the structure. This resulted in a broad corner support. The resulting shapes are presented below:

4.1.4.1 Physical and Computer Model

Figure 4.28: Physical model with broad corner supports

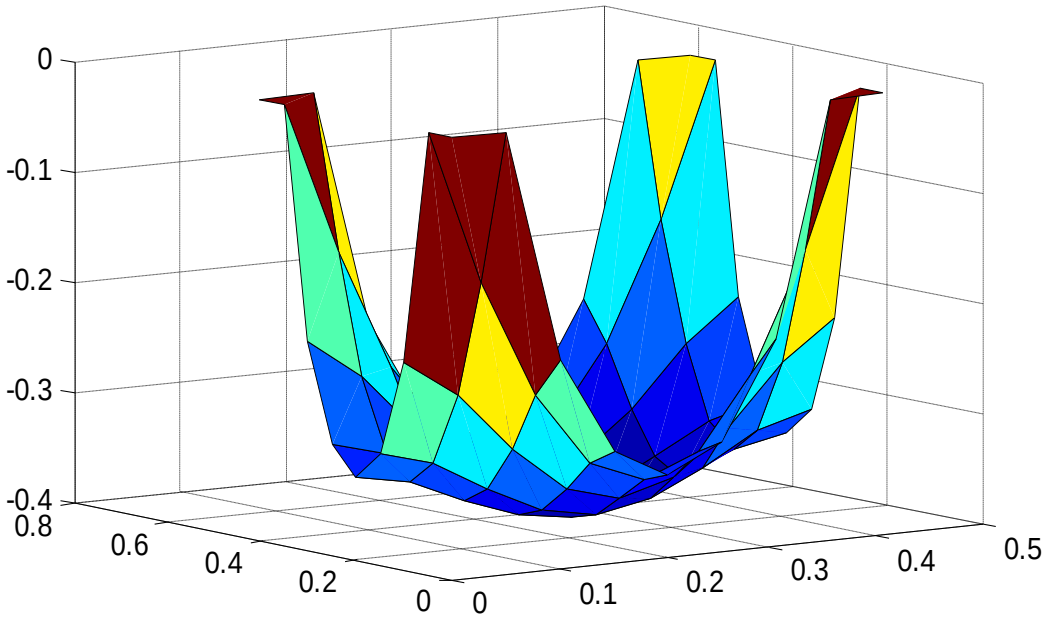

Figure 4.29: Computer model with broad corner supports

A comparison of the shapes formed by the computer and physical models indicate that the overall shape of the two models was very similar. However, the computer model produced a slight reverse bending towards the edge of the structure.

The results of the more detailed analyses are presented below:

4.1.4.2 Computer Model vs Mathematical Model

4.1.4.2.1 Centre Arch

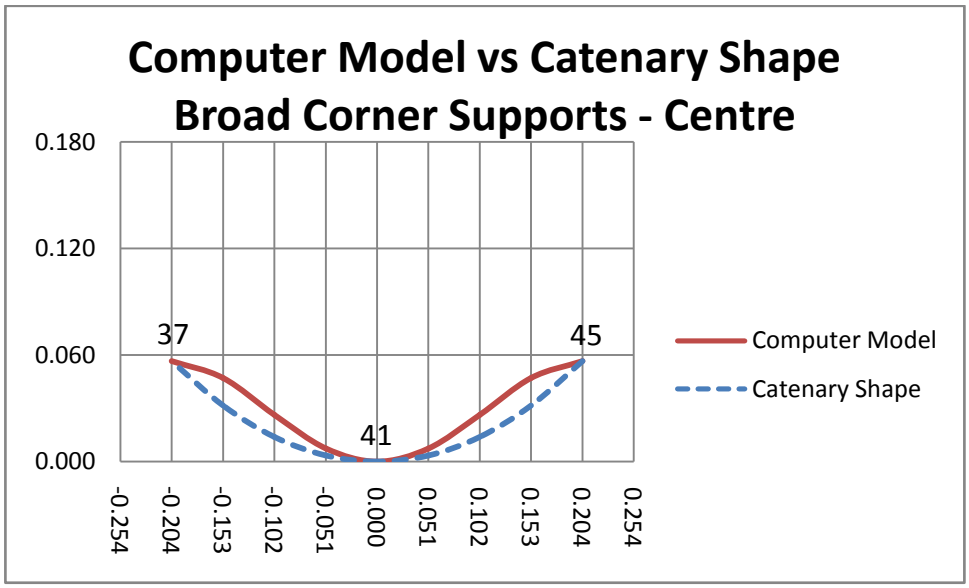

Figure 4.30: Broad corner supports – centre arches – computer model vs catenary shape

Table 4.18: 64 ACM – Computer Model vs Catenary Shape – Centre Comparison – Broad Corner Supports

Node	Distance (m)	Computer (m)	Catenary (m)	% Error
37	0.2035	0.057	0.057	0.0
38	0.1526	0.047	0.031	27.4
39	0.1018	0.026	0.014	21.7
40	0.0509	0.007	0.003	6.9
41	0.0000	0.000	0.000	0.0
42	-0.0509	0.0074	0.003	6.9
43	-0.1018	0.0263	0.014	21.7
44	-0.1526	0.0471	0.031	27.4
45	-0.2035	0.0565	0.057	0.0

With regards to the centre arches, the above graph and table clearly indicate the variation that occurred between the shape of the computer model and the shape of the mathematical model i.e. the catenary shape. The maximum variation of 27.4% occurred at the node closest to the edge. From the above

graph it can be seen that a slight reverse bending or lip occurred towards the edge of the structure.

Again, as has been fully explained earlier, the formation of this lip is more commonly found in the designs of previous engineers, who modelled their shell structures using fabric models. The absence of this lip in the catenary model resulted in the variation between the two shapes as indicated by the above graph.

Therefore, for this particular sag distance and support condition, the centre arch of the computer model did not correspond to the catenary shape.

4.1.4.2.2 Diagonal Arch

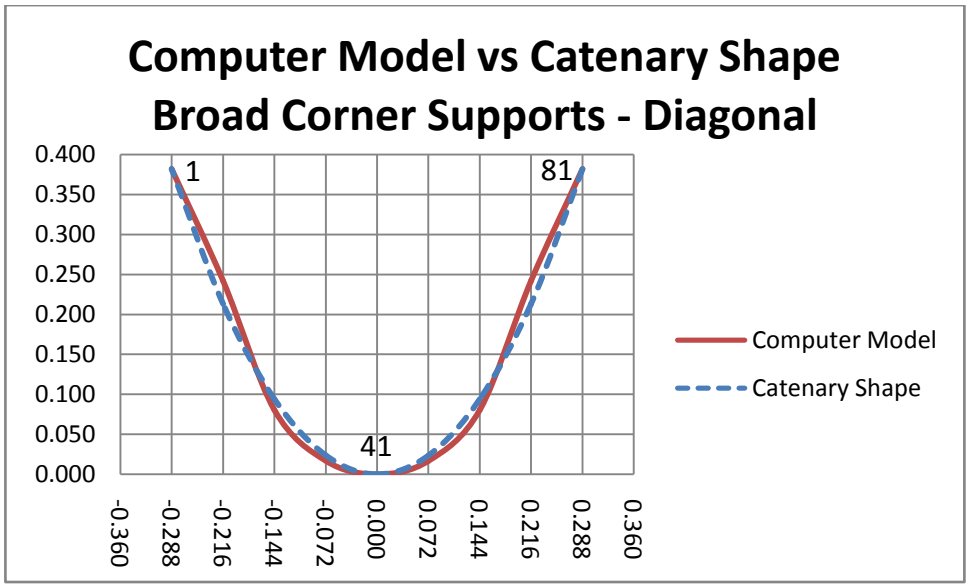

Figure 4.31: Broad corner supports – diagonal arches – computer model vs catenary shape

Table 4.19: 64 ACM – Computer Model vs Catenary Shape – Diagonal Comparison – Broad Corner Supports

Node	Distance (m)	Computer (m)	Catenary (m)	% Error
1	0.288	0.382	0.382	0.0
11	0.216	0.242	0.213	7.5
21	0.144	0.080	0.094	3.6
31	0.072	0.017	0.023	1.8
41	0.000	0.000	0.000	0.0
51	-0.072	0.017	0.023	1.8
61	-0.144	0.080	0.094	3.6
71	-0.216	0.242	0.213	7.5
81	-0.288	0.382	0.382	0.0

From the above graph and table it is clear that there was a small variation in the shape along the diagonal arch of the computer model and the catenary shape. From the table it can be seen that the maximum variation of 7.5% occurred at the node closest to the support. From the graph it can be seen that the arch of the computer model produced a slight reverse bending. However, this reverse bending was not significant and it only resulted in a small variation between the two models.

Therefore, for this particular sag distance and support condition, the diagonal arch of the computer model corresponded to the catenary shape.

4.1.4.3 Physical Model vs Mathematical Model

4.1.4.3.1 Centre Arch

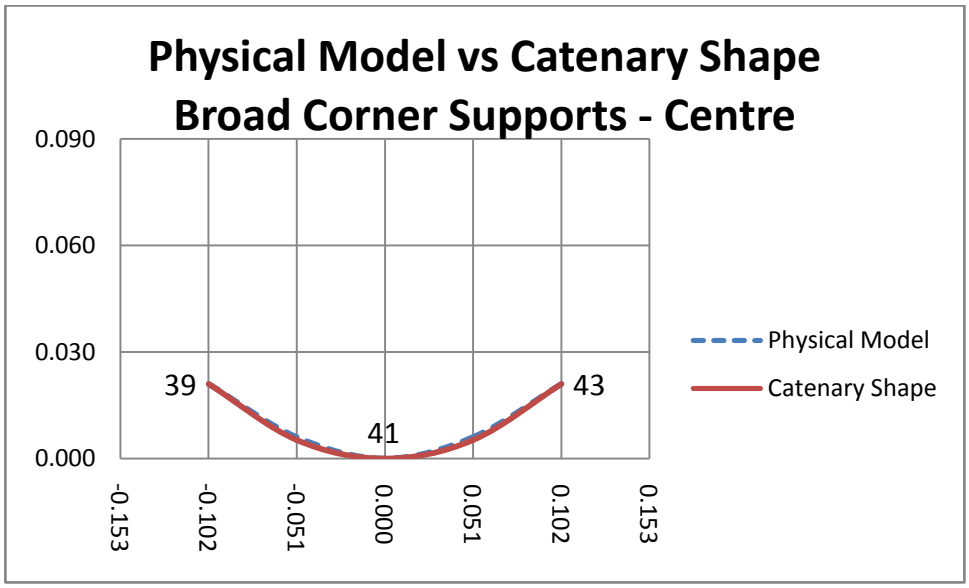

Figure 4.32: Broad corner supports – centre arches – physical model vs catenary shape

Table 4.20: 64 ACM – Physical Model vs Catenary Shape – Centre Comparison – Broad Corner Supports

Node	Distance (m)	Physical (m)	Catenary (m)	% Error
39	0.102	0.021	0.021	0.0
40	0.051	0.006	0.005	4.0
41	0.000	0.000	0.000	0.0
42	-0.051	0.006	0.005	4.0
43	-0.102	0.021	0.021	0.0

From the above graph and table it is clear that the shape of the centre arch of the physical model corresponded closely to the catenary shape. The two shapes were almost identical, with only a very small variation of 4% between

the two models. Therefore, for this particular sag distance and support condition, the centre arch of the physical model corresponded closely to the shape of the catenary model.

4.1.4.3.2 Diagonal Arch

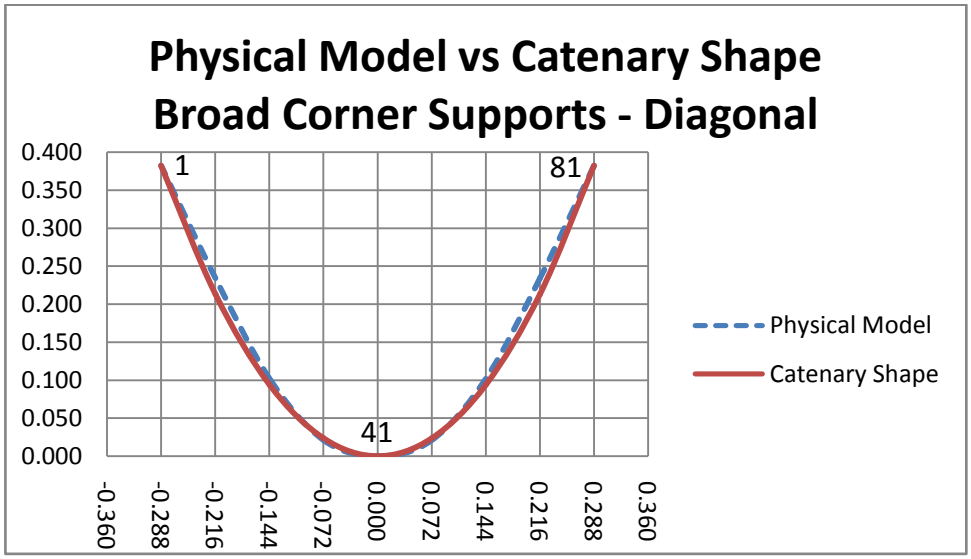

Figure 4.33: Broad corner supports – diagonal arches – physical model vs catenary shape

Table 4.21: 64 ACM – Physical Model vs Catenary Shape – Diagonal Comparison – Broad Corner Supports

Node	Distance (m)	Physical (m)	Catenary (m)	% Error
1	0.288	0.382	0.382	0.0
11	0.216	0.234	0.213	5.5
21	0.144	0.102	0.094	2.1
31	0.072	0.021	0.023	0.6
41	0.000	0.000	0.000	0.0
51	-0.072	0.021	0.023	0.6
61	-0.144	0.102	0.094	2.1
71	-0.216	0.234	0.213	5.5
81	-0.288	0.382	0.382	0.0

With regards to the form of the diagonal arch of the physical model and catenary shape, the above graph and table indicate a small variation in the two forms. The largest variation of 5.5% occurred at the node closest to the support. Since the form produced by the physical model had to be correct, the slight variation can be attributed to either errors in modelling or the difficulties in accurately measuring the co-ordinances of the physical model.

Here again, as has been fully explained earlier, the errors could have occurred due to the one very apparent shortcoming of the physical modelling process, which occurred when constructing the three-dimensional shape from individual arches along the model. The varying lengths of the adjacent hanging chain arches produced a three-dimensional shape that had slight inconsistencies along the model. This definitely caused slight inaccuracies in the arches of the physical model and could explain the variations seen above.

Therefore, for this particular sag distance and support condition, the diagonal arch of the physical model corresponded to the shape of the catenary model.

4.1.4.4 Computer Model vs Physical Model

4.1.4.4.1 Centre Arch

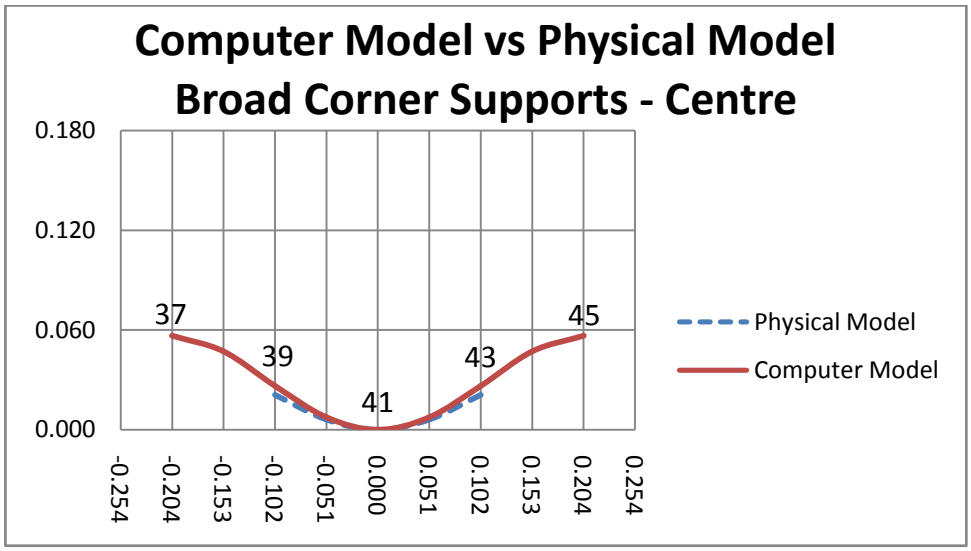

Figure 4.34: Broad corner supports – centre arches – computer model vs physical model

Table 4.22: 64 ACM – Computer Model vs Physical Model – Centre Comparison – Broad Corner Supports

Node	Distance (m)	Computer (m)	Physical (m)	% Error
37	0.204	0.057		
38	0.153	0.047		
39	0.102	0.026	0.021	9.3
40	0.051	0.007	0.006	2.5
41	0.000	0.000	0.000	0.0
42	-0.051	0.0074	0.006	2.5
43	-0.102	0.0263	0.021	9.3
44	-0.153	0.0471		
45	-0.204	0.0565		

The above graph and table indicate the variation in the shape of the centre arch of the computer model and the physical model. From the table it can be seen that the maximum variation of 9.3% occurred two nodes away from the centre node. In addition to the variation in the two shapes, the above graph also indicates that the arch of the physical model did not span the full length of the computer model arch. It can also be seen that the computer model produced a slight reverse bending or lip towards the edge of the structure.

As was explained earlier, the formation of this lip can be more commonly found in the designs of previous engineers, who modelled their shell structures using fabric models instead of chain models. As opposed to the fabric model, the chain model was not capable of producing this lip and therefore formed a shape completely different to the computer model. This explains the variation between the two shapes as indicated by the above graph.

Therefore, for this particular sag distance and support condition, the physical chain model may not be a correct representation of the shape produced by the computer model.

4.1.4.4.2 Diagonal Arch

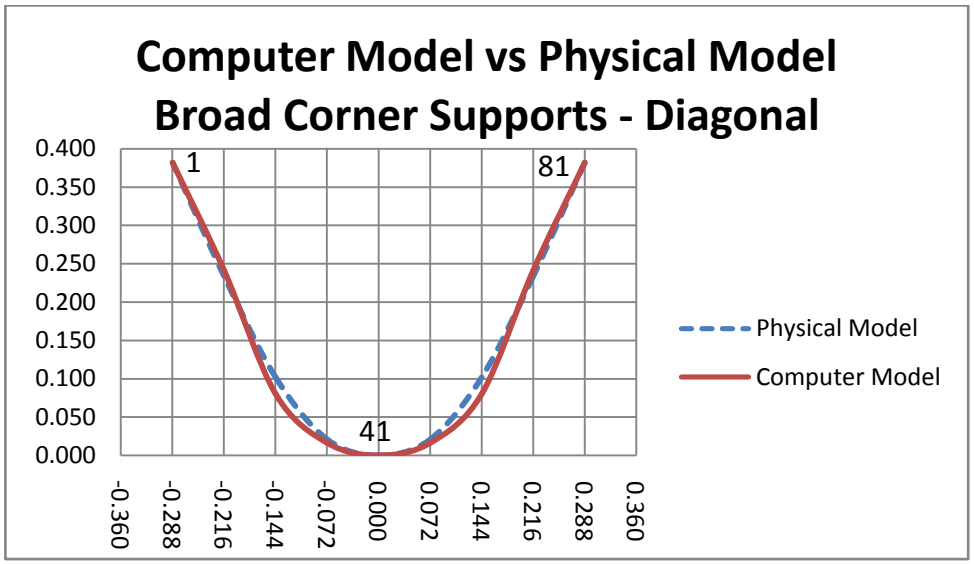

Figure 4.35: Broad corner supports – diagonal arches – computer model vs physical model

Table 4.23: 64 ACM – Computer Model vs Physical Model – Diagonal Comparison – Broad Corner Supports

Node	Distance (m)	Computer (m)	Physical (m)	% Error
1	0.288	0.382	0.382	0.0
11	0.216	0.242	0.234	2.0
21	0.144	0.080	0.102	5.7
31	0.072	0.017	0.021	1.2
41	0.000	0.000	0.000	0.0
51	-0.072	0.017	0.021	1.2
61	-0.144	0.080	0.102	5.7
71	-0.216	0.242	0.234	2.0
81	-0.288	0.382	0.382	0.0

From the above graph and table it is clear that there was a small variation in the shape along the diagonal arch of the computer model and the physical model. From the table it can be seen that a maximum variation of 5.7%

occurred along the arch. From the graph it can be seen that the arch of the computer model produced a slight reverse bending. However, this reverse bending was not significant and it only resulted in a small variation between the two models.

Nevertheless, this small variation can be accommodated by increasing the thickness of the constructed arch such that the arch of the physical model fits within this constructed arch.

Therefore, for this particular sag distance and support condition, the diagonal arch of the computer model corresponded to the physical chain model.

4.1.5 Shape 5: Broad Corner and Centre Supports

For the fifth shape, the models were supported at the corner points, the adjacent points on either side of the corner points and along the centre points of the structure. The resulting shapes are presented below:

4.1.5.1 Physical and Computer Model

Figure 4.36: Physical model with broad corner and centre supports

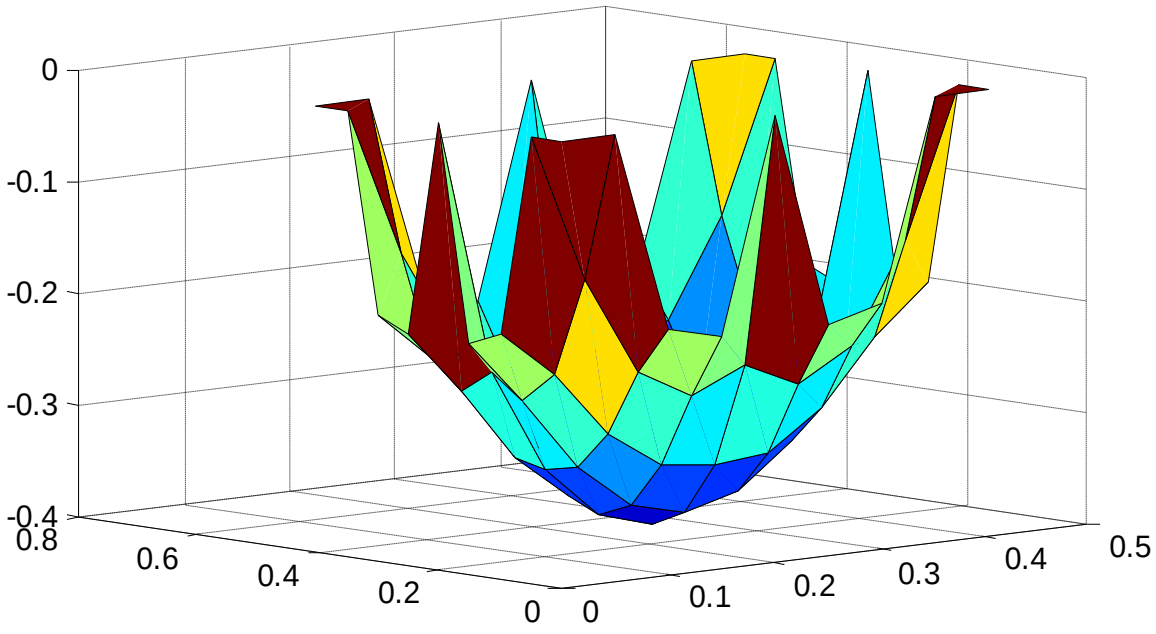

Figure 4.37: Computer model with broad corner and centre supports

A comparison of the shapes formed by the computer and physical models indicate that the overall shape between the two models was similar, although some variations are visible. For instance, the computer model produced a slight reverse bending towards the edge of the structure.

The results of the more detailed analyses are presented below:

4.1.5.2 Computer Model vs Mathematical Model

4.1.5.2.1 Centre Arch

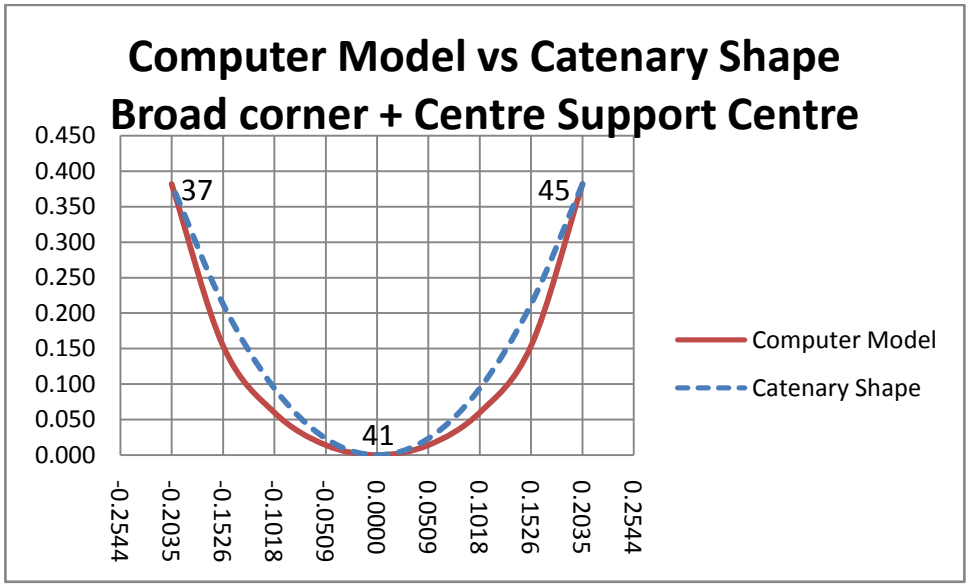

Figure 4.38: Broad corner and centre supports – centre arches – computer model vs catenary shape

Table 4.24: 64 ACM – Computer Model vs Catenary Shape – Centre Comparison – Broad Corner and Centre Supports

Node	Distance (m)	Computer (m)	Catenary (m)	% Error
37	0.2035	0.382	0.382	0.0
38	0.1526	0.154	0.213	15.4
39	0.1018	0.060	0.094	8.9
40	0.0509	0.014	0.023	2.4
41	0.0000	0.000	0.000	0.0
42	-0.0509	0.014	0.023	2.4
43	-0.1018	0.060	0.094	8.9
44	-0.1526	0.154	0.213	15.4
45	-0.2035	0.382	0.382	0.0

The above graph and table indicate some variation in the shape of the centre arch of the computer model and that of the catenary shape. It is clear that the arch of the computer model did not correspond to the arch of the catenary model. The computer model developed a significantly broader arch, with the largest variation of 15.4% occurring at the node closest to the support.

This variation could have occurred due to the formation of the lip along the free edges of the computer model, as is evident from the three-dimensional model presented earlier. This lip is not evident along the centre arch since the model was supported at this arch. Nevertheless, due to computer model being fully interconnected at every point within the structure, it is very possible that the lip that occurred at the edge of the structure affected the centre arch of the structure in a manner that contributed to the variations indicated above.

Therefore, for this particular sag distance and support condition, the centre arch of the computer model did not correspond to the catenary shape.

4.1.5.2.2 Diagonal Arch

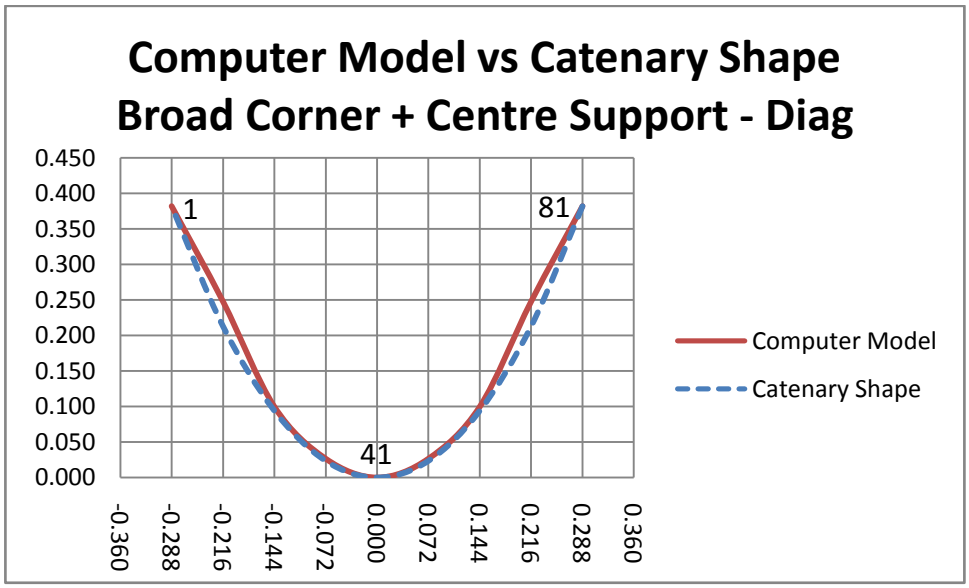

Figure 4.39: Broad corner and centre supports – diagonal arches – computer model vs catenary shape

Table 4.25: 64 ACM – Computer Model vs Catenary Shape – Diagonal Comparison – Broad Corner and Centre Supports

Node	Distance (m)	Computer (m)	Catenary (m)	% Error
1	0.288	0.382	0.382	0.0
11	0.216	0.248	0.213	9.1
21	0.144	0.100	0.094	1.5
31	0.072	0.027	0.023	0.8
41	0.000	0.000	0.000	0.0
51	-0.072	0.027	0.023	0.8
61	-0.144	0.100	0.094	1.5
71	-0.216	0.2478	0.213	9.1
81	-0.288	0.382	0.382	0.0

From the above graph and table it is clear that there was a variation in the shape along the diagonal arch of the computer model and the catenary shape. From the table it can be seen that a maximum variation of 9.1% occurred at the node closest to the support. From the graph it can be seen that the arch of the computer model produced a slight reverse bending. However, this reverse bending was not significant and it only resulted in a small variation between the two models.

Therefore, for this particular sag distance and support condition, the diagonal arch of the computer model corresponded to the catenary shape.

4.1.5.3 Physical Model vs Mathematical Model

4.1.5.3.1 Centre Arch

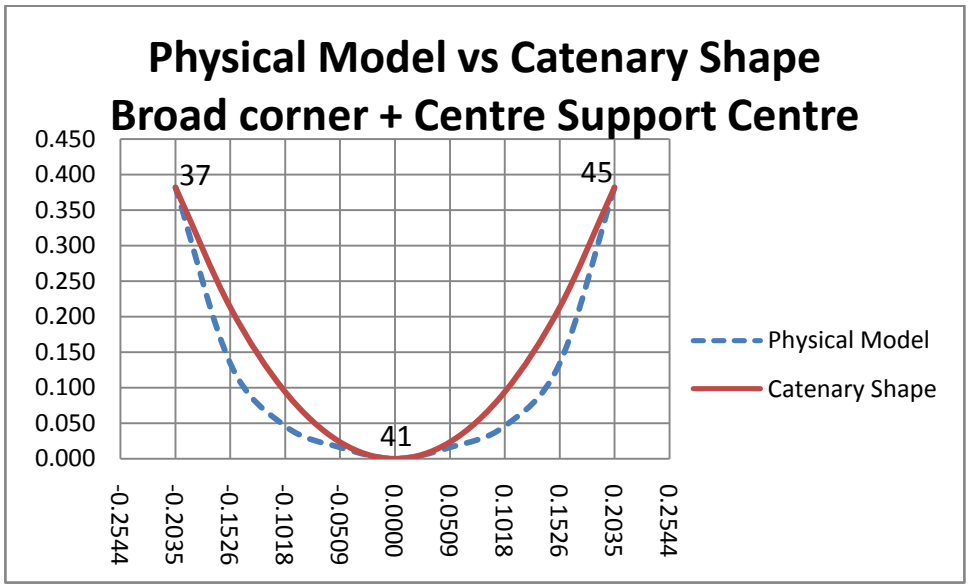

Figure 4.40: Broad corner and centre supports – centre arches – physical model vs catenary shape

Table 4.26: 64 ACM – Physical Model vs Catenary Shape – Centre Comparison – Broad Corner and Centre Supports

Node	Distance (m)	Physical (m)	Catenary (m)	% Error
37	0.2035	0.382	0.382	0.0
38	0.1526	0.134	0.213	20.7
39	0.1018	0.046	0.094	12.6
40	0.0509	0.016	0.023	1.9
41	0.0000	0.000	0.000	0.0
42	-0.0509	0.016	0.023	1.9
43	-0.1018	0.046	0.094	12.6
44	-0.1526	0.134	0.213	20.7
45	-0.2035	0.382	0.382	0.0

The above graph and table clearly indicate the significant variation in the centre arch of the physical model and the catenary shape. The physical model was much broader than the catenary shape, with a maximum variation of 20.7 %. This does not necessarily mean that the shape formed by the physical model was incorrect, since the physical model was a valid pure compression shape formed by its own self-weight. Therefore, the above comparison puts forward an additional observation that a pure compression structure does not necessarily have to be a catenary shape.

This highlights the fact that different physical modelling techniques using different materials would exhibit different pure compression shapes. This important observation added a new dimension to the research, in that it becomes necessary to not only fit the computer model to the physical model

but also the physical model to the computer model. These observations require further investigation.

4.1.5.3.2 Diagonal Arch

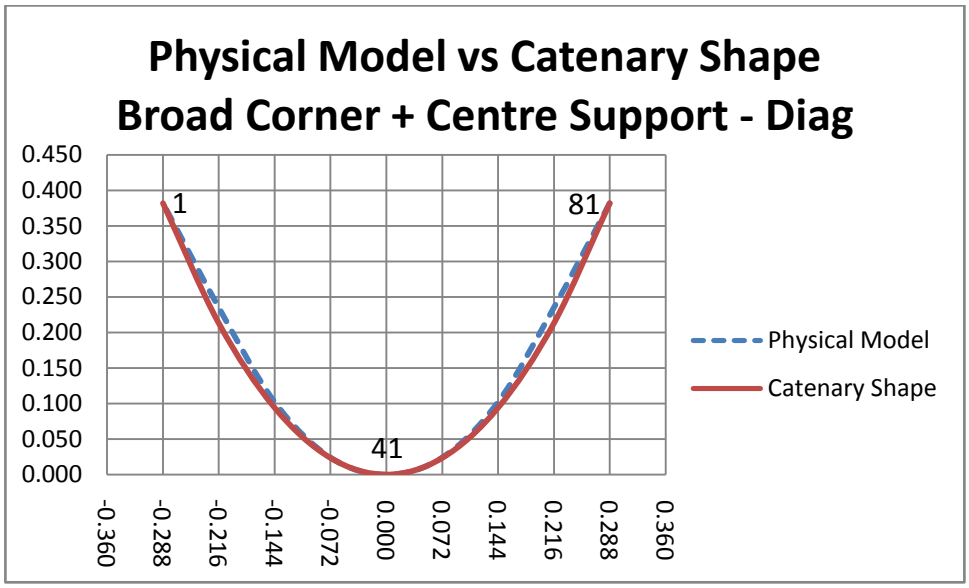

Figure 4.41: Broad corner and centre supports – diagonal arches – physical model vs catenary shape

Table 4.27: 64 ACM – Physical Model vs Catenary Shape – Diagonal Comparison – Broad Corner and Centre Supports

Node	Distance (m)	Physical (m)	Catenary (m)	% Error
1	0.288	0.382	0.382	0.0
11	0.216	0.235	0.213	5.8
21	0.144	0.102	0.094	2.1
31	0.072	0.024	0.023	0.2
41	0.000	0.000	0.000	0.0
51	-0.072	0.024	0.023	0.2
61	-0.144	0.102	0.094	2.1
71	-0.216	0.235	0.213	5.8
81	-0.288	0.382	0.382	0.0

With regards to the form of the diagonal arch of the physical model and catenary shape, the above graph and table indicate a small variation in the two forms. The largest variation of 5.8% occurred at the node closest to the support. Since the form produced by the physical model had to be correct, the slight variation can be attributed to either errors in modelling or the difficulties in accurately measuring the co-ordinances of the physical model.

Again, these errors can be attributed to the one very apparent shortcoming of the physical modelling process that occurred when constructing the three-dimensional shape from individual arches along the model. The differing lengths of the hanging chain arches produced a three-dimensional shape that had slight inconsistencies along the model. This definitely caused slight inaccuracies in the arches of the physical model and could explain the variations seen above.

Therefore, for this particular sag distance and support condition, the diagonal arch of the physical model corresponded to the shape of the catenary model.

4.1.5.4 Computer Model vs Physical Model

4.1.5.4.1 Centre Arch

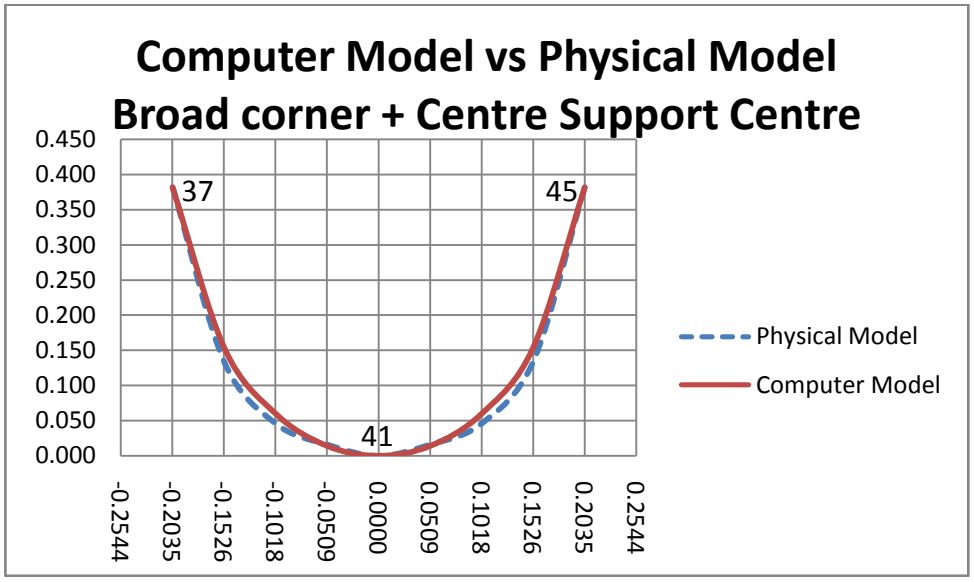

Figure 4.42: Broad corner and centre supports – centre arches – computer model vs physical model

Table 4.28: 64 ACM – Computer Model vs Physical Model – Centre Comparison – Broad Corner and Centre Supports

Node	Distance (m)	Computer (m)	Physical (m)	% Error
37	0.2035	0.382	0.382	0.0
38	0.1526	0.154	0.134	5.3
39	0.1018	0.060	0.046	3.7
40	0.0509	0.014	0.016	0.5
41	0.0000	0.000	0.000	0.0
42	-0.0509	0.014	0.016	0.5
43	-0.1018	0.060	0.046	3.7
44	-0.1526	0.154	0.134	5.3
45	-0.2035	0.382	0.382	0.0

From the above graph and table, the shape of the centre arch of the computer model corresponded to the shape of the centre arch of the physical

model. The two shapes were very similar, with a maximum variation of 5.3% occurring at the node closest to the support. This variation could be due to a combination of errors in the computer model and physical model. For the physical model the errors arose due to the differing lengths of arches along the three-dimensional model and for the computer model the errors arose due to the rigid nature of the finite elements used in the analysis.

It can therefore be concluded that the shape of the centre arch of the computer model corresponded to the shape of the centre arch of the physical model.

4.1.5.4.2 Diagonal Arch

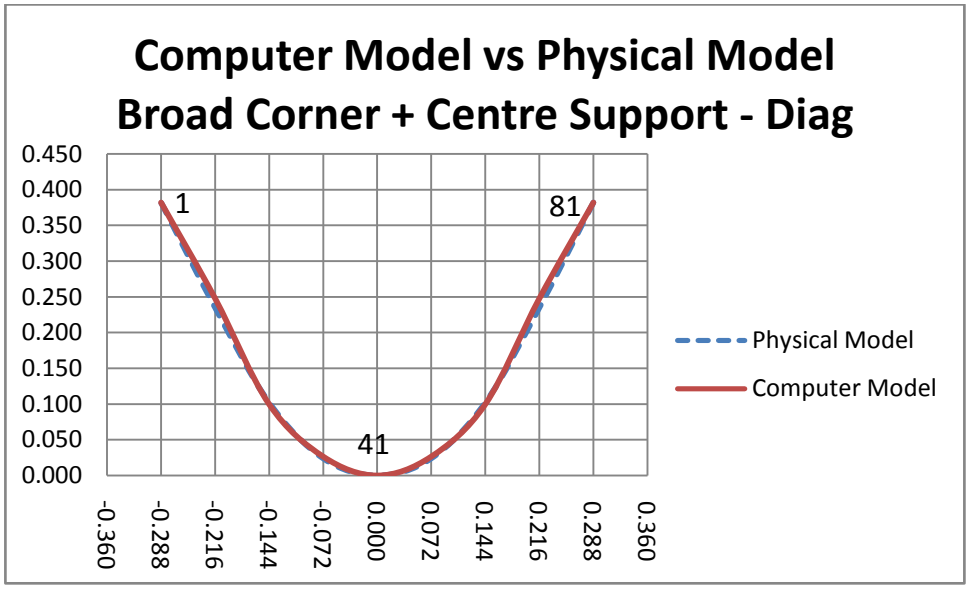

Figure 4.43: Broad corner and centre supports – diagonal arches – computer model vs physical model

Table 4.29: 64 ACM – Computer Model vs Physical Model – Diagonal Comparison – Broad Corner and Centre Supports

Node	Distance (m)	Computer (m)	Physical (m)	% Error
1	0.288	0.382	0.382	0.0
11	0.216	0.248	0.235	3.4
21	0.144	0.100	0.102	0.6
31	0.072	0.027	0.024	0.7
41	0.000	0.000	0.000	0.0
51	-0.072	0.027	0.024	0.7
61	-0.144	0.100	0.102	0.6
71	-0.216	0.248	0.235	3.4
81	-0.288	0.382	0.382	0.0

From the above graph and table it is clear that there was a small variation in the shape along the diagonal arch of the computer model and the physical model. From the table it can be seen that a maximum variation of 3.4% occurred along the arch. From the graph it can be seen that the arch of the computer model produced a slight reverse bending. However, this reverse bending was not significant and it only resulted in a small variation between the two models.

Therefore, for this particular sag distance and support condition, the diagonal arch of the computer model corresponded to the diagonal arch of the physical chain model.

4.1.6 Shape 6: Corner and Centre Point Supports

For the sixth shape, the corner points and the centre points of the structure were supported. The resulting shapes are presented below:

4.1.6.1 Physical and Computer Model

Figure 4.44: Physical model with corner and centre point supports

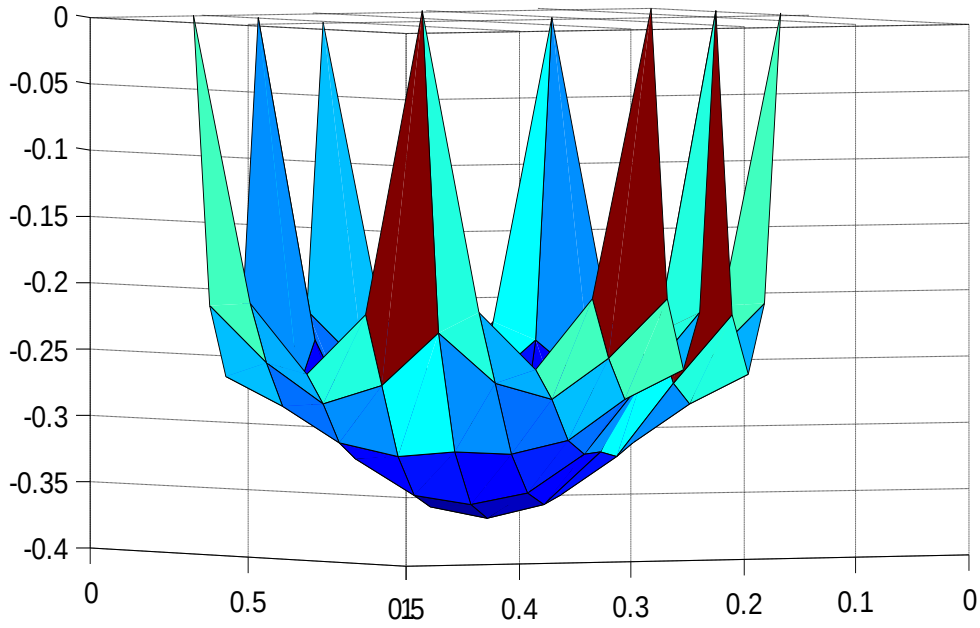

Figure 4.45: Computer model with corner and centre point supports

A comparison of the shapes formed by the computer and physical models indicate that the overall shape between the two models was similar, although some variations are visible. For instance, the computer model produced a slight reverse bending towards the edge of the structure.

The results of the more detailed analyses are presented below:

4.1.6.2 Computer Model vs Mathematical Model

4.1.6.2.1 Centre Arch

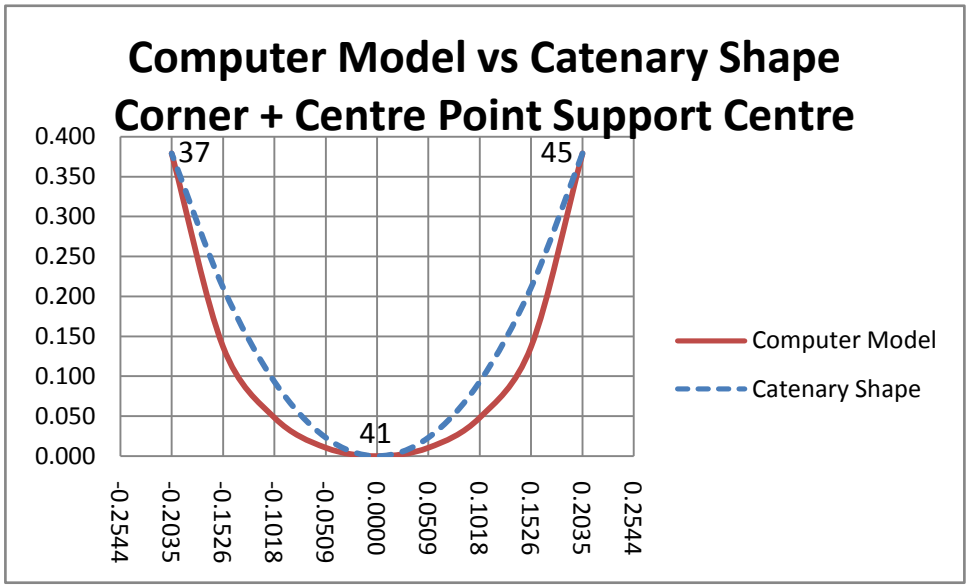

Figure 4.46: Corner and centre point supports – centre arches – computer model vs catenary shape

Table 4.30: 64 ACM – Computer Model vs Catenary Shape – Centre Comparison – Corner and Centre Point Supports

Node	Distance (m)	Computer (m)	Catenary (m)	% Error
37	0.2035	0.379	0.379	0.0
38	0.1526	0.137	0.211	19.6
39	0.1018	0.048	0.093	11.9
40	0.0509	0.011	0.023	3.4
41	0.0000	0.000	0.000	0.0
42	-0.0509	0.011	0.023	3.4
43	-0.1018	0.048	0.093	11.9
44	-0.1526	0.137	0.211	19.6
45	-0.2035	0.379	0.379	0.0

The above graph and table indicate the variation in the shape of the centre arch of the computer model and that of the catenary shape. It is clear that the arch of the computer model did not correspond to the arch of the catenary model. The computer model developed a significantly broader arch, with the largest variation of 19.6% occurring at the node closest to the support.

Again, this variation could have occurred due to the formation of the lip along the free edges of the computer model, as is evident from the three-dimensional model presented earlier. This lip is not evident along the centre arch since the model was supported at this arch. Nevertheless, due to the computer model being fully interconnected at every point within the structure, it is very possible that the lip that occurred at the edge of the structure affected the centre arch of the structure in a manner that contributed to the variations indicated above.

Therefore, for this particular sag distance and support condition, the centre arch of the computer model did not correspond to the catenary shape.

4.1.6.2.2 Diagonal Arch

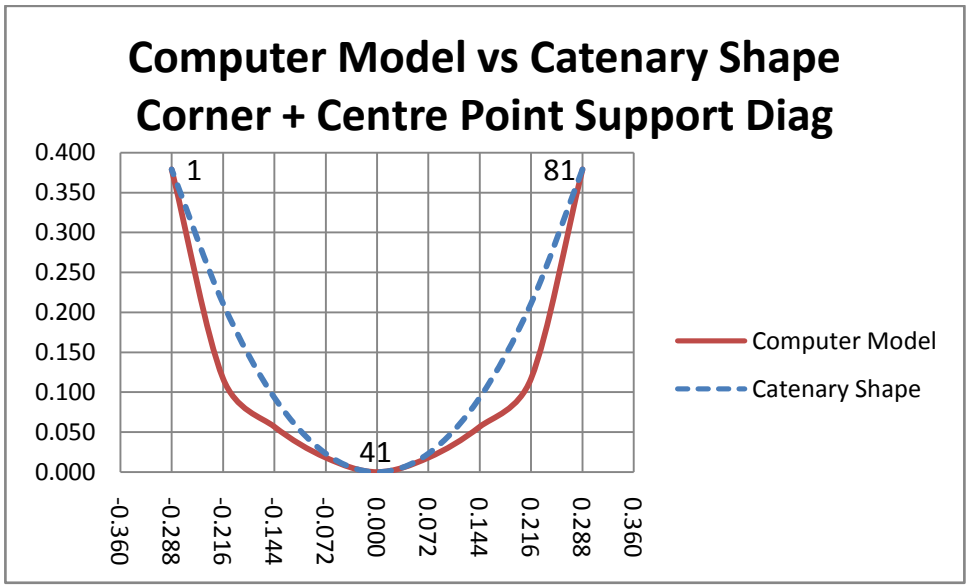

Figure 4.47: Corner and centre point supports – diagonal arches – computer model vs catenary shape

Table 4.31: 64 ACM – Computer Model vs Catenary Shape – Diagonal Comparison – Corner and Centre Point Supports

Node	Distance (m)	Computer (m)	Catenary (m)	% Error
1	0.288	0.379	0.379	0.0
11	0.216	0.117	0.211	24.8
21	0.144	0.057	0.093	9.6
31	0.072	0.018	0.023	1.4
41	0.000	0.000	0.000	0.0
51	-0.072	0.018	0.023	1.4
61	-0.144	0.057	0.093	9.6
71	-0.216	0.117	0.211	24.8
81	-0.288	0.379	0.379	0.0

The above graph and table indicate the significant variation in the shape of the diagonal arch of the computer model and that of the catenary shape. It is clear that the arch of the computer model did not correspond to the arch of the catenary model. The computer model developed a significantly broader arch, with the largest variation of 24.8% occurring at the node closest to the support.

As with the previous case, the variation could have occurred due to the formation of the lip along the free edges of the computer model, as is evident from the three-dimensional model presented earlier. This lip is not evident along the diagonal arch since the model was supported at this arch. Nevertheless, due to the computer model being fully interconnected at every point within the structure, it is very possible that the lip that occurred at the edge of the structure affected the diagonal arch of the structure in a manner that contributed to the variations indicated above.

Therefore, for this particular sag distance and support condition, the diagonal arch of the computer model did not correspond to the catenary shape.

4.1.6.3 Physical Model vs Mathematical Model

4.1.6.3.1 Centre Arch

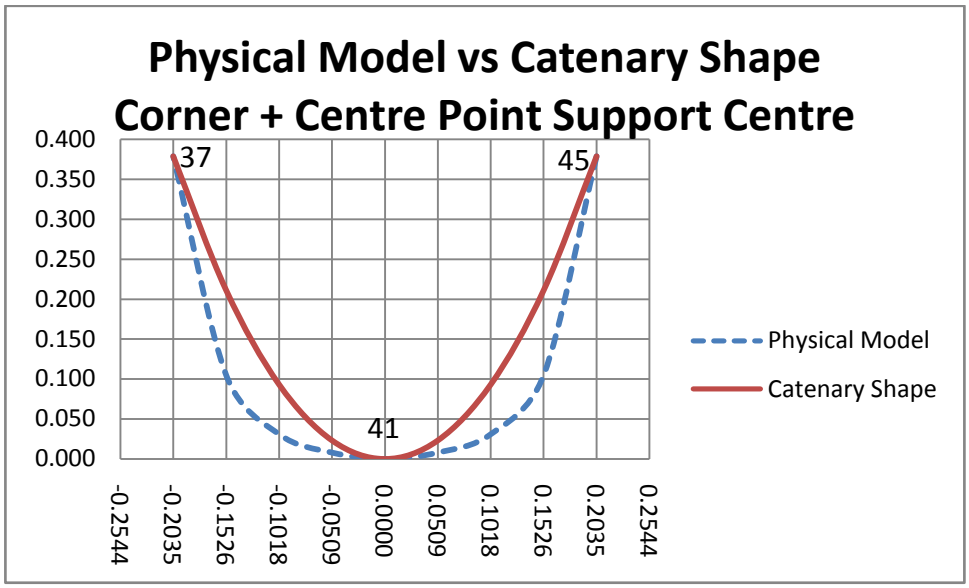

Figure 4.48: Corner and centre point supports – centre arches – physical model vs catenary shape

Table 4.32: 64 ACM – Physical Model vs Catenary Shape – Centre Comparison – Corner and Centre Point Supports

Node	Distance (m)	Physical (m)	Catenary (m)	% Error
37	0.2035	0.379	0.379	0.0
38	0.1526	0.105	0.211	28.0
39	0.1018	0.031	0.093	16.4
40	0.0509	0.008	0.023	4.0
41	0.0000	0.000	0.000	0.0
42	-0.0509	0.008	0.023	4.0
43	-0.1018	0.031	0.093	16.4
44	-0.1526	0.105	0.211	28.0
45	-0.2035	0.379	0.379	0.0

The above graph and table clearly indicate the large variation in the centre arch of the physical model and the catenary shape. The physical model was much broader than the catenary shape, with a maximum variation of 28%. Here again, this does not mean that the shape formed by the physical model

was incorrect; since the physical model was a valid pure compression shape formed by its own self-weight. The variation in the two shapes again puts forward the observation that a pure compression structure does not necessarily have to be a catenary shape.

Similarly, it highlights the fact that different physical modelling techniques using different materials would exhibit different pure compression shapes. This important observation added a new dimension to the research, in that it becomes necessary to not only fit the computer model to the physical model but also the physical model to the computer model.

4.1.6.3.2 Diagonal Arch

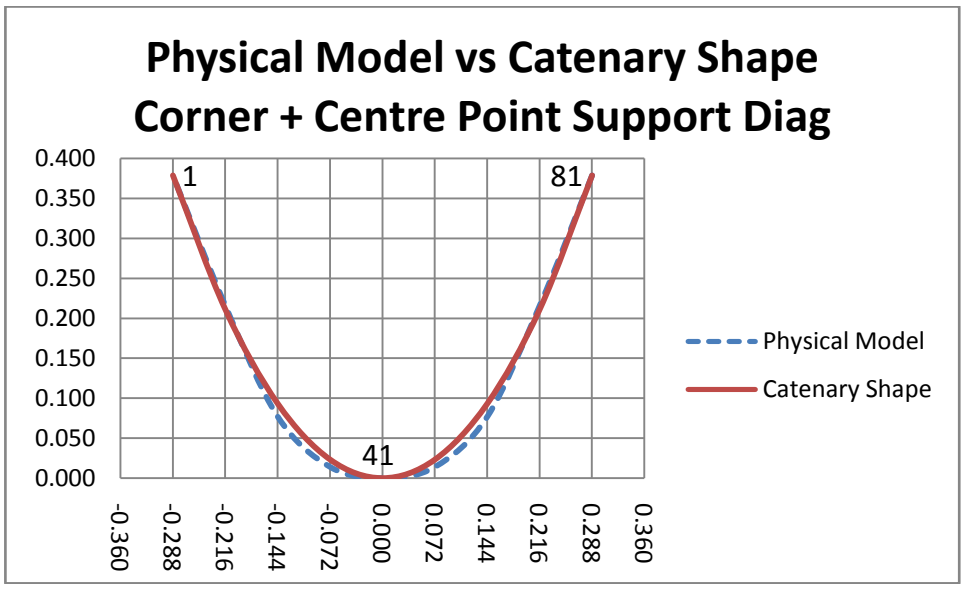

Figure 4.49: Corner and centre point supports – diagonal arches – physical model vs catenary shape

Table 4.33: 64 ACM – Physical Model vs Catenary Shape – Diagonal Comparison – Corner and Centre Point Supports

Node	Distance (m)	Physical (m)	Catenary (m)	% Error
1	0.288	0.379	0.379	0.0
11	0.216	0.216	0.211	1.3
21	0.144	0.077	0.093	4.3
31	0.072	0.014	0.023	2.4
41	0.000	0.000	0.000	0.0
51	-0.072	0.014	0.023	2.4
61	-0.144	0.077	0.093	4.3
71	-0.216	0.216	0.211	1.3
81	-0.288	0.379	0.379	0.0

The above graph and table indicate a small variation between the diagonal arch of the physical model and that of the catenary shape. This variation made the physical model slightly broader than the catenary shape towards the middle of the structure, where a maximum variation of 4.3% occurred. This small variation could have been due to the inconsistencies in the physical modelling process and the difficulties in measuring the co-ordinances of the physical model.

As with some of the earlier shapes, the errors could be due to the one very apparent shortcoming of the physical modelling process, which occurred when constructing the three-dimensional shape from individual arches along the model. The differing lengths of the arches produced a three-dimensional shape that had slight inconsistencies along the model. This definitely caused

slight inaccuracies in the arches of the physical model and could explain the variations seen above.

However, it can be concluded that the physical model corresponded to the catenary shape for this particular case.

4.1.6.4 Computer Model vs Physical Model

4.1.6.4.1 Centre Arch

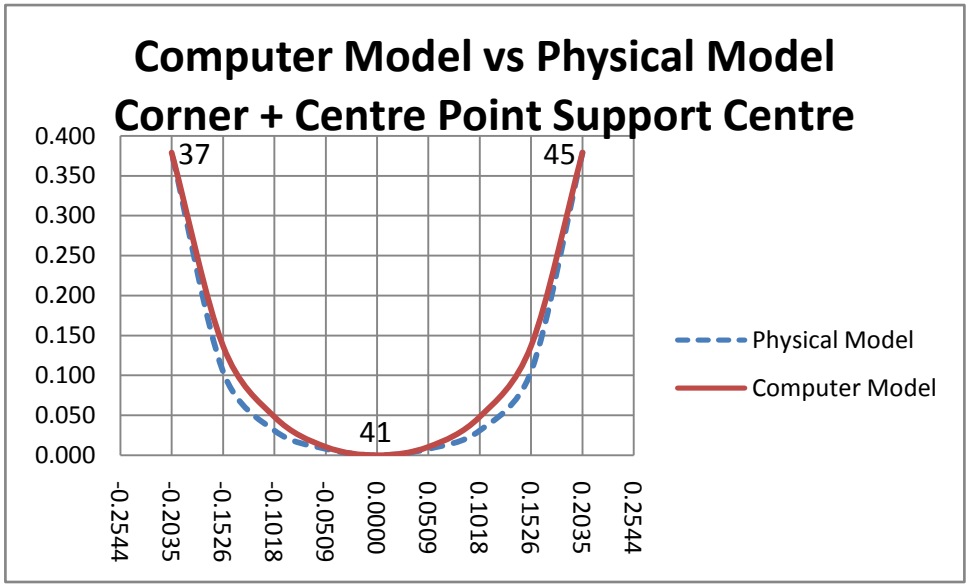

Figure 4.50: Corner and centre point supports – centre arches – computer model vs physical model

Table 4.34: 64 ACM – Computer Model vs Physical Model – Centre Comparison – Corner and Centre Point Supports

Node	Distance (m)	Computer (m)	Physical (m)	% Error
37	0.2035	0.379	0.379	0.0
38	0.1526	0.137	0.105	8.5
39	0.1018	0.048	0.031	4.5
40	0.0509	0.011	0.008	0.7
41	0.0000	0.000	0.000	0.0
42	-0.0509	0.011	0.008	0.7
43	-0.1018	0.048	0.031	4.5
44	-0.1526	0.137	0.105	8.5
45	-0.2035	0.379	0.379	0.0

The above graph and table indicate the small variation between the centre arch of the computer model and the physical model. The physical model was a bit broader than the computer model and a maximum variation of 8.5% occurred at the node closest to the support. This variation could be due to a combination of errors in the computer model and physical model. For the physical model the errors arose due to the differing lengths of arches along the three-dimensional model and for the computer model the errors arose due to the rigid finite elements used in the analysis.

Nevertheless, this variation can be accommodated by increasing the thickness of the constructed arch such that the arch of the computer model falls within the perimeters of the constructed arch.

4.1.6.4.2 Diagonal Arch

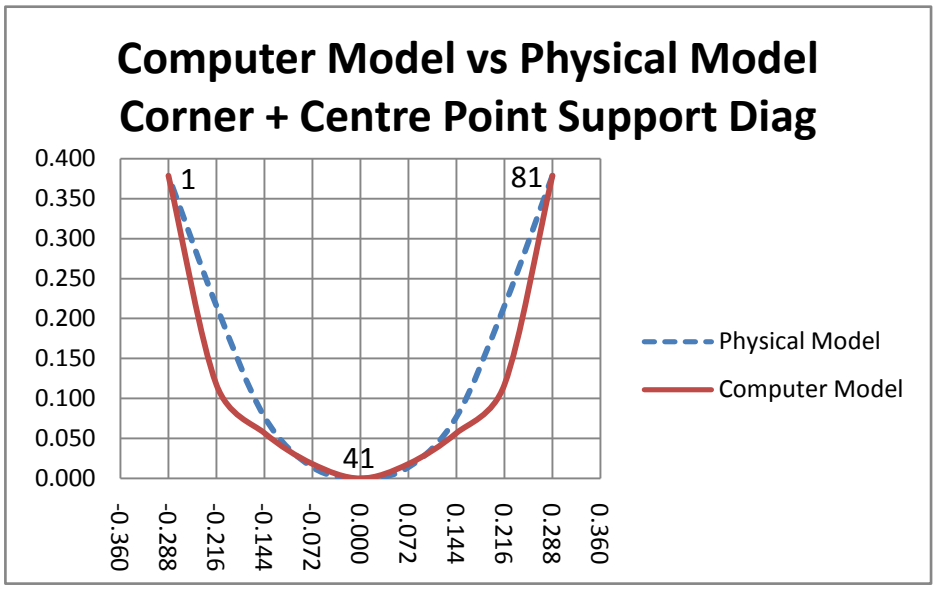

Figure 4.51: Corner and centre point supports – diagonal arches – computer model vs physical model

Table 4.35: 64 ACM – Computer Model vs Physical Model – Diagonal Comparison – Corner and Centre Point Supports

Node	Distance (m)	Computer (m)	Physical (m)	% Error
1	0.288	0.379	0.379	0.0
11	0.216	0.117	0.216	26.0
21	0.144	0.057	0.077	5.3
31	0.072	0.018	0.014	1.1
41	0.000	0.000	0.000	0.0
51	-0.072	0.018	0.014	1.1
61	-0.144	0.057	0.077	5.3
71	-0.216	0.117	0.216	26.0
81	-0.288	0.379	0.379	0.0

The above graph and table indicate the significant variation in the shape of the diagonal arch of the computer model and the physical model. It is clear

that the arch of the computer model did not correspond to the arch of the physical model. The computer model developed a significantly broader arch, with the largest variation of 26% occurring at the node closest to the support.

Here again, the variation could have occurred due to the formation of the lip along the free edges of the computer model, as is evident from the three-dimensional model presented earlier. This lip is not evident along the diagonal arch since the model was supported at this arch. Nevertheless, due to the computer model being fully interconnected at every point within the structure, it is very possible that the lip that occurred at the edge of the structure affected the diagonal arch of the structure in a manner that contributed to the variations indicated above. The physical chain model was not capable of producing this lip and therefore formed a shape completely different to the computer model. This explains the variation between the two shapes as indicated by the above graph.

Therefore, for this particular sag distance and support condition, the diagonal arch of the computer model did not correspond to the physical model.

4.2 Summary of Results

4.2.1 Shape 1: Barrel Vault

- The arch produced by the REGN finite element method did not correspond to the shape of the catenary arch. Therefore, the REGN method was not capable of modelling a pure compression barrel vault
- The arch produced by the ACM finite element method had an excellent correspondence to the shape of the catenary arch. The two forms were almost identical. Therefore, the ACM method is fully capable of modelling a pure compression barrel vault

4.2.2 Shape 2: All Edges Simply Supported

- The centre arch of the computer model corresponded to the catenary shape
- The diagonal arch of the computer model was narrower than the catenary shape with a reverse bending towards the edge of the structure
- Both the centre and diagonal arches of the physical model corresponded to the catenary shape
- The centre arch of the computer model corresponded to that of the physical model with a slight variation
- The diagonal arch of the computer model was narrower than that of the physical model, with the computer model producing a reverse bending towards the edge of the structure

4.2.3 Shape 3: Corner Point Supports

- The centre arch of the computer model was narrower than the catenary shape, with the computer model producing a reverse bending towards the edge of the structure
- The diagonal arch of the computer model was much broader than the catenary shape
- Both the centre and diagonal arches of the physical model corresponded to the catenary shape
- The centre arch of the computer model was much narrower than the physical model, with the computer model producing a reverse bending towards the edge of the structure. The physical model was not capable of producing this reverse bending
- The diagonal arch of the computer model was much broader than that of the physical model

4.2.4 Shape 4: Broad Corner Supports

- The centre arch of the computer model was narrower than the catenary shape, with the computer model producing a reverse bending towards the edge of the structure
- The diagonal arch of the computer model corresponded to the catenary shape, although the computer model produced a reverse bending along the arch, which was not significant

- Both the centre and diagonal arches of the physical model corresponded to the catenary shape
- The centre arch of the computer model was narrower than the physical model, with the computer model producing a reverse bending towards the edge of the structure. The physical model was not capable of producing this reverse bending
- The diagonal arch of the computer model corresponded to the shape of the physical model, although the computer model produced a reverse bending along the arch, which was not significant

4.2.5 Shape 5: Broad Corner and Centre Supports

- The centre arch of the computer model was broader than that of the catenary shape
- The diagonal arch of the computer model corresponded to that of the catenary shape, although the computer model produced a reverse bending along the arch, which was not significant
- The centre arch of the physical model was much broader than that of the catenary shape
- The diagonal arch of the physical model corresponded closely to that of the catenary shape
- The centre arch of the computer model corresponded to the shape of the physical model with a slight variation

- The diagonal arch of the computer model corresponded to the shape of the physical model, although the computer model produced a reverse bending along the arch, which was not significant

4.2.6 Shape 6: Corner and Centre Point Supports

- The centre arch of the computer model was broader than that of the catenary shape
- The diagonal arch of the computer model was much broader than that of the catenary shape. This arch also had a kink in it, which was representative of the reverse bending that occurred within the structure
- The centre arch of the physical model was much broader than that of the catenary shape
- The diagonal arch of the physical model corresponded to that of the catenary shape with a slight variation
- The centre arch of the computer model corresponded to that of the physical model with a slight variation
- The diagonal arch of the computer model was much broader than that of the physical model. This arch also had a kink in it, which was representative of the reverse bending that occurred within the structure

The results show that with regards to the correspondence of the computer model and the catenary shape, none of the five doubly-curved shell structures corresponded to the catenary shape in both the centre and diagonal arches.

In shape 2, the centre arch of the computer model corresponded to that of the catenary shape, whilst the diagonal arch was narrower than the catenary shape. In shape 3, the centre arch of the computer model was narrower than the catenary shape, whilst the diagonal arch was broader than the catenary shape. In shape 4, the centre arch of the computer model was narrower than the catenary shape, whilst the diagonal arch corresponded to that of the catenary shape. In shape 5, the centre arch of the computer model was broader than the catenary shape, whilst the diagonal arch corresponded to that of the catenary shape. For shape 6, both the centre and diagonal arches of the computer model were broader than the catenary shape.

With regards to the physical model and the catenary shape, shapes 2, 3 and 4 corresponded in both the centre and diagonal arches of the two models. In shapes 5 and 6, the diagonal arches of the physical models corresponded to that of the catenary shape, whilst the centre arches were much broader than that of the catenary shape.

With regards to the computer model and the physical model, only shape 5 corresponded in both the centre and diagonal arches of the two models. In shape 2, the centre arch of the computer model corresponded to the physical model, whilst the diagonal arch was narrower than the physical model. In shape 3, the centre arch of the computer model was narrower than the physical model, whilst the diagonal arch was broader than the physical model.

In shape 4, the centre arch of the computer model was narrower than the physical model, whilst the diagonal arch corresponded to that of the physical model. For shape 6, the centre arch of the computer model corresponded to the physical model, whilst the diagonal arch was broader than the physical model.

It is interesting to note that in some of the models developed, the physical model formed a catenary shape for both the centre and diagonal arches, whereas in the other models, the physical model only conformed to a catenary shape along the diagonal arches.

4.3 Discussion of Results

From the six shapes analyzed, the computer model corresponded closely to the shape of the singly-curved barrel vault, i.e. shape 1, and one of the doubly-curved structures, i.e. shape 5. For the remaining four shapes, i.e. shapes 2, 3, 4 and 6, the computer model did not correspond to the shape of both the centre and diagonal arches of the physical hanging chain model.

All five of the doubly-curved shapes generated by the computer model produced a reverse bending or lip along the structure. This reverse bending or lip resulted in major variations between the computer and physical models in four of the doubly-curved shapes and minor variations in one of the doubly

curved shapes i.e. shape 5. The reason for these variations was due to the physical model not being able to produce this reverse bending or lip. The minor variation in shape 5 was due to the less pronounced lip produced by the computer model and this allowed for it to correspond more closely to the shape of the physical hanging chain model. The reduction in the extent of the reverse bending in shape 5 was most probably due the manner in which the model was supported.

The formation of this reverse bending can also be observed in two other scenarios. In the first scenario, the formation of this reverse bending at the corners of the computer model corresponds closely to the corner effects that are manifested in yield-line analysis - when a uniformly distributed load is applied to a square slab that is simply supported along the edges. These corner effects produce what is known as “corner levers” at the corner edges of the slab. Johansen (1962) maintains that the existence of these corner levers is solely due to the shape of the edge of the slab and does not depend on whether it is anchored or not.

In the second scenario, the formation of this lip can be found in the designs of previous engineers, who modelled their shell structures using fabric models as opposed to chain models. These fabric models were able to accurately predict the shape of shallow shells. Since the fabric model is interconnected at every point within the structure, the formation of the lip at the edge of the

structure also affected the other points towards the interior of the structure. In a similar manner, the computer model was also interconnected at every point within the structure and it therefore behaved in exactly the same manner as the fabric model.

In addition to the major inconsistencies that occurred due to the formation of the reverse bending or lip, other minor inconsistencies also occurred within the models. These minor inconsistencies were as a result of a combination of errors in both the computer and physical hanging chain models. For the physical models, the minor errors arose due to the inconsistencies in the physical modelling process and the difficulties in measuring the co-ordinances of the physical model.

One very apparent shortcoming of the physical modelling process occurred when constructing the three-dimensional shape from individual arches along the model. Each arch was constructed using identical links that were combined together to form a chain. The uniform size of the link meant that the length of each chain could only be increased or decreased according to the link size. This resulted in adjacent arches being either too long or too short as one moved along the physical hanging chain model. This produced a three-dimensional shape that had slight inconsistencies along the model.

For the computer models, the minor errors arose due to the way in which the computer model formed the arches along the model. The computer model formed the arches by approximating it by a series of rigid finite elements that had no bending capacity. The finite elements were connected to each other at nodal points and the intersection of the adjacent finite elements produced a curve that was not completely smooth. This lack of smoothness along the curve resulted in minor variations when compared to a curve that was completely smooth. Nevertheless, the accuracy of the computer model can be further increased by decreasing the size of the finite elements.

The results also suggest that the ideal shape of a pure compression structure does not necessarily have to be entirely a catenary shape. The physical models of shapes 5 and 6 produced centre arches that were much broader than the catenary shape, whilst the diagonal arches of these same structures corresponded to that of the catenary shape. Therefore, within the same structure along different arches, there existed a combination of both a catenary and non-catenary shape.

Similarly, the computer model of shape 5 corresponded to the shape of the physical model by producing a centre arch that was much broader than the catenary shape, and a diagonal arch that corresponded to the catenary shape. Since the physical model was definitely a pure compression structure, this indicated that shape 5 of the computer model was in fact a pure

compression structure. Furthermore, the computer model also accurately defined the form of a fully catenary shaped pure compression structure i.e. the barrel vault. This proves that the computer model is capable of producing both a fully catenary shaped pure compression structure and a pure compression structure that is a combination of a catenary and a non-catenary shape.

The physical modelling process also led to the important observation that the most consistent shapes were obtained when the model was set up on a circular grid i.e. when the structure was supported along points that formed a circular pattern. This observation was only made after the physical models were constructed and the computer model had already been formulated on a square grid using the rectangular finite element.

This realisation led to attempts to transform the square grid into a circular grid. However, these attempts were unsuccessful, because in order to produce this circular grid and still maintain the accuracy of the computer model, the rectangular finite elements needed to be extremely small. This extremity resulted in a large number of elements, which resulted in an even larger number of nodes. This made it difficult to model the boundary conditions i.e. the support conditions, due to the difficulties in identifying the exact nodes where the supports needed to be positioned from amongst the large number of nodes that existed within the structure. This caused the

computer program to become very cumbersome, especially when the support conditions needed to be changed so that a new shape of structure could be defined. Therefore, the rectangular finite element only allowed the model to be developed on a square grid and therefore the physical models had to be developed on this square grid.

5 CONCLUSIONS AND RECOMMENDATIONS

From the above results, important conclusions have been made. These conclusions allow for a better understanding of both the physical and computer modelling processes. These conclusions are presented below.

Firstly, since the computer model was capable of generating a barrel vault shape that corresponded very closely to the actual shape of a pure compression barrel vault, it can be concluded that the design philosophy employed in developing the computer design tool is in fact capable of defining the shape of a pure compression thin shell structure. Furthermore, the analysis also proved that the ACM finite element method was much more accurate than the REGN finite element method.

The second conclusion became evident from the computer model that fully corresponded to the doubly-curved shape of the physical hanging chain model. This model produced a form that was a combination of both a

catenary and non-catenary shape. Therefore, it can be concluded that a pure compression thin shell structure can comprise of a combination of catenary and non-catenary arches within the same structure. It can also be concluded that the computer model is capable of modelling both a fully catenary shaped structure i.e. the barrel vault and a partly catenary shaped structure i.e. shape 5.

The third conclusion is that the physical hanging chain models need to be developed on a circular grid instead of a rectangular grid. This was realised during the physical modelling process when it became apparent that the most consistent shapes were obtained when the physical hanging chain model was set up on a circular grid i.e. when the structure was supported along points that formed a circular pattern. The more consistent shapes will reduce the inconsistencies between the computer and physical hanging chain models and will allow for a better correspondence between the models.

The final and most important conclusion stems from the fact that all five of the doubly-curved shapes generated by the computer model produced a reverse bending or lip along the structure, whilst none of the physical hanging chain models produced this reverse bending or lip. The formation of this reverse bending or lip can be more commonly found in the square slabs of yield-line analysis or the physical models developed using the hanging fabric modelling technique.

The hanging chain models were not capable of producing this lip and it therefore produced shapes that did not correspond to the shapes generated by the computer models. This suggests that the structure is not only influenced by the support conditions but it is also dependant on the physical modelling process, which needs to be taken into consideration when comparing the computer model to the physical model. This leads to the main conclusion that the physical hanging chain model may not be a correct representation of the shape produced by the computer model and it therefore does not provide a suitable comparison for the computer model.

The first recommendation would be to compare the present form of the computer model to a more suitable physical model. This physical model should be able to produce the corner effects and/or lip formed by the computer model. This will allow for a more accurate comparison between the computer and physical models.

The next recommendation would be to re-develop the computer model, by utilizing a more versatile finite element in the analysis, like that of the triangular or quadrilateral element. This will allow the computer model to be developed on a circular grid, which should prevent the reverse bending or lip from being produced by the computer model. This will lead to a computer model that corresponds more closely to the physical hanging chain model and will result in a reduction in the inconsistencies between the two models.

If the more versatile triangular or quadrilateral elements are still not capable of accurately modelling the pure compression structure, then the next recommendation would be to develop a new or modified finite element that more accurately defines the behaviour of a pure compression thin shell structure.

The above recommendations seek to rectify the major challenge of providing a more suitable and closer comparison between the computer and physical models. Exploring these possibilities will allow for more definite and conclusive results to be obtained. This will determine with certainty whether the computer design tool is in fact capable of consistently predicting the shape of a pure compression thin shell structure.

References

Aaron, H. (1874), *Das gleichgewicht und die bewegung einer unendlich dunnen, beliebig gekrummten, elastischen schale,* journal fur reine und ange. Math.

Allen, E and Zalewski, W. (2010), *Form & Forces: Designing Efficient, Expressive Structures,* John Wiley & Sons, New Jersey.

Anderson, S. (2004), *Eladio Dieste: Innovation in Structural Art,* Princeton Architectural Press, New York.

Angerer, F. (1961), *Surface structures in building,* Verlag G.D.W. Callwey, Munich.

Ashwell, D G. & Gallagher, R H. (1976), *Finite elements for thin shells & curved members,* John Wiley & Sons Ltd, London.

Baker, A J and Pepper, D W. (1991), *Finite Elements 1-2-3,* McGraw Hill.

Bassegoda, J (1989) (in Spanish), *El gran Gaudí*, Barcelona: Sabadell.

Billington, D P. (1965), *Thin shell concrete structures,* McGraw Hill, New York.

Bulovic, I and Bhikhoo, N. (2011), *Structural Forms of the Future,* University of the Witwatersrand, Johannesburg, South Africa

Calladine, C R. (1983), *Theory of shell structures,* Cambridge University Press, Cambridge.

Cheung, Y K and Yeo, M F. (1979), *A Practical Introduction to Finite Element Analysis,* Pitman Publishing Limited, Massachusetts

Chilton, J. (2000), *Heinz Isler: The Engineer's Contribution to Contemporary Architecture,* Thomas Telford Publishing, London.

Chilton, J. (2010), *Heinz Isler's Infinite Spectrum Form-Finding in Design,* John Wiley & Sons

DoH. 2000. *National Housing Code*. Department of Housing. Pretoria, South Africa.

Flores, C. (2002) (in Catalan), *Les lliçons de Gaudí*. Translated by Glòria Bohigas. Barcelona: Empúries.

Flugge, W. (1961), *Stresses in shells,* Springer-Verlag, Berlin.

Fung, Y C & Sechler, E E. (1974), *Thin shell structures: theory, experiment &design,* Prentice Hall, New Jersey.

Gohnert, M. (n.d.), *Low cost thin shell structures*, University of the Witwatersrand, Johannesburg

Johansen, K W. (1962), *Yield-line theory*, William Clowes and Sons Limited, London

Killian, A.(2004), *Linking Hanging Chain Models to Fabrication,* Massachusetts Institute of Technology, Cambridge, MA

Killian, A and Ochsendorf, J. (2005), *Particle Spring Systems for Structural Form-Finding,* Massachusetts Institute of Technology, Cambridge, MA

Kotnik, T and Schwarts, J. (2011), *The Architecture of Heinz Isler,* Journal of the International Association for Shell and Spatial Structures, Vol 52, No 3, pp. 185-190

Lamé, G and Clapeyron. (1828), *Memoires sur l'equilibre interieur des corps solides homogenes,* Memoirs presents a l'academia des sciences de institute de France; second series.

Liem , Y (2011), *Graphic statics in funicular design: calculating force equilibrium through complementary energy,* TU Delft, Delft.

Love, A E H. (1888), *On the small free vibrations and deformations of thin elastic shells*, Phil.Trans.Royal Soc, London.

Ochsendorf, J. (2010), *Guastavino vaulting: the art of structural tile*, Princeton architectural press, New York.

Osserman, R. (2010), *How the Gateway Arch Got its Shape,* Nexus Network Journal, Vol 12, No 2, pp. 167-189

Pendergrast, R A. (2010), *Thin Shell Structure Design Tool,* Rensseler Polytechnic Institute, Troy, New York.

Rao, S S, (2011), *The finite element method in engineering: fifth edition,* Elsevier Inc, USA

Rockey, K C, Evans, H R, Griffiths, D W & Nethercot, D A (1983), *The finite element method: a basic introduction,* Granada Publishing, London.

Rutten, H S. (n.d.), *Forty years of theory, design and construction of thin shells,* Eidenhoven University of Technology.

Saudi, A. (2002), "Gaudí i els seus col·laboradors: artistes i industrials a l'entorn del 1900". In Casanova, Rossend (in Catalan), *Gaudí 2002. Miscel·lània*, Barcelona: Planeta.

Seegers, J. (2011), *Heinz Isler and his New Shapes for Shells*

Tomlow, J., Graefe, R., Otto, F., Szeemann, H., (1989), *Das Modell, The Model,* Institut fur Leichte Flachentragwerke, Stuttgart, Germany.

Van Hensbergen, G (2004) (in Spanish). *Antoni Gaudí*, London, UK: Debolsillo.

Wegmuller, A W. & Kostem, C N. (n.d.), *Finite element analysis of plates and eccentrically stiffened plates,* Lehigh University, Pennsylvania.

Weller, W M. (2011), *Form Finding, Force and Function: Mass-Spring Simulation for a Thin Shell Concrete Trolley Barn,* University of Washington.

Weller, W M. (2010), *Form-Finding, Force and Function: a Thin Shell Concrete Trolley Barn for Seattle's Waterfront,* University of Washington.

Zienkiewics, O C. (1977), *The finite element method,* McGraw Hill, London.

APPENDIX 1

$$[A] = \begin{bmatrix}
0 & 0 & -1 & 0 & 0 & 0 & 0 & 0 & 0 & 0 & 0 & 0 \\
0 & 1 & 0 & 0 & 0 & 0 & 0 & 0 & 0 & 0 & 0 & 0 \\
1 & 0 & 0 & 0 & 0 & 0 & 0 & 0 & 0 & 0 & 0 & 0 \\
0 & 0 & -1 & 0 & 0 & -2b & 0 & 0 & 0 & & 0 & 0 \\
0 & 1 & 0 & 0 & b & 0 & 0 & 0 & b^2 & 0 & 0 & b^3 \\
1 & 0 & b & 0 & 0 & b^2 & 0 & 0 & 0 & b^3 & 0 & 0 \\
0 & 0 & -1 & 0 & -a & 0 & 0 & -a & 0 & 0 & -a^3 & 0 \\
0 & 1 & 0 & 2a & 0 & 0 & 3a^2 & 0 & 0 & 0 & 0 & 0 \\
1 & a & 0 & a^2 & 0 & 0 & a^2 & 0 & 0 & 0 & 0 & 0 \\
0 & 0 & -1 & 0 & -a & -2b & 0 & -a^2 & -2ab & -3b^2 & -a^3 & -3ab^2 \\
0 & 1 & 0 & 2a & b & 0 & 3a^2 & 2ab & b^2 & 0 & 3a^2b & b^3 \\
1 & a & b & a^2 & ab & b^2 & a^3 & a^2b & ab^2 & b^3 & a^3b & ab^3
\end{bmatrix}$$

$$[\underline{B}] = \begin{bmatrix}
1 & -1 & 1 & 1 & -1 & 1 & -1 & 1 & -1 & 1 & -1 & -1 \\
0 & 0 & 1 & 0 & -1 & 2 & 0 & 1 & -2 & 3 & -1 & -3 \\
0 & -1 & 0 & 2 & -1 & 0 & -3 & 2 & -1 & 0 & -3 & -1 \\
1 & -1 & -1 & 1 & 1 & 1 & -1 & -1 & -1 & -1 & 1 & 1 \\
0 & 0 & 1 & 0 & -1 & -2 & 0 & 1 & 2 & 3 & -1 & -3 \\
0 & -1 & 0 & 2 & 1 & 0 & -3 & -2 & -1 & 0 & 3 & 1 \\
1 & 1 & 1 & 1 & 1 & 1 & 1 & 1 & 1 & 1 & 1 & 1 \\
0 & 0 & 1 & 0 & 1 & 2 & 0 & 1 & 2 & 3 & 1 & 3 \\
0 & -1 & 0 & -2 & -1 & 0 & -3 & -2 & -1 & 0 & -3 & -1 \\
1 & 1 & -1 & 1 & -1 & 1 & 1 & -1 & 1 & -1 & -1 & -1 \\
0 & 0 & 1 & 0 & 1 & -2 & 0 & 1 & -2 & 3 & 1 & 3 \\
0 & -1 & 0 & -2 & 1 & 0 & -3 & 2 & -1 & 0 & 3 & 1
\end{bmatrix}$$

$$K1 = (16b) / (15a^3)$$

$$\begin{bmatrix}
0 & 0 & 0 & 0 & 0 & 0 & 0 & 0 & 0 & 0 & 0 & 0 \\
0 & 0 & 0 & 0 & 0 & 0 & 0 & 0 & 0 & 0 & 0 & 0 \\
0 & 0 & 0 & 0 & 0 & 0 & 0 & 0 & 0 & 0 & 0 & 0 \\
0 & 0 & 0 & 15 & 0 & 0 & 0 & 0 & 0 & 0 & 0 & 0 \\
0 & 0 & 0 & 0 & 0 & 0 & 0 & 0 & 0 & 0 & 0 & 0 \\
0 & 0 & 0 & 0 & 0 & 0 & 0 & 0 & 0 & 0 & 0 & 0 \\
0 & 0 & 0 & 0 & 0 & 0 & 45 & 0 & 0 & 0 & 0 & 0 \\
0 & 0 & 0 & 0 & 0 & 0 & 0 & 5 & 0 & 0 & 0 & 0 \\
0 & 0 & 0 & 0 & 0 & 0 & 0 & 0 & 0 & 0 & 0 & 0 \\
0 & 0 & 0 & 0 & 0 & 0 & 0 & 0 & 0 & 0 & 0 & 0 \\
0 & 0 & 0 & 0 & 0 & 0 & 0 & 0 & 0 & 0 & 15 & 0 \\
0 & 0 & 0 & 0 & 0 & 0 & 0 & 0 & 0 & 0 & 0 & 0
\end{bmatrix}$$

$$K2 = 16 / (15ab)$$

$$\begin{bmatrix}
0 & 0 & 0 & 0 & 0 & 0 & 0 & 0 & 0 & 0 & 0 & 0 \\
0 & 0 & 0 & 0 & 0 & 0 & 0 & 0 & 0 & 0 & 0 & 0 \\
0 & 0 & 0 & 0 & 0 & 0 & 0 & 0 & 0 & 0 & 0 & 0 \\
0 & 0 & 0 & 0 & 0 & 15 & 0 & 0 & 0 & 0 & 0 & 0 \\
0 & 0 & 0 & 0 & 0 & 0 & 0 & 0 & 0 & 0 & 0 & 0 \\
0 & 0 & 0 & 15 & 0 & 0 & 0 & 0 & 0 & 0 & 0 & 0 \\
0 & 0 & 0 & 0 & 0 & 0 & 0 & 0 & 15 & 0 & 0 & 0 \\
0 & 0 & 0 & 0 & 0 & 0 & 0 & 0 & 0 & 15 & 0 & 0 \\
0 & 0 & 0 & 0 & 0 & 0 & 15 & 0 & 0 & 0 & 0 & 0 \\
0 & 0 & 0 & 0 & 0 & 0 & 0 & 15 & 0 & 0 & 0 & 0 \\
0 & 0 & 0 & 0 & 0 & 0 & 0 & 0 & 0 & 0 & 0 & 15 \\
0 & 0 & 0 & 0 & 0 & 0 & 0 & 0 & 0 & 0 & 15 & 0
\end{bmatrix}$$

$$K3 = 16 / (15a^2) \begin{bmatrix} 0 & 0 & 0 & 0 & 0 & 0 & 0 & 0 & 0 & 0 & 0 & 0 \\ 0 & 0 & 0 & 0 & 0 & 0 & 0 & 0 & 0 & 0 & 0 & 0 \\ 0 & 0 & 0 & 0 & 0 & 0 & 0 & 0 & 0 & 0 & 0 & 0 \\ 0 & 0 & 0 & 0 & -15 & 0 & 0 & 0 & 0 & 0 & -15 & -15 \\ 0 & 0 & 0 & -15 & 0 & 0 & 0 & 0 & 0 & 0 & 0 & 0 \\ 0 & 0 & 0 & 0 & 0 & 0 & 0 & 0 & 0 & 0 & 0 & 0 \\ 0 & 0 & 0 & 0 & 0 & 0 & 0 & -30 & 0 & 0 & 0 & 0 \\ 0 & 0 & 0 & 0 & 0 & 0 & -30 & 0 & -10 & 0 & 0 & 0 \\ 0 & 0 & 0 & 0 & 0 & 0 & 0 & -10 & 0 & 0 & 0 & 0 \\ 0 & 0 & 0 & 0 & 0 & 0 & 0 & 0 & 0 & 0 & 0 & 0 \\ 0 & 0 & 0 & -15 & 0 & 0 & 0 & 0 & 0 & 0 & 0 & 0 \\ 0 & 0 & 0 & -15 & 0 & 0 & 0 & 0 & 0 & 0 & 0 & 0 \end{bmatrix}$$

$$K4 = (16a)/(15b^3) \begin{bmatrix} 0 & 0 & 0 & 0 & 0 & 0 & 0 & 0 & 0 & 0 & 0 & 0 \\ 0 & 0 & 0 & 0 & 0 & 0 & 0 & 0 & 0 & 0 & 0 & 0 \\ 0 & 0 & 0 & 0 & 0 & 0 & 0 & 0 & 0 & 0 & 0 & 0 \\ 0 & 0 & 0 & 0 & 0 & 0 & 0 & 0 & 0 & 0 & 0 & 0 \\ 0 & 0 & 0 & 0 & 0 & 0 & 0 & 0 & 0 & 0 & 0 & 0 \\ 0 & 0 & 0 & 0 & 0 & 15 & 0 & 0 & 0 & 0 & 0 & 0 \\ 0 & 0 & 0 & 0 & 0 & 0 & 0 & 0 & 0 & 0 & 0 & 0 \\ 0 & 0 & 0 & 0 & 0 & 0 & 0 & 0 & 0 & 0 & 0 & 0 \\ 0 & 0 & 0 & 0 & 0 & 0 & 0 & 0 & 5 & 0 & 0 & 0 \\ 0 & 0 & 0 & 0 & 0 & 0 & 0 & 0 & 0 & 45 & 0 & 0 \\ 0 & 0 & 0 & 0 & 0 & 0 & 0 & 0 & 0 & 0 & 0 & 0 \\ 0 & 0 & 0 & 0 & 0 & 0 & 0 & 0 & 0 & 0 & 0 & 15 \end{bmatrix}$$

$$K5 = \frac{16}{15b^2} \begin{bmatrix} 0 & 0 & 0 & 0 & 0 & 0 & 0 & 0 & 0 & 0 & 0 & 0 \\ 0 & 0 & 0 & 0 & 0 & 0 & 0 & 0 & 0 & 0 & 0 & 0 \\ 0 & 0 & 0 & 0 & 0 & 0 & 0 & 0 & 0 & 0 & 0 & 0 \\ 0 & 0 & 0 & 0 & 0 & 0 & 0 & 0 & 0 & 0 & 0 & 0 \\ 0 & 0 & 0 & 0 & 0 & -15 & 0 & 0 & 0 & 0 & 0 & 0 \\ 0 & 0 & 0 & 0 & -15 & 0 & 0 & 0 & 0 & 0 & -15 & -15 \\ 0 & 0 & 0 & 0 & 0 & 0 & 0 & 0 & 0 & 0 & 0 & 0 \\ 0 & 0 & 0 & 0 & 0 & 0 & 0 & 0 & -10 & 0 & 0 & 0 \\ 0 & 0 & 0 & 0 & 0 & 0 & 0 & -10 & 0 & -30 & 0 & 0 \\ 0 & 0 & 0 & 0 & 0 & 0 & 0 & 0 & -30 & 0 & 0 & 0 \\ 0 & 0 & 0 & 0 & 0 & -15 & 0 & 0 & 0 & 0 & 0 & 0 \\ 0 & 0 & 0 & 0 & 0 & -15 & 0 & 0 & 0 & 0 & 0 & 0 \end{bmatrix}$$

$$K6 = \frac{16}{15ab} \begin{bmatrix} 0 & 0 & 0 & 0 & 0 & 0 & 0 & 0 & 0 & 0 & 0 & 0 \\ 0 & 0 & 0 & 0 & 0 & 0 & 0 & 0 & 0 & 0 & 0 & 0 \\ 0 & 0 & 0 & 0 & 0 & 0 & 0 & 0 & 0 & 0 & 0 & 0 \\ 0 & 0 & 0 & 0 & 0 & 0 & 0 & 0 & 0 & 0 & 0 & 0 \\ 0 & 0 & 0 & 0 & 15 & 0 & 0 & 0 & 0 & 0 & 15 & 15 \\ 0 & 0 & 0 & 0 & 0 & 0 & 0 & 0 & 0 & 0 & 0 & 0 \\ 0 & 0 & 0 & 0 & 0 & 0 & 0 & 0 & 0 & 0 & 0 & 0 \\ 0 & 0 & 0 & 0 & 0 & 0 & 0 & 20 & 0 & 0 & 0 & 0 \\ 0 & 0 & 0 & 0 & 0 & 0 & 0 & 0 & 20 & 0 & 0 & 0 \\ 0 & 0 & 0 & 0 & 0 & 0 & 0 & 0 & 0 & 0 & 0 & 0 \\ 0 & 0 & 0 & 0 & 15 & 0 & 0 & 0 & 0 & 0 & 27 & 15 \\ 0 & 0 & 0 & 0 & 15 & 0 & 0 & 0 & 0 & 0 & 15 & 27 \end{bmatrix}$$